

Physics  
University of Pisa

Master Thesis

---

# Quantum Communication through finite dimensional lossy channels

---

by  
Marco Cocciaretto

Supervisor: Vittorio Giovannetti  
CdS Tutor: Davide Rossini  
Date: October, 2023



# Abstract

Quantum Information Theory (QIT) is a relatively new field of physics that is attracting a growing number of researchers. Although some elements of QIT can be found at the dawn of Quantum Mechanics (e.g. the EPR paradox), its first formal definition dates back to the 1960's[[Gor62](#)] (Bell published his paper on the EPR paradox in 1964[[Bel64](#)]).

The new framework provided by the QIT allowed for the study of open systems, i.e. systems subject to external noise; this is accomplished by defining any quantum process, or quantum channel, as a **Linear, Completely Positive and Trace-preserving** (LCPT) map, which interprets the set of initial density matrices as input and outputs new density matrices in a (possibly) different Hilbert space. This paved the way for an information theoretic approach to the study of quantum processes relevant to Quantum Computation and Quantum Communication, in the same way Shannon's noisy channel theorem did for classical communication and computation.

The question then becomes, in this context, what quantity can we interpret as "information"? And how well is this information preserved during the quantum process? In other words, how well can we store and reliably transmit information through a given quantum channel? It turns out that, in the quantum case, the amount of "stored information" of a system is given by the Von Neumann entropy, while there are a number of quantities called "capacities" that describe the amount of transmittable information through a given channel based on the nature of the information to be transmitted and the availability of additional resources (e.g. classical communication lines, entanglement...). This thesis work focuses on the study of some of these capacities, with a particular focus on quantum capacity and 2-way quantum capacity, for a specific family of channels, called Multilevel Amplitude Damping (MAD) channels.

MAD channels are the  $d$ -dimensional extension of the well understood 2-dimensional case of Amplitude Damping Channels. The foundations for how to treat these kind of channels were already laid out in an earlier work in [[CG21a](#)], which explored the channels in the case of  $d = 3$ .

The quantum capacity is generally not computable, as its underlying quantity (the coherent information) is not subadditive when one considers multiple uses of a channel. The only cases in which the quantum capacity is computable correspond to degradable channels (i.e. there exists a LCPT map that connects the output state of the system to the output state of the environment, which takes on the role of the induced noise) and anti-degradable channels (i.e. there exists a LCPT map that connects the output state of the environment to the output state of the system; in this case the quantum capacity is 0). When neither of these conditions is satisfied, it is usually only possible to set upper and lower bounds on the quantum capacity.

In [[CG21a](#)] it has been shown that it is possible to find the value for the quantum

capacity of 3-dimensional MAD channels even in regions where those channels are neither degradable nor anti-degradable. This was accomplished by employing pipeline inequalities, which led to the derivation of some monotonicity properties for the capacity that allowed to extend the values of the capacity found at the border of the degradability regions to the outside of these regions. Expanding upon this work, some general results for  $d$ -dimensional MAD channels were found (i.e. composition, monotonicity properties, inverse maps, degradability conditions), which enabled a generalization of the technique used to find the quantum capacity in non-degradability zones in [CG21a]. This paved the way for the numerical evaluation of the quantum capacity for various configurations of 4-dimensional MAD's, again, even where those channels are not degradable.

The 2-way quantum capacity of 3-dimensional MAD channels was also studied, as the literature was lacking in that regard, and lower bounds (which are always computable, as seen in [PLOB17]) were found.

The results of the thesis are to be added in the context of those related to the computation of the quantum capacity for qudit channels (which suggest that these channels could be more convenient with respect to their qubit counterparts) and to those related to the limits of repeater-less quantum communication. The techniques illustrated in the thesis can be ideally expanded to bigger dimension, the limit being the computational power of the machine used to arrive at the values of the capacities.

# Contents

<b>Abstract</b>	<b>i</b>
<b>Nomenclature</b>	<b>vii</b>
<b>1 Introduction</b>	<b>1</b>
<b>2 Theory of Quantum Information and Communication</b>	<b>5</b>
2.1 Open Systems . . . . .	5
2.2 Composite quantum states . . . . .	7
2.3 Stinespring Dilation . . . . .	7
2.4 Intuitive description of quantum channels . . . . .	8
2.5 Channel representations . . . . .	9
2.5.a Stinespring representation . . . . .	10
2.5.b Kraus Representation . . . . .	10
2.5.c Choi-Jamiołkowski representation . . . . .	11
2.6 Complementary channels . . . . .	12
2.7 Degradability and antidegradability . . . . .	13
2.8 Covariant channels . . . . .	14
2.9 Shannon entropy . . . . .	14
2.10 Von Neumann entropy . . . . .	16
2.11 Quantum entropic quantities . . . . .	17
2.12 Quantum capacity . . . . .	19
2.13 2-way capacity . . . . .	19
2.13.a Lower bound . . . . .	20
2.13.b Upper Bound . . . . .	21
2.14 Pipeline inequalities . . . . .	23
2.15 Classical private capacity . . . . .	23
<b>3 Finite dimensional lossy channels</b>	<b>25</b>
3.1 Amplitude Damping Channels . . . . .	25
3.1.a Composition of ADC's . . . . .	26
3.1.b Complementary channel of an ADC . . . . .	26
3.1.c Degradability and antidegradability . . . . .	26
3.1.d Quantum Capacity of ADC's . . . . .	27
3.2 PCDS channels . . . . .	28
3.2.a Direct Sum channels . . . . .	29
3.3 MAD3 . . . . .	29
3.3.a Settings for $d$ -dimensional MAD channels . . . . .	29

3.3.b	Settings for 3-dimensional MAD channels . . . . .	30
3.3.c	Composition rules . . . . .	31
3.3.d	Covariance . . . . .	32
3.3.e	Maximum of coherent information for degradable MAD channels	32
3.3.f	Single decays . . . . .	33
3.3.g	Monotonicity . . . . .	33
3.3.h	Quantum capacity and private classical capacity . . . . .	35
3.3.i	Degradability regions . . . . .	35
3.3.j	Quantum capacity of 3-dimensional MAD channels . . . . .	39
<b>4</b>	<b>Properties of MAD channels</b>	<b>41</b>
4.1	Settings for $d$ -dimensional MAD channels . . . . .	41
4.2	Composition of MAD channels . . . . .	42
4.2.a	Useful decompositions of MAD channels . . . . .	44
4.3	Equivalence of single decay MAD channels . . . . .	47
4.4	Composition of degradable channels . . . . .	47
4.5	MAD inverse . . . . .	49
4.5.a	Inverse maps of ADC's . . . . .	49
4.5.b	Inverse of single decay MAD channels . . . . .	50
4.5.c	Inverse map as composition of inverse maps of single decays . .	51
4.6	Degradability of MAD channels . . . . .	51
4.7	Degradability of 4-dimensional MAD channels . . . . .	52
4.7.a	Class 1A . . . . .	52
4.7.b	Class 2A . . . . .	53
4.7.c	Class 2B . . . . .	54
4.7.d	Class 2C . . . . .	54
4.7.e	Class 2D . . . . .	55
4.7.f	Class 3A . . . . .	55
4.7.g	Class 3B . . . . .	56
4.7.h	Class 3C . . . . .	57
4.7.i	Class 3D . . . . .	58
4.7.j	Class 3E . . . . .	58
4.7.k	Class 3F . . . . .	59
4.7.l	Class 3G . . . . .	60
4.7.m	Class 3H . . . . .	60
4.7.n	Class 3I . . . . .	61
4.8	Degradability in higher dimensions . . . . .	62
4.9	Monotonicity properties . . . . .	62
4.10	Complete damping of level $ 3\rangle$ . . . . .	65
<b>5</b>	<b>Capacity computations for MAD channels in <math>d = 4</math></b>	<b>67</b>
5.1	Single decay 4-dimensional MAD channel . . . . .	67
5.1.a	Class 1A . . . . .	67
5.2	2-decay 4-dimensional MAD channels . . . . .	68

5.2.a	Class 2A . . . . .	68
5.2.b	Class 2B . . . . .	71
5.2.c	Class 2C . . . . .	73
5.2.d	Class 2D . . . . .	74
5.3	3-decay 4-dimensional MAD channels . . . . .	76
5.3.a	Class 3A . . . . .	76
5.3.b	Class 3B . . . . .	77
5.3.c	Class 3C . . . . .	84
5.3.d	Class 3D . . . . .	85
5.3.e	Class 3E . . . . .	86
5.3.f	Class 3F . . . . .	93
5.3.g	Class 3G . . . . .	98
5.3.h	Class 3H . . . . .	99
5.3.i	Class 3I . . . . .	100
5.4	4-decay 4-dimensional MAD channels . . . . .	101
5.4.a	Class 4A . . . . .	101
<b>6</b>	<b>2-way capacity for 3-dimensional MAD channels</b>	<b>105</b>
6.1	Class 1A3 . . . . .	105
6.2	Class 2A3 . . . . .	105
6.3	Class 2B3 . . . . .	106
6.4	Class 2C3 . . . . .	107
<b>7</b>	<b>Conclusion</b>	<b>109</b>
7.1	Summary . . . . .	109
7.2	Future research . . . . .	110
<b>Appendix</b>		<b>117</b>
	Computation methods . . . . .	117



# Nomenclature

## Abbreviations

Abbreviation	Definition
ADC	Amplitude Damping Channel
EPR	Einstein, Podolsky, Rosen
LCPT	Linear, Completely Positive, Trace-preserving
MAD	Multi-level Amplitude Damping
QCT	Quantum Communication Theory
QIT	Quantum Information Theory
ReMAD	Resonant MAD



# Introduction

In an ever more interconnected world, the secure sharing of information is paramount to a functioning global society. The impact that the advent of the internet had on the human civilization can not be overstated, as it changed entire dynamics of human behavior and it rendered physical distances between people wanting to communicate or share resources (e.g. money) with each other virtually meaningless. The work of Shannon [Sha48] laid the mathematical foundations to this process of information sharing; it provided the scientific community with the tools necessary to understand how well a message, which could be represented by a string of characters, can be transmitted through a physical medium from one party to another.

However, the findings of Shannon present a limitation in the fact that they only encompass classical messages (which can be encoded in *bits*) being transmitted through a classical medium (e.g. a copper wire).

In the EPR paper [EPR35], the authors were baffled by a strange property of quantum mechanics, which one of them, Einstein, famously called "spooky action at a distance", to the point where they came to doubt the entire foundations of quantum mechanics itself and propose a different interpretation of reality. This property is now known as *entanglement*, and it can be considered the defining aspect of quantum mechanics, what sets it apart from classical mechanics. Consider two electrons in the same energy state of an atom; by the laws of quantum mechanics, these electrons must be in opposite spin states. Then, assume that these electrons are separated and that one party performs a measurement on the spin state of one of the electrons; automatically, the other electron is fixed in the opposite spin state, as if the information was transmitted instantly in space, violating special relativity. Of course, this is not exactly what happens, and this "paradox" was solved by the introduction of Bell's inequalities [Bel64] in what may be considered one of the first works of *Quantum Information Theory*.

Quantum Information Theory (QIT) is the confluence of quantum mechanics and information science, and it allows for the harnessing of the property of entanglement for information-sharing purposes. In the context of QIT, the messages to be shared are *quantum states* (e.g *qubits*) and the media through which these states are shared

are called *quantum channels* (e.g. a fiber optic cable). A branch of QIT, Quantum Communication Theory (QCT), concerns itself with the sharing of quantum information between two parties over somewhat long distances. Usually, in order to better understand the problems treated by QCT, one resorts to the "Alice and Bob" framework: Alice sends a message to Bob, how well can Bob read this message? The messages, as already stated, in this case, are quantum states, which are subject to external perturbations, or *noise*, along the communication line. Bob receives a garbled up message, which he must try to decode. An understanding and characterization of the QCT framework could pave the way to the development of technologies that employ the advantages presented by quantum mechanics in the context of long-distance communication, potentially giving rise to what some have begun to call *quantum internet*. In this scenario, the attention of this Thesis work is devoted to a particular class of quantum channels, called *Multi-level Amplitude Damping channels*, or MAD channels.

MAD channels are lossy, finite-dimensional channels that describe an energy decay of a *qudit*, i.e. the  $d$ -dimensional equivalent of a qubit. The relevance of this kind of channels lies in their wide range of applicability: in fact, energy decays are commonplace over long distance communications, as can be exemplified by a fiber optic cable which is not completely isolated and can therefore lose an electron to the external environment. Furthermore, the focus on higher-dimensional channels, i.e. channels built upon qudit transmission, which replace the more traditional qubits, is justified by the fact that recent results highlight how these kinds of architectures may present advantages both in terms of computation [WHSK20] and communication [CDLBO19].

Existing literature treated MAD channels for  $d = 2$ , in which case the channels send are called Amplitude Damping Channels (ADC) [GF05] and are very well understood, and for  $d = 3$  [CG21a]. The study of 3-dimensional MAD channels [CG21a] was carried out through an analysis of some capacity functionals, which represent the rate at which classical or quantum information can be shared when the parties involved can access possible additional resources (e.g. telephone lines, entanglement..); most importantly, the authors were able to derive the *quantum capacity* of those channels (i.e. the rate at which quantum states can be reliably transmitted through the channels), even under conditions that normally render the computation of that capacity impossible. Using the techniques first developed in the paper [CG21a], the main objective of this Thesis work is to derive the quantum capacity for a wide range of configurations of 4-dimensional MAD channels, even when a direct computation of this quantity is normally not attainable. To this end, this work has been structured as follows:

1. provide a picture of the theoretical landscape of QIT and QCT, see Chapter 2;
2. report previous literature on Quantum Communication through lossy, finite-dimensional channels, see Chapter 3;
3. derive general properties of MAD channels, with special emphasis on the case  $d = 4$ , see Chapter 4;

4. compute, where possible, the quantum capacities of 4-dimensional MAD channels, see 5.

Furthermore, it was shown in Section 2.15 that the values obtained for the quantum capacity are the same as those of another capacity functional, the *classical private capacity*, which represents the rate of reliably sharing classical information through a quantum channel in a secure way (meaning that possible eavesdroppers are not able to access that information).

Finally, in Chapter 6, in the case of 3-dimensional MAD channels, lower bounds were provided for yet another capacity functional, known as the *2-way capacity*, which represent the same rate of information-sharing as the quantum capacity under the additional assumption that "Alice and Bob" can perform local operations in their respective laboratories and communicate with each other through a classical communication line (e.g. a telephone).



## 2

# Theory of Quantum Information and Communication

In this chapter, the reader will be presented with all the tools necessary to understand this thesis work. The theories that encompass these tools are called Quantum Information Theory (QIT) are Quantum Communication Theory (QCT); see e.g. [NC10] for an introduction on these subjects and [Hol13] for a deeper dive into their mathematical foundations and for more recent developments. The strength of these theories lies in the fact that they provide a framework that makes it possible to study the behavior of *open systems*, which will be defined in the following section. The reason behind the necessity of a coherent structure describing open system is a practical one: in any real world scenario, physicists will find themselves having to deal with *noise*, which is something that only an open system can take into account. The work of Shannon [Sha48] taught the scientific community how information is transmitted through a classical, noisy communication line. Quantum Information Theory allows for the study of *quantum noise*, which in turns paves the way for the development of technologies that could allow the long distance sharing of quantum states, which would be the stepping stone of *quantum internet*.

## 2.1 Open Systems

Usually, in quantum mechanics, the time evolution of the system in a state can be summarized by defining a unitary operator, dependent on the Hamiltonian of the system. This is done through the Schrödinger equation:

$$i\hbar \frac{\partial}{\partial t} |\psi(t)\rangle = H |\psi(t)\rangle, \quad (2.1.1)$$

where  $|\psi(t)\rangle$  is the state of the system at time  $t$  and  $H$  is the Hamiltonian operator. Solving (2.1.1) yields:

$$|\psi(t')\rangle = \exp [iH(t' - t)/\hbar] |\psi(t)\rangle. \quad (2.1.2)$$

This picture only works for time-independent Hamiltonians<sup>1</sup> and for *closed systems*, i.e. systems whose interactions are confined within said systems. This is not generally the case in a real-world setting, as physicists often have to deal with noise, which can be represented as an interaction of the *laboratory system* (i.e. the system upon which one is able to make measurements) with an external system, usually called *environment*. Before defining a framework capable of describing this scenario, a precise definition of *quantum state* is needed. The most generic quantum state of a system  $\mathcal{H}$  takes the form of a *density matrix operator*  $\rho$ , which satisfies the following properties:

- $\rho$  is a hermitian operator,  $\rho^\dagger = \rho$ ;
- $\text{tr } \rho = 1$ ;
- $\text{tr } \rho^2 \leq 1$ ; if  $\text{tr } \rho^2 = 1$  then the state is called a *pure state*, i.e.  $\exists |\psi\rangle \in \mathcal{H} : \rho = |\psi\rangle\langle\psi|$ . A state that is not pure is called *mixed state*;
- $\rho$  is positive-semidefinite,  $\rho \geq 0$ .

The set of all the elements that satisfy the properties above is denoted as  $\sigma(\mathcal{H})$ . In order to characterize the interaction of a system  $\mathcal{H}_S$  with an environment  $\mathcal{H}_E$ , one needs to consider *joint states*  $\rho_{SE} \in \sigma(\mathcal{H}_S \otimes \mathcal{H}_E)$ , which represent the total states of the system laboratory-environment. In general, given a joint state  $\rho_{AB} \in \sigma(\mathcal{H}_A \otimes \mathcal{H}_B)$ , one could obtain the *reduced density matrices*, representing the states of the systems  $\mathcal{H}_A$  and  $\mathcal{H}_B$  through the use of the *partial trace* operation, defined as:

$$\begin{aligned}\rho_B &= \text{tr}_A \rho_{AB} \equiv \sum_i {}_A\langle\phi_i|\rho_{AB}|\phi_i\rangle_A, \\ \rho_A &= \text{tr}_B \rho_{AB} \equiv \sum_i {}_B\langle\psi_i|\rho_{AB}|\psi_i\rangle_B,\end{aligned}\tag{2.1.3}$$

where  $\{|\phi_i\rangle_A\}_i$  and  $\{|\psi_i\rangle_B\}_i$  are, respectively, bases of  $\mathcal{H}_A$  and  $\mathcal{H}_B$ . Then, let  $\rho_S \in \sigma(\mathcal{H}_S)$  and let the state of the environment be a pure state<sup>2</sup> which will be denoted as  $\tau_E = |0\rangle_E\langle 0| \in \sigma(\mathcal{H}_E)$ , then the state of the composite system  $\mathcal{H}_S \otimes \mathcal{H}_E$  is the tensor product<sup>3</sup>:

$$\rho_{SE} \equiv \rho_S \otimes |0\rangle_E\langle 0| \in \sigma(\mathcal{H}_S \otimes \mathcal{H}_E).\tag{2.1.4}$$

In Section 2.3, the mechanism behind the evolution of  $\rho_S$ , in the setting illustrated above, will be explained.

---

<sup>1</sup>A solution for time-dependent Hamiltonians (which might not commute between themselves at different times) exists and is called *Dyson series*, see [Dys49]

<sup>2</sup>This is because, since the environment represents anything that is external to the system  $A$ , even if  $\tau_E$  was, in fact, a mixed state, it could always be *purified*, see Section 2.2

<sup>3</sup>In order to lighten the notation, when possible, the symbol  $\otimes$  of tensor product will usually be omitted, as indices referring to specific quantum systems make it redundant.

## 2.2 Composite quantum states

Before moving on, it might be useful to label composite quantum states in a more precise way. Given a joint system  $\mathcal{H}_S \otimes \mathcal{H}_R$ , its quantum states  $\rho_{SR}$  can be classified in one of the three following categories:

- *Factorized states* present the form:

$$\rho_{SR} = \rho_S \tau_R, \quad (2.2.1)$$

- *Separable states* present the form:

$$\rho_{SR} = \sum_i p_i \rho_S^{(i)} \tau_R^{(i)}, \quad (2.2.2)$$

where  $\{p_i\}_i$  forms a probability distribution,  $\sum_i p_i = 1$ . Separable states are convex combination of factorized states; furthermore, the convex combination of separable states is still a separable state. Note that (2.2.2) reduces to (2.2.1) if  $p_i = \delta_{i,i_0}$

- *Non separable (entangled) states* are all the joint states that do not satisfy (2.2.2)

### Purification

Let  $\rho_S$  be a state in  $\mathcal{H}_S$ , suppose that  $\rho_S$  is a mixed state and let  $\mathcal{H}_R$  be another system, called, in this case, *auxiliary system*. Through the *purification* process, it is **always** possible to build a composite state  $\rho_{SR} \in \sigma(\mathcal{H}_S \otimes \mathcal{H}_R)$ ,  $\text{tr}_R \rho_{SR} = \rho_S$  such that  $\rho_{SR}$  is a pure state. In fact, in its diagonal basis  $\{|\psi_i\rangle_S\}_i$ ,  $\rho_S$  can be written as:

$$\rho_S = \sum_i p_i |\psi_i\rangle_S \langle \psi_i|, \quad (2.2.3)$$

where  $\{p_i\}_i$  forms a probability distribution. Then, fixing  $\dim \mathcal{H}_R = \dim \mathcal{H}_S$  and choosing a basis  $\{|i\rangle_R\}_i$  for  $\mathcal{H}_R$ , one could build the pure state:

$$\begin{aligned} |\psi_i\rangle_{SR} &\equiv \sum_i \sqrt{p_i} |\psi_i\rangle_S |i\rangle_R, \\ \rho_{SR} &= |\psi_i\rangle_{SR} \langle \psi_i|, \end{aligned} \quad (2.2.4)$$

which clearly satisfies  $\text{tr}_R \rho_{SR} = \rho_S$ .

## 2.3 Stinespring Dilation

Since the composite system  $\mathcal{H}_S \otimes \mathcal{H}_E$  is a closed system, its state in (2.1.4) will evolve following a unitary operator  $U_{SE} : \mathcal{H}_S \otimes \mathcal{H}_E \mapsto \mathcal{H}_S \otimes \mathcal{H}_E$ , which acts on density matrices as:

$$\rho_{SE} \mapsto U_{SE} (\rho_S |0\rangle_E \langle 0|) U_{SE}^\dagger. \quad (2.3.1)$$

Then, combining (2.3.1) with (2.1.3), one could find the evolved state of the system  $S$  by defining a *superoperator* (i.e. an object that maps linear operators into linear operators)  $\Phi$  such that:

$$\rho_S \mapsto \Phi(\rho_S) = \text{tr}_E \left[ U_{SE} (\rho_S |0\rangle_E \langle 0|) U_{SE}^\dagger \right]. \quad (2.3.2)$$

This equation defines a very specific family of maps: in fact any map  $\Phi$  which can be cast in the form of (2.3.4) needs to satisfy the following properties:

- $\Phi$  is Linear,
- $\Phi$  is Completely Positive, meaning that its Choi matrix (see (2.5.12)) is positive [Cho75],
- $\Phi$  is Trace preserving, meaning that  $\text{tr } \theta = \text{tr } \Phi(\theta)$  for all  $\theta$ .

The maps satisfying these properties are named through the acronym LCPT maps, or, in the context of QIT, simply *quantum channels*.

One could also consider quantum channels whose input and output systems are different from each other. In this case, an input state  $\rho_A \in \sigma(\mathcal{H}_A)$  is sent into an output state  $\Phi(\rho_A) \in \sigma(\mathcal{H}_B)$ . The channel

$$\Phi : \sigma(\mathcal{H}_A) \mapsto \sigma(\mathcal{H}_B) \quad (2.3.3)$$

can be defined by introducing an isometry  $U_{BE \leftarrow AE}$ , so that:

$$\rho_A \mapsto \Phi(\rho_A) = \text{tr}_E \left[ U_{BE \leftarrow AE} (\rho_A |0\rangle_E \langle 0|) U_{BE \leftarrow AE}^\dagger \right]. \quad (2.3.4)$$

In general, the map  $\rho_A \mapsto U_{BE \leftarrow AE} (\rho_A |0\rangle_E \langle 0|) U_{BE \leftarrow AE}^\dagger$  is called *Stinespring dilation* [Sti55], while the map in (2.3.4) is the *Stinespring representation* of the quantum channel  $\Phi$ ; in fact, as will be explained in Section 2.5, a given LCPT map admits different but equivalent representations.

## 2.4 Intuitive description of quantum channels

Before moving on, it might be a good idea to provide an intuitive understanding of quantum channels. Usually, one refers to the experimental setting known as the "Alice and Bob" framework: Alice wants to send a message to Bob, what happens to this message before reaching Bob? Alice needs to send the message, which in the context of this Thesis is a quantum state, through a medium in order to communicate with Bob; the signals (which might be, for example electrons, with the information encoded in their spin state, or photons, in which case the information could be encoded in their number) passing through this medium are, realistically, subject to noise, which may be caused by a number of external factors, e.g. suppose Alice and Bob are using a

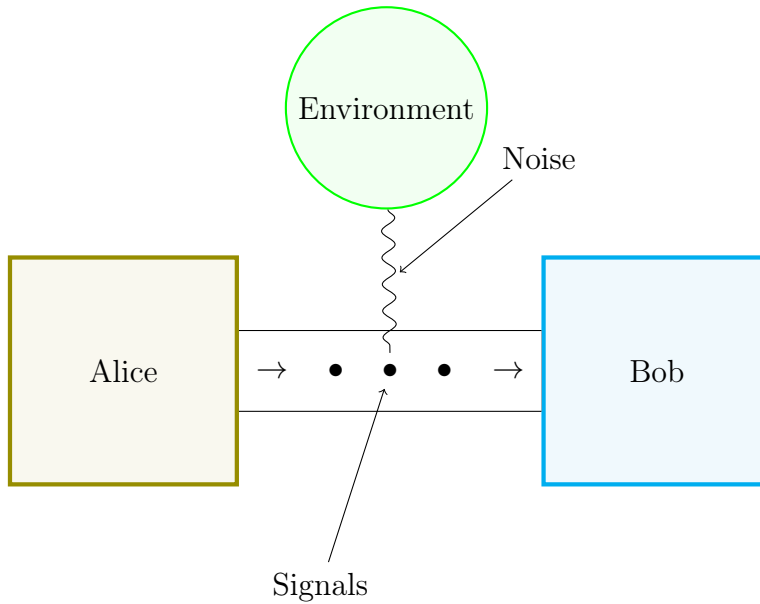


**Figure 2.4.1:** Visual depiction of the "Alice and Bob" framework: Alice sends a message to Bob, this message is subject to noise caused by interactions with an external environment. Bob receives a different signal compared to the one originally sent by Alice. The state received by Bob is the output of the quantum channel associated to this process, while the state sent by Alice is the input of that quantum channel.

fiber optic cable that is not completely isolated, resulting in a loss of a photon to the environment. Therefore, Bob receives a signal different from the one sent by Alice. This process is depicted in Figure 2.4.1.

The transformations that the signals undergo while in the medium of communication can be represented mathematically by quantum channels (2.3.4), and the signal received by Bob is the output state of a quantum channel which takes as inputs the signal sent by Alice.

## 2.5 Channel representations

The Stinespring representation is not the only possible representation of quantum channels. In fact, it can be shown that there exist different representations equivalent to each other; the most important ones are reported below

### 2.5.a Stinespring representation

As seen in Section 2.3, the Stinespring dilation  $\mathfrak{U}_{S \mapsto SE}$ :

$$\begin{aligned} \mathfrak{U}_{S \mapsto SE}(\bullet) &\equiv U_{S \mapsto SE} \bullet U_{S \mapsto SE}^\dagger, \\ U_{S \mapsto SE} &\equiv U_{SE} |0\rangle_E, \\ \rho_S &\xrightarrow{\mathfrak{U}_{S \mapsto SE}} U_{SE} (\rho_S |0\rangle_E \langle 0|) U_{SE}^\dagger, \end{aligned} \quad (2.5.1)$$

is an isometry that maps an input state in  $\sigma(\mathcal{H}_S)$  onto a state in  $\sigma(\mathcal{H}_S \otimes \mathcal{H}_E)$ ; tracing this *dilated* state over the environment  $E$  returns the output state  $\Phi(\rho_S)$  (2.3.4). Note that the input and output system of the quantum channel do not need to coincide. This can be achieved by replacing the unitary  $U_{SE}$  with an isometry  $U_{BE \leftarrow AE}$ . This leads to a more general form of (2.5.1).

$$\begin{aligned} \mathfrak{U}_{A \mapsto BE}(\bullet) &\equiv U_{BE \leftarrow A} \bullet U_{BE \leftarrow A}^\dagger, \\ U_{BE \leftarrow A} &\equiv U_{BE \leftarrow AE} |0\rangle_E, \\ \rho_A &\xrightarrow{\mathfrak{U}_{A \mapsto BE}} U_{BE \leftarrow AE} (\rho_A |0\rangle_E \langle 0|) U_{BE \leftarrow AE}^\dagger. \end{aligned} \quad (2.5.2)$$

### 2.5.b Kraus Representation

The Kraus representation is characterized by a set of operators  $\mathcal{K} = \{K_i\}_i$  on  $\mathcal{H}$  such that:

$$\sum_i K_i^\dagger K_i = \mathbb{1}, \quad (2.5.3)$$

where  $\mathbb{1}$  is the identity operator on  $\mathcal{H}$ . The set  $\mathcal{K}$  describes a unique quantum channel  $\Phi$ , defined by:

$$\Phi(\rho) = \sum_i K_i \rho K_i^\dagger. \quad (2.5.4)$$

The set  $\mathcal{K}$  is called *Kraus set*, while the  $K_i$ 's are called *Kraus operators*. Note that unitary transformations are a particular class of quantum channels, as given the unitary operator  $U$ , one could build the trivial Kraus set  $\mathcal{K} = \{U\}$  which satisfies (2.5.3) and the corresponding unitary transformation is given in the Kraus representation,  $\rho \mapsto U\rho U^\dagger$ .

It is possible, given a Stinespring representation of a channel, to derive (one of) its Kraus representations, in fact from (2.3.4):

$$\Phi(\rho_S) = \text{tr}_E \left[ U_{SE} (\rho_S |0\rangle_E \langle 0|) U_{SE}^\dagger \right] = \sum_l {}_E \langle l | U_{SE} |0\rangle_E \rho_S |0\rangle_E \langle 0| U_{SE}^\dagger |l\rangle_E. \quad (2.5.5)$$

Then, one could define:

$$K_i \equiv {}_E \langle i | U_{SE} |0\rangle_E, \quad (2.5.6)$$

which is an operator acting on  $\mathcal{H}_S$  and that clearly satisfies (2.5.3), so that (2.5.4) is obtained. Conversely, one could derive the action of the unitary operator  $U_{SE}$  in (2.3.4) on the states  $|\psi\rangle_S |0\rangle_E$  of  $\mathcal{H}_S \otimes \mathcal{H}_E$  through the Kraus operators of the channel:

$$|\psi_i\rangle_S |0\rangle_E \xrightarrow{U_{SE}} \sum_i K_i |\psi_i\rangle_S |0\rangle_E. \quad (2.5.7)$$

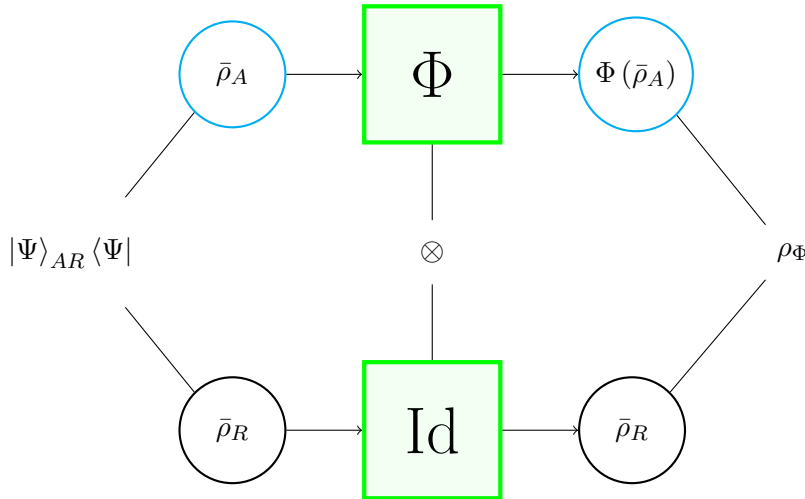


**Figure 2.5.1:** The Choi state  $\rho_\Phi$  for a channel  $\Phi$  can be built using the scheme described in this figure

### Equivalence of Kraus representations

While a certain  $\mathcal{K}$  identifies a specific  $\Phi$ , given a channel  $\Phi$  one may find different Kraus sets associated with it. It is then reasonable to ask under which condition two Kraus sets represent the same quantum channel. The answer is that, given the Kraus sets  $\mathcal{K} = \{K_i\}_i$  and  $\mathcal{K}' = \{K'_i\}_i$ , they represent the same channel if and only if:

$$K'_i = \sum_j \mathcal{U}_{ij} K_j, \quad (2.5.8)$$

where the  $\mathcal{U}_{ij}$  are the matrix elements of an isometry and they satisfy the conditions:

$$\sum_k \mathcal{U}_{ik} \mathcal{U}_{jk}^* = \sum_k \mathcal{U}_{ki} \mathcal{U}_{kj}^* = \delta_{ij}. \quad (2.5.9)$$

### 2.5.c Choi-Jamiołkowski representation

The Choi-Jamiołkowski isomorphism [Cho75], [Jam72] introduces a one-to-one mapping between a channel and a specific density matrix. Consider the channel  $\Phi$  acting on the system  $\mathcal{H}_A$  of dimension  $d$  and a reference system  $\mathcal{H}_R$ ; given the completely chaotic state  $\bar{\rho}_A$ :

$$\bar{\rho}_A \equiv \frac{1}{d} \sum_i |i\rangle\langle i|, \quad (2.5.10)$$

it can be purified using the reference system  $R$ , leading to the maximally entangled state  $|\Psi\rangle_{AR}$ :

$$|\Psi\rangle_{AR} = \frac{1}{\sqrt{d}} \sum_i |i\rangle_A |i\rangle_R. \quad (2.5.11)$$

If the state in system  $A$  is sent through the channel  $\Phi$  the corresponding state in  $AR$  is sent through  $\Phi \otimes \text{Id}_R$ , where  $\text{Id}_R$  is the identity superoperator on  $\sigma(\mathcal{H}_R)$ ; if the maximally entangled state in (2.5.11) is sent through  $\Phi \otimes \text{Id}_R$ , the output of this channel is called *Choi state* of the channel:

$$\begin{aligned} \rho_\Phi & \text{ Choi state,} \\ \rho_\Phi & \equiv [\Phi \otimes \text{Id}_R] (|\Psi\rangle_{AR} \langle \Psi|). \end{aligned} \quad (2.5.12)$$

Figure 2.5.1 provides a visual depiction of Choi states. It is possible to prove (see [Cho75], [Jam72]) that:

$$\Phi (|\psi\rangle_A \langle \psi|) = d_R \langle \psi^* | \rho_\Phi | \psi^* \rangle_R = d \text{tr}_R \left( |\psi\rangle_R \langle \psi| (\rho_\Phi)^{T_A} \right), \quad (2.5.13)$$

where

$$|\psi\rangle = \sum_{i=0}^{d-1} \alpha_i |i\rangle \Rightarrow |\psi^*\rangle = \sum_{i=0}^{d-1} \alpha_i^* |i\rangle. \quad (2.5.14)$$

and the operation of *partial transpose* has been introduced:

$$\begin{aligned} \theta_{AR} &= \sum_{ijmn} \theta_{ijmn} |i\rangle_A \langle j| |m\rangle_R \langle n|, \\ \Rightarrow (\theta_{AR})^{T_A} &= \sum_{ijmn} \theta_{ijmn} |j\rangle_A \langle i| |m\rangle_R \langle n|. \end{aligned} \quad (2.5.15)$$

Due to the linearity of  $\Phi$ , one could easily extend (2.5.13) to the mixed state case:

$$\Phi(\theta_A) = d \text{tr}_R \left( \theta_R (\rho_\Phi)^{T_A} \right). \quad (2.5.16)$$

### Choi theorem

The complete positiveness of a map can be verified by checking the positivity of the associated Choi matrix (2.5.12). This is a consequence of Choi's theorem illustrated in [Cho75], [Jam72]:

$$\Psi \text{ is completely positive} \Leftrightarrow \rho_\Psi \text{ is positive.} \quad (2.5.17)$$

## 2.6 Complementary channels

The Stinespring dilation (2.5.2) allows to define another type of quantum channels; in fact, one may wonder what happens when one traces the dilation of a state over the output system instead of the environment. This leads to the definition of the *complementary channels*, which act as the "output state of the environment".

$$\tilde{\Phi}(\rho_A) \equiv \text{tr}_B \left( U_{BE \leftarrow AE} (\rho_A |0\rangle_E \langle 0|) U_{BE \leftarrow AE}^\dagger \right) \in \sigma(\mathcal{H}_E). \quad (2.6.1)$$

The map  $\tilde{\Phi} : \sigma(\mathcal{H}_A) \mapsto (\mathcal{H}_E)$  in (2.6.1) is a LCPT map, therefore complementary "channels" are actually quantum channels. In Figure 2.6.1 the reader can find a schematic depiction of quantum channels and complementary channels.

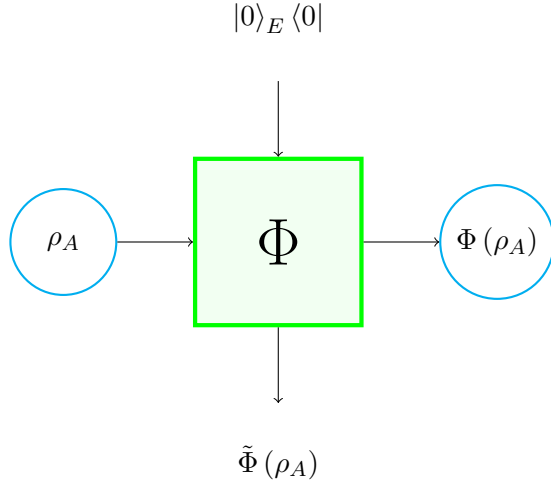


**Figure 2.6.1:** The quantum channel  $\Phi$  depicted as a "black box" that takes as inputs  $\rho_S$  from the system  $S$  and  $|0\rangle_E \langle 0|$  while it outputs  $\Phi(\rho_S)$  in  $S$  and  $\tilde{\Phi}(\rho_S)$  in  $E$ .

### Complementary channel from Kraus representation

It is possible to find the complementary channel from a Kraus set by employing (2.5.6) into (2.6.1), yielding:

$$\tilde{\Phi}(\rho) = \sum_{ij} \text{tr} \left( K_i \rho K_j^\dagger \right) |i\rangle_E \langle j|. \quad (2.6.2)$$

Different Kraus representations correspond to different complementary channel, which are unitarily equivalent; in fact, given the Kraus sets  $\mathcal{K}, \mathcal{K}'$ :

$$\begin{aligned} \tilde{\Phi}(\rho) &= \sum_{ij} \text{tr} \left( K_i \rho K_j^\dagger \right) |i\rangle_E \langle j|, \\ \tilde{\Phi}'(\rho) &= \sum_{ij} \text{tr} \left( K'_i \rho K'^\dagger_j \right) |e_i\rangle_E \langle e_j|. \end{aligned} \quad (2.6.3)$$

Suppose  $\mathcal{K}, \mathcal{K}'$ , satisfy (2.5.8), then defining the isometry  $U \equiv \sum_{i,j} \mathcal{U}_{ij} |e_i\rangle_E \langle j|$ , one could verify that:

$$\tilde{\Phi}'(\rho) = U \tilde{\Phi}(\rho) U^\dagger. \quad (2.6.4)$$

## 2.7 Degradability and antidegradability

A quantum channel  $\Phi$  is said to be *degradable* if and only if, given its complementary channel  $\tilde{\Phi}$ , there exists a LCPT map  $\Lambda$  such that the composition  $\Lambda \circ \Phi$  is equal to the complementary channel  $\tilde{\Phi}$ :

$$\Phi \text{ is degradable} \Leftrightarrow \exists \Lambda \text{ LCPT s.t. } \tilde{\Phi} = \Lambda \circ \Phi. \quad (2.7.1)$$

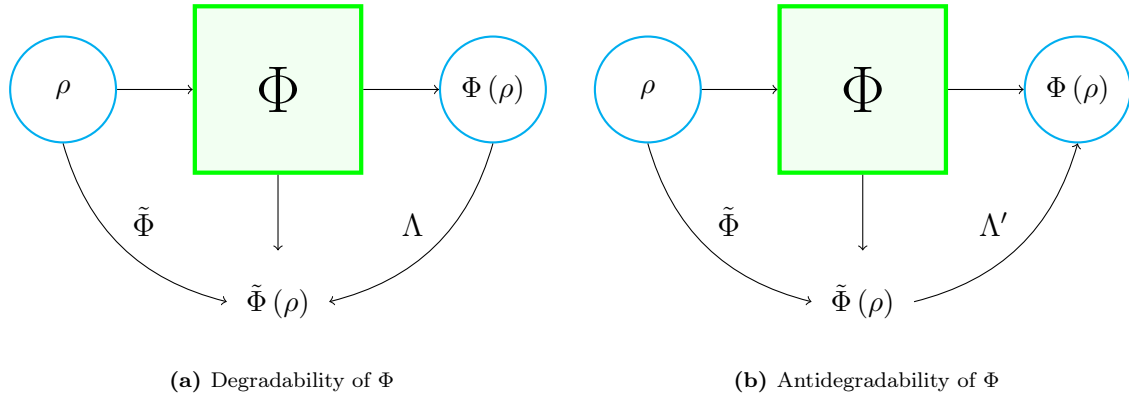


**Figure 2.7.1:** On the left, a visual representation for the degradability condition given in (2.7.1); on the right, a visual representation for the antidegradability condition given in (2.7.2);

Conversely  $\Phi$  is said to be *antidegradable* if and only if there exists a LCPT map  $\Lambda'$  such that the composition  $\Lambda' \circ \tilde{\Phi}$  is equal to the channel  $\Phi$ :

$$\Phi \text{ is antidegradable} \Leftrightarrow \exists \Lambda' \text{ LCPT s.t. } \Phi = \Lambda' \circ \tilde{\Phi}. \quad (2.7.2)$$

Figure 2.7.1 provides a visual representation of the degradability and antidegradability conditions outlined in this section.

## 2.8 Covariant channels

Consider a quantum channel  $\Phi : \sigma(\mathcal{H}_A) \mapsto \sigma(\mathcal{H}_B)$  and a group  $\mathfrak{G}$  which has unitary representations on  $\mathcal{H}_A$ ,  $\mathcal{H}_B$  and the environment  $\mathcal{H}_E$ , so that  $\forall g \in \mathfrak{G}, \exists U_g^X$  unitary operator on  $\mathcal{H}_X$ . The channel  $\Phi$  is called *covariant* under the action of  $\mathfrak{G}$  if:

$$\Phi \left( U_g^A \rho U_g^{A\dagger} \right) = U_g^B \Phi(\rho) U_g^{B\dagger} \quad \forall g \in \mathfrak{G}, \forall \rho \in \sigma(\mathcal{H}_A). \quad (2.8.1)$$

It can be proven that, if  $\tilde{\Phi}$  is the complementary channel of  $\Phi$  and  $\Phi$  satisfies (2.8.1), then [Hol07] also its complementary channel must be covariant under the same group  $\mathfrak{G}$ :

$$\tilde{\Phi} \left( U_g^A \rho U_g^{A\dagger} \right) = U_g^E \tilde{\Phi}(\rho) U_g^{E\dagger} \quad \forall g \in \mathfrak{G}, \forall \rho \in \sigma(\mathcal{H}_A), \quad (2.8.2)$$

$$\Phi \text{ covariant under } \mathfrak{G} \Rightarrow \tilde{\Phi} \text{ covariant under } \mathfrak{G}. \quad (2.8.3)$$

## 2.9 Shannon entropy

In this section, the basic tool that allows for the study of (classical) information will be introduced. Given a probability distribution  $X = \{p_x\}_x$ , the *Shannon entropy* (or

classical entropy) is defined as:

$$H(X) \equiv - \sum_x p_x \log_2 p_x. \quad (2.9.1)$$

From the Shannon entropy, a number of information theoretic quantities can be derived, as exposed in what follows. It is important to note that, if for some  $x_0$  one finds  $p_{x_0} = 0$ , one needs to set a convention to treat the indefinite form of  $0 \log_2 0$  found in (2.9.1). Therefore, in the context of entropies, the reader needs to assume:

$$0 \log_2 0 \equiv 0. \quad (2.9.2)$$

One can think of the Shannon entropy as the "classical information" content that can be gained by measuring the system, or the amount of *bits* needed to store the information contained in the system.

### Classical relative entropy

The classical relative entropy provides a way to measure the closeness of two probability distributions  $X = \{p_x\}_x$  and  $Y = \{q_x\}_x$ , which are defined over the same indexes. The relative entropy is defined as:

$$H(p_x || q_x) \equiv -H(X) - \sum_x p_x \log_2 q_x = \sum_x p_x \log_2 \frac{p_x}{q_x}. \quad (2.9.3)$$

An important property of the classical relative entropy is its non-negativity:

$$H(p_x || q_x) \geq 0. \quad (2.9.4)$$

Using this property, it is possible to find an upper bound for the Shannon entropy. In fact, using  $q_x = 1/d \forall x$ :

$$H(p_x || 1/d) = \log_2 d - H(X) \geq 0 \Rightarrow H(X) \leq \log_2 d. \quad (2.9.5)$$

This upper bound is achievable by selecting  $p_x = 1/d \forall x$ .

### Joint classical entropy

Given a pair of random variables  $x, y$  and a probability distribution over those variables  $XY = \{p(x, y)\}_{x,y}$ , then the *joint classical entropy* is a natural extension of (2.9.1):

$$H(XY) \equiv - \sum_{x,y} p(x, y) \log_2 p(x, y). \quad (2.9.6)$$

### Classical conditional entropy

In the case of two random variables  $x, y$ , the knowledge of one of those variables, for example  $y$ , changes the information content that can be gained by measuring the system  $X$ ; this quantity is represented by the *conditional entropy*:

$$H(X|Y) \equiv H(XY) - H(Y). \quad (2.9.7)$$

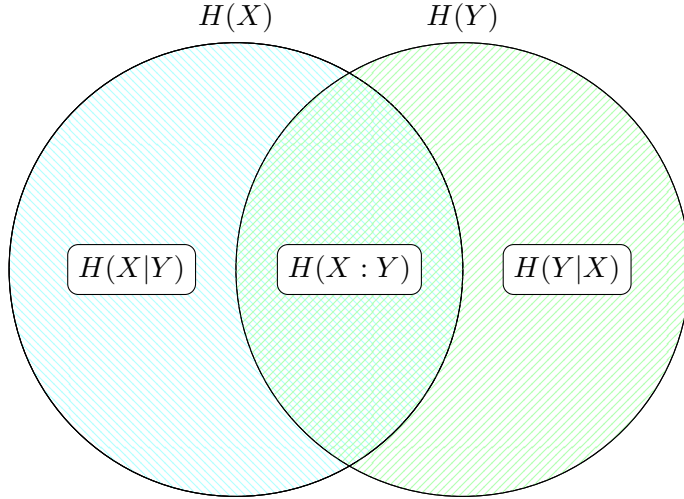


**Figure 2.9.1:** This pseudo-Venn diagram provides a powerful mnemonic tool that depicts the relationship between the classical entropic quantities.

### Classical mutual information

The *mutual information* measures the information content in  $XY$  accessible to both the observers that only have access to either  $X$  or  $Y$ :

$$\begin{aligned} H(X : Y) &\equiv H(X) + H(Y) - H(XY), \\ H(X : Y) &\equiv H(X) - H(X|Y). \end{aligned} \tag{2.9.8}$$

The relationships between the classical entropic quantities can be (improperly) visually derived using the Venn diagram drawn in Figure 2.9.1.

## 2.10 Von Neumann entropy

The quantum equivalent of the Shannon entropy in (2.9.1) is the Von Neumann entropy; it describes the amount of *qubits* needed to store the information contained in a quantum system. The Von Neumann entropy is defined by:

$$S(\rho) \equiv -\text{tr}(\rho \log_2 \rho), \tag{2.10.1}$$

where  $\rho$  is a quantum state. The  $\log_2$  in (2.10.1) is the logarithm base 2 of a matrix; formally speaking, it is the inverse operator of taking the power of that matrix base 2, while practically speaking,  $\log_2 \theta$  returns a matrix  $\theta'$  obtained by taking the element-wise  $\log_2$  of  $\theta$  in its diagonal basis and then transforming back to the original basis for  $\theta$ . Since the trace operator is invariant under change of basis, this means that, denoting with  $\{\lambda_x\}_x$  the eigenvalues of  $\rho$ , (2.10.1) can be reduced to the form of (2.9.1):

$$S(\rho) = -\sum_x \lambda_x \log_2 \lambda_x, \tag{2.10.2}$$

(2.9.2) still holds.

## 2.11 Quantum entropic quantities

In this Section, the most important quantum entropic quantities, built from the Von Neumann entropy, are listed.

### Relative entropy

The quantum relative entropy is the extension to the quantum case of the quantity in (2.9.3). Its definition is given by:

$$S(\rho||\tau) \equiv \text{tr}(\rho \log_2 \rho) - \text{tr}(\rho \log_2 \tau) = -S(\rho) - \text{tr}(\rho \log_2 \tau). \quad (2.11.1)$$

The Klein's inequality guarantees that the relative entropy is non-negative:

$$S(\rho||\tau) \geq 0, \quad (2.11.2)$$

where the inequality is saturated if and only if  $\rho = \tau$ . The relation (2.11.2) offers a way of setting an upper bound on the Von Neumann entropy; in fact, assuming  $\tau = \frac{1}{d}\mathbb{1}_d$ :

$$0 \leq S(\rho||\tau) = -S(\rho) + \log_2 d, \quad (2.11.3)$$

$$S(\rho) \leq \log_2 d. \quad (2.11.4)$$

This bound is achievable when  $\rho = \frac{1}{d}\mathbb{1}_d$ ; this state is often called the *completely chaotic state*.

### Joint entropy

The joint quantum entropy is the extension of the Von Neumann entropy to a joint quantum system.

$$S(AB)_\rho \equiv \text{tr}_{AB}(\rho_{AB} \log_2 \rho_{AB}). \quad (2.11.5)$$

The index  $\rho$  signifies the state over which the entropy is to be calculated. This notation will also occur in later definitions.

### Conditional entropy

When one part of a joint system  $AB$  is already known, the information content of the remaining system is given by the quantum conditional entropy:

$$S(A|B)_\rho \equiv S(AB)_\rho - S(B)_\rho, \quad (2.11.6)$$

where  $\rho_{A/B} = \text{tr}_{B/A} \rho_{AB}$ .

## Mutual information

The quantum mutual information represents the amount of information stored in a joint state in the system  $AB$  accessible to both parties  $A, B$ :

$$I(A : B)_\rho \equiv S(A)_\rho + S(B)_\rho - S(AB)_\rho, \quad (2.11.7)$$

where  $\rho_{A/B} = \text{tr}_{B/A} \rho_{AB}$ . If  $B$  is the output system of a channel  $\Psi_{A \rightarrow B}$  whose input is the system  $A$ , then the mutual information associated with  $\Psi_{A \rightarrow B}$  can be written as:

$$\begin{aligned} I(\rho_A, \Psi_{A \rightarrow B}) &= S(A)_\rho + S(B)_\rho - S(E)_\rho \\ &= S(\rho_A) + S(\Psi_{A \rightarrow B}(\rho_A)) - S(\tilde{\Psi}_{A \rightarrow E}(\rho_A)), \end{aligned} \quad (2.11.8)$$

refer to Figure 2.13.1 for a clearer understanding of the quantities in play. The main properties of the mutual information [Hol13] are listed below:

- $I(\rho, \Psi)$  is concave in  $\rho$ ,
- $I(\rho, \Psi)$  is concave in  $\Psi$ ,
- $I(\rho, \Psi)$  is subadditive,
- $I(\rho, \Psi)$  satisfies the following data-processing inequalities:

$$I(\rho, \Psi_2 \circ \Psi_1) \leq \min \{I(\rho, \Psi_1), I(\Psi_1(\rho), \Psi_2)\}. \quad (2.11.9)$$

## Coherent information

The coherent information is the basic building block for the quantum capacity, defined in Section 2.12; its definition is given by:

$$\begin{aligned} I_C(\Psi_{A \rightarrow B}, \rho_A) &\equiv S(B)_\rho - S(E)_\rho \\ &= S(\Psi_{A \rightarrow B}(\rho_A)) - S(\tilde{\Psi}_{A \rightarrow E}(\rho_A)). \end{aligned} \quad (2.11.10)$$

Uncomfortably, the coherent information does not satisfy many of the properties of the mutual information, such as the subadditivity property [DSS98]:

$$I_C(\rho_{12}, \Psi_1 \otimes \Psi_2) \not\leq I_C(\rho_1, \Psi_1) + I_C(\rho_2, \Psi_2), \quad (2.11.11)$$

where  $\rho_{1/2} = \text{tr}_{2/1} \rho_{12}$ , the concavity in the input states or one of the data-processing inequalities:

$$\begin{aligned} I_C(\rho, \Psi_2 \circ \Psi_1) &\leq I_C(\rho, \Psi_1), \\ I_C(\rho, \Psi_2 \circ \Psi_1) &\not\leq I_C(\Psi_1(\rho), \Psi_2). \end{aligned} \quad (2.11.12)$$

If a channel satisfies (2.7.1), then its coherent information is concave [YHD08]:

$$\Psi \text{ is degradable} \Rightarrow I_C \left( \sum_i p_i \rho_i, \Psi \right) \geq \sum_i p_i I_C(\rho_i, \Psi). \quad (2.11.13)$$

## 2.12 Quantum capacity

The *quantum capacity* of a quantum channel represents the rate for reliably transmitting quantum information, encoded in quantum states, through the channel. Intuitively, in the qubit case<sup>4</sup>, the quantum capacity  $Q$  is the (maximum) ratio between the number of states that can be transmitted through the channel and the uses of the channel needed to achieve that number:

$$Q \sim \frac{\# \text{ of faithfully transmitted qubits}}{\# \text{ of uses of the channel}}. \quad (2.12.1)$$

Basically, if a qubit-to-qubit channel has a quantum capacity = 0.5, then, in order to faithfully transmit 1 qubit, one needs 2 uses of the channel. Channels whose quantum capacity is 0 can not be used to reliably transmit quantum states.

The formal expression of the quantum capacity for a given noisy channel  $\Psi$  can be found in the paper by Devetak [Dev05]:

$$Q(\Psi) \equiv \lim_{n \rightarrow \infty} \frac{Q^{(n)}(\Psi)}{n} \equiv \lim_{n \rightarrow \infty} \frac{1}{n} \max_{\rho^{(n)} \in \sigma(\mathcal{H}^{\otimes n})} I_c(\rho^{(n)}, \Psi^{\otimes n}). \quad (2.12.2)$$

The quantity  $Q^{(n)}(\Psi)$  represents the maximization of the coherent information for  $n$  uses of the channel over all possible inputs. Due to the property in (2.11.11), the limit for  $n$  uses of the channel can not be dropped, rendering the actual computation of the quantum capacity impossible. However [DS05], if a channel satisfies (2.7.1), then its coherent information is subadditive and the limit over  $n$  can be dropped, allowing to write:

$$\Psi \text{ is degradable} \Rightarrow Q(\Psi) = Q^{(1)}(\Psi) = \max_{\rho \in \sigma(\mathcal{H})} I_c(\rho, \Psi). \quad (2.12.3)$$

## 2.13 2-way capacity

The *2-way capacity*  $Q_2$  represents the maximum rate for reliably transmitting quantum information under the assumption that the two parties involved are able to perform LOCC's (Local Operations and Classical Communication), which means that, in the "Alice and Bob" framework, both Alice and Bob can act on their respective systems, carrying out e.g. transformations or measurements in their respective "laboratories", and are able to communicate with each other via a classical communication line (e.g. a telephone), which they may use to share the outcomes of their local operations. By definition, the 2-way capacity represents the same rate of information-sharing as the

---

<sup>4</sup>Since in the definitions of the underlying quantities that form the quantum capacity the logarithms are in base 2, then the intuitive definition in (2.12.1) only works in the qubit case; however, since one could always encode the information of a quantum state in a series of qubits, this intuitive understanding of the quantum capacity remains useful also in higher-dimensional systems.

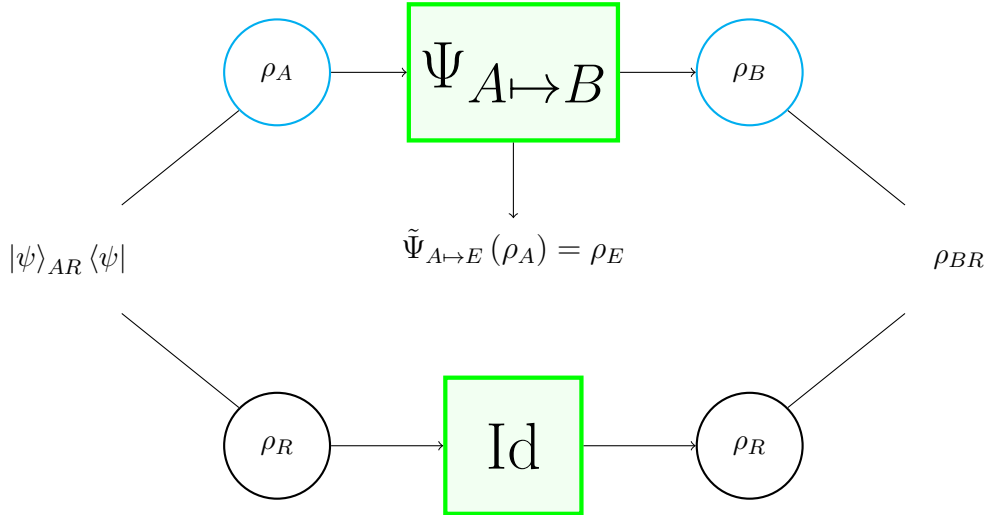


**Figure 2.13.1:** Figure 2.5.1 is a specific case of the general configuration illustrated in this scheme; Alice sends the message  $\rho_A$  to Bob, who receives the state  $\rho_B$ ; Alice also has access to a reference system in the state  $\rho_R$ , which is isospectral to  $\rho_A$  (due to the Schmidt decomposition, see e.g. [Hol13], page 37).

quantum capacity, with the additional resource of LOCC's accessible to both parties, which means that the quantum capacity of a channel  $\Psi$  is a natural lower bound on the 2-way capacity of  $\Psi$ :

$$Q(\Psi) \leq Q_2(\Psi). \quad (2.13.1)$$

At the moment of writing, there is no known formula that outputs the  $Q_2$  of a channel; however, it is always possible to find upper and lower bounds, as illustrated in [PLOB17]

### 2.13.a Lower bound

A natural lower bound of the 2-way capacity is the quantum capacity itself; another lower bound on the  $Q_2$  of a quantum channel  $\Psi_{A \mapsto B}$  can be set by:

$$Q_2(\Psi_{A \mapsto B}) \geq \max_{\rho_A} \{I_C(\Psi_{A \mapsto B}, \rho_A), I_{RC}(\Psi_{A \mapsto B}, \rho_A)\}, \quad (2.13.2)$$

where  $I_C$  is the coherent information of the channel, while  $I_{RC}$  is called the reverse coherent information of the channel:

$$\begin{aligned} I_C(\Psi_{A \mapsto B}, \rho_A) &= S(\text{tr}_R(\rho_{BR})) - S(\rho_{BR}), \\ I_{RC}(\Psi_{A \mapsto B}, \rho_A) &\equiv S(\text{tr}_B(\rho_{BR})) - S(\rho_{BR}). \end{aligned} \quad (2.13.3)$$

Note that the expression for the coherent information  $I_C$  in (2.13.3) is equivalent to the definition (2.11.10). The system  $R$  is used to purify the input state  $\rho_A$  into  $|\psi\rangle_{AR}\langle\psi|$ . Refer to Figure 2.13.1 for a visual representation of the quantities in play. Since in (2.13.2) there is a maximization over all possible inputs, a fixed choice of  $\rho_A$  gives still

rise to a (possibly non optimal) lower bound. In particular, a common choice of  $\rho_A$  is the completely chaotic state  $\bar{\rho}_A$ , so that  $\rho_{BR}$  is the Choi state [Cho75] of the channel  $\rho_\Psi$ . In this case, if the channel is finite dimensional and the output of the channel has the same dimensionality as its input (as it is the case for ReMAD's), then the reverse coherent information is always bigger than the coherent information, so that:

$$Q_2(\Psi_{A \rightarrow B}) \geq I_{RC}(\Psi_{A \rightarrow B}, \bar{\rho}_A) = \log_2 d - S(\rho_\Psi), \quad (2.13.4)$$

where  $d = \dim \mathcal{H}_A$ . The relation (2.13.4) was used to find lower bounds on the 2-way capacity of 3-dimensional MAD channels in Chapter 6.

## 2.13.b Upper Bound

The computation of the upper bound of the  $Q_2$  of a channel is more difficult than that of the lower bound. One quantity that is always bigger than  $Q_2$  under any condition is the squashed entanglement.

### Squashed entanglement

Given a noisy channel  $\mathcal{N}$ , its squashed entanglement is defined by (see e.g. [KW20]):

$$\begin{aligned} E_{sq}(\mathcal{N}) &\equiv \sup_{|\psi\rangle_{AR}\langle\psi|} E_{sq}(R; B)_\psi, \\ E_{sq}(R; B)_\psi &\equiv \frac{1}{2} \inf_{\Omega_{E \rightarrow E'}} \left( I(R; B|E')_\rho : \rho_{BRE'} = \Omega_{E \rightarrow E'}(|\psi\rangle_{BRE} \langle\psi|) \right). \end{aligned} \quad (2.13.5)$$

where  $|\psi\rangle_{BRE} \langle\psi|$  is the output of the Stinespring dilation that corresponds to a pure state input  $|\psi\rangle_{AR} \langle\psi|$ ,  $(\mathcal{N}_{A \rightarrow B} \otimes \text{Id}_R)(|\psi\rangle_{AR} \langle\psi|) = \text{tr}_E(|\psi\rangle_{BRE} \langle\psi|)$ , while  $I(R; B|E')_\rho$  is the quantum conditional mutual information:

$$\begin{aligned} I(R; B|E')_\rho &\equiv S(R|E')_\rho + S(B|E')_\rho - S(BR|E')_\rho, \\ &= S(B|E')_\rho - S(B|RE')_\rho. \end{aligned} \quad (2.13.6)$$

From [Chr06]:

$$Q_2(\mathcal{N}) \leq E_{sq}(\mathcal{N}). \quad (2.13.7)$$

The  $\inf_{\Omega_{E \rightarrow E'}}$  in (2.13.5) can be dropped by choosing  $\Omega_{E \rightarrow E'} = \text{Id}_{E \rightarrow E}$ , the remaining quantity is still an upper bound, albeit possibly non optimal.

### Teleportation covariance

One defines (see [PLOB17])  $\sigma$ -stretchable channels as channels  $\mathcal{E}$  satisfying the condition:

$$\mathcal{E}(\rho) = \mathcal{T}(\sigma \otimes \rho) \quad \forall \rho, \quad (2.13.8)$$

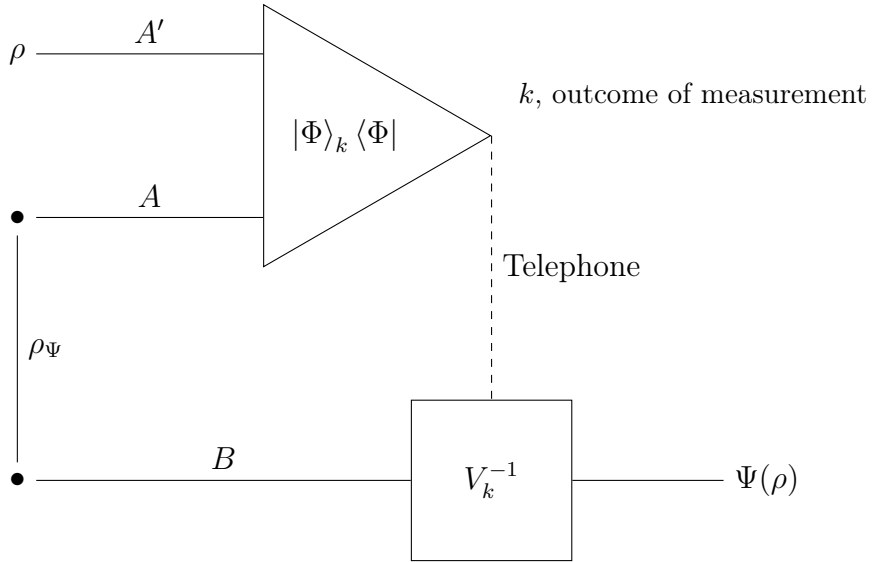


**Figure 2.13.2:** Schematic representation of the simulation of a telecovariant channel  $\Psi$ . Alice has access to the systems  $A$ ,  $A'$ , while Bob has access to system  $B$ . They share two halves of a composite system  $AB$ , which is in the Choi state  $\rho_\Psi$ . Alice wants to send the state  $\Psi(\rho)$  to Bob, while having the state  $\rho$  in her system  $A'$ . She makes a projective measurement of the Bell states in the system  $AA'$ , communicates the outcome to Bob who then performs an appropriate unitary transformation on his system  $B$  to obtain the desired state.

where  $\sigma$  is to be considered a shared resource between the two parties "Alice and Bob" while  $\mathcal{T}$  is a set of LOCC's. Accordingly, one can define "Choi-stretchable" channels that can be simulated over their Choi states  $\rho_{\mathcal{E}}$  using LOCC's, i.e.  $\exists \mathcal{T} \text{ LOCC}$ :

$$\mathcal{E}(\rho) = \mathcal{T}(\rho_{\mathcal{E}} \otimes \rho) \quad \forall \rho. \quad (2.13.9)$$

A channel  $\mathcal{E}$  is said to be teleportation covariant if, under a teleportation unitary  $U$  and another unitary (not necessarily a teleportation unitary)  $V$  one has:

$$\mathcal{E}(U\rho U^\dagger) = V\mathcal{E}(\rho)V^\dagger. \quad (2.13.10)$$

A teleportation covariant channel is Choi-stretchable; the protocol with which these channels can be simulated is the same as the qudit teleportation protocol (see e.g. [PEW<sup>+</sup>15]), with the only difference being that the shared resource is not the maximally entangled state but the Choi matrix of the channel to be simulated. See [PLOB17] for details and Figure 2.13.2 for a visual representation of the protocol. A sufficient and necessary condition for tele-covariance is given by:

$$[\rho_{\mathcal{E}}, U_k \otimes V_k] = 0 \quad \forall k, \quad (2.13.11)$$

where  $U_k$ 's are the teleportation unitaries and  $V_k$ 's are (possibly) different representations of the same group elements as the  $U_k$ 's. Amplitude damping channels are not tele-covariant; however, they can be mapped into bosonic lossy channels, which, since they are gaussian channels, are also Choi-stretchable.

### Relative Entropy of Entanglement

The relative entropy of entanglement (REE) can be thought of a kind of distance from an input entangled state to its "closest" separable state (2.2.2) and is defined by:

$$E_R(\rho) \equiv \inf_{\sigma_s} S(\rho || \sigma_s) \quad \sigma_s \text{ separable.} \quad (2.13.12)$$

If the channel  $\mathcal{E}$  satisfies (2.13.11), then an upper bound on  $Q_2(\mathcal{E})$  can be found with relative ease:

$$Q_2(\mathcal{E}) \leq E_R(\rho_{\mathcal{E}}). \quad (2.13.13)$$

## 2.14 Pipeline inequalities

Given a generic capacity functional  $\mathfrak{C}$ , such as the quantum capacity  $Q$  or the 2-way capacity  $Q_2$ , one may derive the pipeline (or data-processing) inequalities [HG12]: given two quantum channels  $\Psi_1, \Psi_2$  and their composition  $\Psi_2 \circ \Psi_1$  the capacity of the composed channel can not be bigger than that of the single channels:

$$\mathfrak{C}[\Psi_2 \circ \Psi_1] \leq \min \{\mathfrak{C}[\Psi_1], \mathfrak{C}[\Psi_2]\}. \quad (2.14.1)$$

The relation (2.14.1) makes intuitive sense: the capacity represents the ability of the receiving party to decipher the information sent through the channel, therefore adding further "noise" (i.e. an additional channel) to a channel can not increase its capacity.

## 2.15 Classical private capacity

Another capacity functional that was implicitly studied during this Thesis work is the *classical private capacity* of a quantum channel. In order to describe what this capacity represents, one needs to think of the environment in the "Alice and Bob" framework as an *eavesdropper*, which means that one needs to treat the information content decayed into the environment as the information content available to the eavesdropper. Assume that Alice wants to send a classical message to Bob, e.g. a string of bits, which is encoded in a mixture of quantum states, then one may ask what is the maximum ratio between the messages faithfully sent to Bob and the uses of the channel through which the messages are sent, under the additional condition that the information content received by the eavesdropper is 0. This rate is quantified by the classical private capacity  $C_P$ :

$$C_P \sim \frac{\# \text{ of bits faithfully transmitted without information leakage}}{\# \text{ of uses of the channel}}. \quad (2.15.1)$$

The curious reader can find a formal definition in [CWY04]. Two properties of the classical private capacity are of interest in this Thesis work:

- the classical private capacity is an upper bound for the quantum capacity [Hol13]:

$$Q(\Psi) \leq C_P(\Psi); \quad (2.15.2)$$

- if the channel  $\Psi$  is degradable, then its quantum and private classical capacities coincide [Hol13]:

$$\Psi \text{ is degradable} \Rightarrow C_P(\Psi) = Q(\Psi) \stackrel{(2.12.3)}{=} Q^{(1)}(\Psi). \quad (2.15.3)$$

In Chapter 7, the values of the quantum capacity for a wide range of configurations of 4-dimensional MAD channels are reported. Those values are the same for the classical private capacity in those configurations. This is obvious in those regions where the channel is degradable as a consequence of (2.15.3), but it is true even when the computation has been extended to non-degradable regions. This extension is possible by proving that the values of the capacity at the border of the degradable region are the same as those at the border of the parameter space.

The border of the degradability region can always be considered to be that region where<sup>5</sup>  $\gamma_{33} = 1/2$ , while the corresponding border of the parameter space is identified by  $\gamma_{33} = 0$ . The case  $\gamma_{33} = 0$  has been treated in Section 4.10, where the quantum capacity of the complete damping of level  $|3\rangle$  has been derived. If the difference  $Q(\gamma_{33} = 0) - Q(\gamma_{33} = 1/2)$  of the quantum capacities at  $\gamma_{33} = 1/2, 0$ , computed numerically, is 0, then, by employing the results in Section 4.9, the quantum capacity in the whole region  $0 \leq \gamma_{33} \leq 1/2$  is given by  $Q(\gamma_{33} = 1/2)$ .

From the relations (2.15.2) (2.15.3) and the monotonicity properties derived in Section 4.9:

$$Q(\gamma_{33} = 1/2) = Q(\gamma_{33} = 0) \leq C_P(\gamma_{33} = 0) \leq C_P(\gamma_{33} = 1/2) = Q(\gamma_{33} = 1/2), \quad (2.15.4)$$

therefore:

$$C_P(\gamma_{33} = 0) = C_P(\gamma_{33} = 1/2), \quad (2.15.5)$$

which, by the monotonicity properties of MAD channels, implies that:

$$C_P(\gamma_{33}) = C_P(\gamma_{33} = 1/2) = Q(\gamma_{33} = 1/2), \quad \forall 0 \leq \gamma_{33} \leq \frac{1}{2}. \quad (2.15.6)$$

The result in (2.15.6) guarantees that the values of the quantum capacities reported in Chapter 5 are the same as those of the classical private capacity even in non-degradable regions.

---

<sup>5</sup>This is a consequence of the covariance of the channels treated in Chapter 5 under unitary transformations of the form (4.3.2)

## 3

# Finite dimensional lossy channels

As already stated in Chapter 1, the purpose of this thesis work is the computation of some capacity functionals for a specific family of quantum channels, called Multi-level Amplitude Damping (MAD) channels; the previous research on MAD channels is exposed in the present chapter.

## 3.1 Amplitude Damping Channels

Amplitude Damping Channels, or ADC's, are qubit-to-qubit channels. They can be thought of as the interaction of a qubit with an infinite external environment at zero temperature, capable of absorbing energy from the qubit, which is transmitted e.g. through a photon, without altering the environment itself. ADC's are therefore very useful for describing energy decay processes, such as the loss of a photon in a fiber optic cable, or the energy decay of an electron in an atom with 2 energy levels. Interactions with an environment at non-zero temperature may be considered, which give rise to Generalized Amplitude Damping Channels (GADC) [KSW20]; however, those channels deviate from the scope of this work.

ADC's are defined by the Kraus set (see for example [NC10] page 380):

$$K_0 \equiv |0\rangle\langle 0| + \sqrt{1-\gamma} |1\rangle\langle 1| \quad K_1 \equiv \sqrt{\gamma} |0\rangle\langle 1|, \quad (3.1.1)$$

where  $\gamma$  is a real parameter satisfying  $0 \leq \gamma \leq 1$ ; it completely identifies an ADC. Given an input density matrix  $\rho$ :

$$\rho = \begin{pmatrix} \rho_{00} & \rho_{01} \\ \rho_{01}^* & \rho_{11} \end{pmatrix}, \quad (3.1.2)$$

the corresponding output state of an ADC is:

$$\begin{aligned} \text{ADC}_\gamma(\rho) &\equiv K_0 \rho K_0^\dagger + K_1 \rho K_1^\dagger, \\ \text{ADC}_\gamma(\rho) &= \begin{pmatrix} \rho_{00} + \gamma \rho_{11} & \sqrt{1-\gamma} \rho_{01} \\ \sqrt{1-\gamma} \rho_{01}^* & (1-\gamma) \rho_{11} \end{pmatrix}. \end{aligned} \quad (3.1.3)$$

For a detailed review on the quantum capacity, classical and quantum entangled assisted capacity, and classical capacity of ADC's see [GF05]. In the present section, a more in-depth analysis will be given only for the quantum capacity (and, consequently, also for the classical private capacity). Upper and lower bounds for the two-way capacity of ADC's can be obtained following the results illustrated in [PLOB17].

### 3.1.a Composition of ADC's

Consider a composition  $\text{ADC}_{\gamma''} \circ \text{ADC}_{\gamma'}$ , its output channel is given by:

$$\text{ADC}_{\gamma''} \circ \text{ADC}_{\gamma'}(\rho) = \begin{pmatrix} \rho_{00} + (\gamma' + \gamma'' - \gamma'\gamma'')\rho_{11} & \sqrt{(1-\gamma')(1-\gamma'')}\rho_{01} \\ \sqrt{(1-\gamma')(1-\gamma'')}\rho_{01}^* & (1-\gamma')(1-\gamma'')\rho_{11} \end{pmatrix}. \quad (3.1.4)$$

One could define a new parameter  $\gamma = \gamma' + \gamma''(1 - \gamma')$ , so that  $\text{ADC}_{\gamma''} \circ \text{ADC}_{\gamma'}(\rho) = \text{ADC}_\gamma(\rho)$ . This implies that ADC's are closed under composition, and the composition rules are:

$$\begin{aligned} \text{ADC}_\gamma &= \text{ADC}_{\gamma''} \circ \text{ADC}_{\gamma'}, \\ \gamma &= \gamma' + \gamma''(1 - \gamma') \geq \gamma', \gamma''. \end{aligned} \quad (3.1.5)$$

Notice that these composition rules, coupled with the bottleneck inequalities (2.14.1), imply that any capacity functional  $\mathfrak{C}$  for ADC's must be monotonous non-increasing for increasing values of  $\gamma$ :

$$\mathfrak{C}(\text{ADC}_\gamma) \leq \mathfrak{C}(\text{ADC}_{\gamma'}) \quad \gamma \geq \gamma'. \quad (3.1.6)$$

### 3.1.b Complementary channel of an ADC

Equation (2.6.2) can be used to find the output of the complementary channel of an ADC given an input matrix  $\rho$  of the form (3.1.2):

$$\widetilde{\text{ADC}}_\gamma(\rho) = \begin{pmatrix} \rho_{00} + (1 - \gamma)\rho_{11} & \sqrt{\gamma}\rho_{01} \\ \sqrt{\gamma}\rho_{01}^* & \gamma\rho_{11} \end{pmatrix}. \quad (3.1.7)$$

From (3.1.7) and (3.1.3), it is apparent that:

$$\text{ADC}_{1-\gamma} = \widetilde{\text{ADC}}_\gamma. \quad (3.1.8)$$

### 3.1.c Degradability and antidegradability

The conditions (2.7.1) and (2.7.2) define what it means for a generic channel  $\Phi$  to be, respectively, degradable or antidegradable. In the context of Amplitude Damping Channels, one finds, from (3.1.8), that the degradability condition reduces to:

$$\exists \Lambda : \text{ADC}_{1-\gamma} = \Lambda \circ \text{ADC}_\gamma, \quad (3.1.9)$$

while the antidegradability condition becomes:

$$\exists \Lambda' : \text{ADC}_\gamma = \Lambda' \circ \text{ADC}_{1-\gamma}. \quad (3.1.10)$$

Heuristically speaking, it would make sense if  $\Lambda$  and  $\Lambda'$  in (3.1.9) and (3.1.10) were both ADC's themselves. Following this hypothesis, one could rewrite (3.1.9) as:

$$\exists \lambda, 0 \leq \lambda \leq 1 : \text{ADC}_{1-\gamma} = \text{ADC}_\lambda \circ \text{ADC}_\gamma. \quad (3.1.11)$$

Employing (3.1.5) into (3.1.11), one finds:

$$\lambda = \frac{1 - 2\gamma}{1 - \gamma}. \quad (3.1.12)$$

In order for  $\lambda$  to satisfy  $0 \leq \lambda \leq 1$ , one needs to set the condition  $0 \leq \gamma \leq 1/2$ ; therefore, if  $0 \leq \gamma \leq 1/2$  the channel  $\text{ADC}_\gamma$  is degradable. One could also follow this line of reasoning in order to find an antidegradability condition; in fact, assuming that the antidegrading channel is itself an ADC, one could rewrite (3.1.10) as:

$$\exists \lambda', 0 \leq \lambda' \leq 1 : \text{ADC}_\gamma = \text{ADC}_{\lambda'} \circ \text{ADC}_{1-\gamma}. \quad (3.1.13)$$

This leads to:

$$\lambda' = \frac{2\gamma - 1}{\gamma}. \quad (3.1.14)$$

Therefore,  $\text{ADC}_\gamma$  is antidegradable if  $1/2 \leq \gamma \leq 1$ . This means that ADC's are either degradable or antidegradable:

$$\begin{cases} 0 \leq \gamma \leq 1/2 \Rightarrow \text{ADC}_\gamma \text{ is degradable}, \\ 1/2 \leq \gamma \leq 1 \Rightarrow \text{ADC}_\gamma \text{ is antidegradable}. \end{cases} \quad (3.1.15)$$

### 3.1.d Quantum Capacity of ADC's

Following the result (3.1.15), the quantum capacity of ADC's turns out to be relatively easy to compute. In fact, for  $1/2 \leq \gamma \leq 1$ , since the channel is antidegradable, the quantum capacity of  $\text{ADC}_\gamma$  is 0, while for  $0 \leq \gamma \leq 1/2$ , due to the property of degradable channels (2.12.3), the quantum capacity of  $\text{ADC}_\gamma$  corresponds to the maximum of the coherent information over all possible inputs for a single use of the channel:

$$Q(\text{ADC}_\gamma) = Q^{(1)}(\text{ADC}_\gamma) = \max_{\rho \in \sigma(\mathcal{H}_2)} I_c(\rho, \text{ADC}_\gamma) \quad \forall 0 \leq \gamma \leq 1/2 \quad (3.1.16)$$

Thanks to a property that MAD channels present for every dimension  $d$  (see (3.3.21)), the maximum in (3.1.16) can be computed over all diagonal density matrices  $\rho^{(\text{diag})}$  [GF05]:

$$\rho^{(\text{diag})} \equiv p |0\rangle\langle 0| + (1-p) |1\rangle\langle 1|, \quad (3.1.17)$$

$$\max_{\rho^{(\text{diag})} \in \sigma(\mathcal{H}_2)} I_c(\rho, \text{ADC}_\gamma) = \max_p \left\{ \begin{array}{l} -(1-p)(1-\gamma) \log_2((1-p)(1-\gamma)) \\ -(\gamma + p(1-\gamma)) \log_2(\gamma + p(1-\gamma)) \\ +(1-\gamma(1-p)) \log_2(1-\gamma(1-p)) \\ +\gamma(1-p) \log_2(\gamma(1-p)) \end{array} \right\}. \quad (3.1.18)$$

The right-hand side of (3.1.18) can be computed using a numerical evaluation, obtaining the plot reported in Figure 3.1.1.

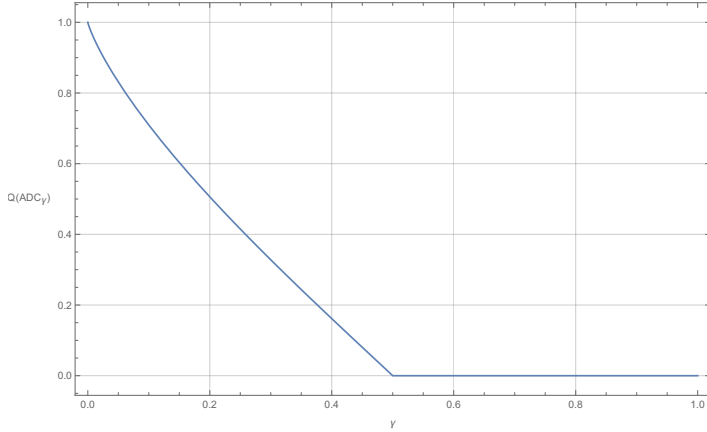


**Figure 3.1.1:** Quantum capacity for an Amplitude Damping Channel  $ADC_\gamma$  as a function of the parameter  $\gamma$ . Notice that (3.1.6) is satisfied.

## 3.2 Partially Coherent Direct Sum channels

In [CG21b], the authors analyze channels of the form:

$$\Phi_{CC}(\Theta_{CC}) \equiv \left[ \begin{array}{c|c} \Phi_{AA}(\Theta_{AA}) & \Phi_{AB}^{(off)}(\Theta_{AB}) \\ \hline \Phi_{BA}^{(off)}(\Theta_{BA}) & \Phi_{BB}(\Theta_{BB}) \end{array} \right], \quad (3.2.1)$$

$$\Theta_{CC} \equiv \left[ \begin{array}{c|c} \Theta_{AA} & \Theta_{AB} \\ \hline \Theta_{BA} & \Theta_{BB} \end{array} \right];$$

these are called Partially Coherent Direct Sum (PCDS) channels. For this type of channels, it was shown that:

$$\Phi_{CC} \text{ is degradable} \Leftrightarrow \Phi_{AA}, \Phi_{BB} \text{ are both degradable.} \quad (3.2.2)$$

If  $\Phi_{CC}$  is degradable, its quantum capacity presents an upper bound:

$$Q(\Phi_{CC}) \leq \log_2 (2^{Q(\Phi_{AA})} + 2^{Q(\Phi_{BB})}). \quad (3.2.3)$$

### Special case of $\Phi_{BB} = \text{Id}_{BB}$

Suppose  $\Phi_{BB}$  is the identity channel on  $\sigma(\mathcal{H}_B)$ ,  $\text{Id}_{BB}$ ; the upper bound (3.2.3) becomes:

$$Q(\Phi_{CC}) \leq \log_2 (2^{Q(\Phi_{AA})} + d_B), \quad (3.2.4)$$

where  $d_B = \dim \mathcal{H}_B$ . In this case, a lower bound for  $Q(\Phi_{CC})$  can also be found:

$$Q(\Phi_{CC}) \geq \log_2 (1 + d_B). \quad (3.2.5)$$

If the degradable channel  $\Phi_{AA}$  has null quantum capacity, then the upper bound (3.2.4) and the lower bound (3.2.5) coincide:

$$Q(\Phi_{AA}) = 0 \Rightarrow Q(\Phi_{CC}) = \log_2 (1 + d_B). \quad (3.2.6)$$

### 3.2.a Direct Sum channels

PCDS channels provide a generalization of Direct Sum (DS) channels [FW07], which suppress the coherence terms between the Hilbert spaces  $\mathcal{H}_A$  and  $\mathcal{H}_B$ :

$$\begin{aligned}\Phi_{CC}^{DS}(\Theta_{CC}) &\equiv \left[ \begin{array}{c|c} \Phi_{AA}(\Theta_{AA}) & 0 \\ \hline 0 & \Phi_{BB}(\Theta_{BB}) \end{array} \right], \\ \Theta_{CC} &\equiv \left[ \begin{array}{c|c} \Theta_{AA} & \Theta_{AB} \\ \hline \Theta_{BA} & \Theta_{BB} \end{array} \right].\end{aligned}\tag{3.2.7}$$

The capacity of these channels is never greater than the capacity of PCDS channels:

$$Q(\Phi_{CC}^{DS}) = \max \{Q(\Phi_{AA}), Q(\Phi_{BB})\} \leq Q(\Phi_{CC}).\tag{3.2.8}$$

## 3.3 3-dimensional Multi-level Amplitude Damping channels

Multi-level Amplitude Damping channels are the generalization to the qudit case of ADC channels; they were first explored in the article [CG21a], which is summarized in the present section.

### 3.3.a Settings for $d$ -dimensional MAD channels

The paper [CG21a] outlines the settings for a  $d$ -dimensional MAD channel, which are also reported here for the sake of completeness. Given a  $d$ -dimensional Hilbert space  $\mathcal{H}$ , spanned by the basis  $\{|i\rangle\}_i$ , for  $i = 0, \dots, d-1$ , the MAD channel has a minimal Kraus representation given by the Kraus operators:

$$\begin{aligned}K_{ij} &\equiv \sqrt{\gamma_{ji}} |i\rangle\langle j| \quad 0 \leq i < j \leq d-1, \\ K_{00} &\equiv \sum_{j=0}^{d-1} \sqrt{\gamma_{jj}} |j\rangle\langle j|.\end{aligned}\tag{3.3.1}$$

The  $\gamma_{ji}$ 's in (3.3.1) describe the probabilities of decay from level  $|j\rangle$  onto level  $|i\rangle$ , while  $\gamma_{jj}$ 's describe the probabilities that level  $|j\rangle$  will not decay during the transformation; as such, these are real quantities satisfying:

$$\gamma_{jj} \equiv 1 - \sum_{i=0}^{j-1} \gamma_{ji},\tag{3.3.2}$$

$$\begin{cases} 0 \leq \gamma_{ji} \leq 1 & \forall 0 \leq i < j \leq d-1, \\ 0 \leq \gamma_{jj} \leq 1 & \forall 0 \leq j \leq d-1, \\ \gamma_{ji} = 0 & \forall i > j. \end{cases}\tag{3.3.3}$$

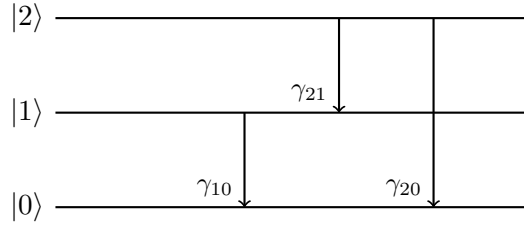


**Figure 3.3.1:** MAD channels represent decay processes, where each level of a system has a fixed probability of decaying onto a lower level. Here, a schematic depiction of a 3-dimensional MAD is reported

These quantities, which will be called *transition probabilities* in what follows, can be grouped into a matrix, which will be called *transition matrix*, defined by:

$$\Gamma \equiv \mathbb{1}_d + \sum_{j=1}^{d-1} \sum_{i=0}^{j-1} \gamma_{ji} |j\rangle\langle i| - \sum_{j=1}^{d-1} \sum_{i=0}^{j-1} \gamma_{ji} |j\rangle\langle j|, \quad (3.3.4)$$

where  $\mathbb{1}_d$  is the  $d$ -dimensional identity operator. There is a one-to-one relation between a specific MAD channel and its transition matrix, so that, given a transition matrix  $\Gamma$ , it is possible to identify the corresponding MAD channel by  $\Phi_\Gamma$ :

$$\Phi_\Gamma \sim \Gamma. \quad (3.3.5)$$

Finally, given an input  $\rho \in \sigma(\mathcal{H})$ , a MAD channel  $\Phi_\Gamma$  outputs the state:

$$\Phi_\Gamma(\rho) = K_{00}\rho K_{00}^\dagger + \sum_{j=1}^{d-1} \sum_{i=0}^{j-1} K_{ij}\rho K_{ij}^\dagger. \quad (3.3.6)$$

Which, in terms of transition probabilities, translates to:

$$\Phi_\Gamma(\rho) = \sum_{m=0}^{d-1} \sum_{n=0}^{d-1} \sqrt{\gamma_{mm}\gamma_{nn}} \rho_{mn} |m\rangle\langle n| + \sum_{j=1}^{d-1} \sum_{i=0}^{j-1} \gamma_{ji} \rho_{ii} |i\rangle\langle i|. \quad (3.3.7)$$

### 3.3.b Settings for 3-dimensional MAD channels

Set  $d = 3$ ; a generic 3-dimensional MAD channel  $\Phi_\Gamma^{(3)}$  is uniquely identified by its transition matrix  $\Gamma$ :

$$\Gamma = \begin{pmatrix} 1 & 0 & 0 \\ \gamma_{10} & 1 - \gamma_{10} & 0 \\ \gamma_{20} & \gamma_{21} & 1 - \gamma_{20} - \gamma_{21} \end{pmatrix}, \quad (3.3.8)$$

while the Kraus set for  $\Phi_{\Gamma}^{(3)}$ , taken from (3.3.1), is:

$$\begin{aligned} K_{00} &= \begin{pmatrix} 1 & 0 & 0 \\ 0 & \sqrt{1-\gamma_{10}} & 0 \\ 0 & 0 & \sqrt{1-\gamma_{20}-\gamma_{21}} \end{pmatrix}, \\ K_{01} &= \begin{pmatrix} 0 & \sqrt{\gamma_{10}} & 0 \\ 0 & 0 & 0 \\ 0 & 0 & 0 \end{pmatrix}, \quad K_{02} = \begin{pmatrix} 0 & 0 & \sqrt{\gamma_{20}} \\ 0 & 0 & 0 \\ 0 & 0 & 0 \end{pmatrix}, \quad K_{12} = \begin{pmatrix} 0 & 0 & 0 \\ 0 & 0 & \sqrt{\gamma_{21}} \\ 0 & 0 & 0 \end{pmatrix}. \end{aligned} \quad (3.3.9)$$

The transition probabilities  $\gamma_{10}, \gamma_{20}, \gamma_{21}$  satisfy the conditions:

$$\begin{cases} 0 \leq \gamma_{10}, \gamma_{20}, \gamma_{21} \leq 1, \\ 0 \leq \gamma_{20} + \gamma_{21} \leq 1. \end{cases} \quad (3.3.10)$$

Given an input density matrix  $\rho$ :

$$\rho = \begin{pmatrix} \rho_{00} & \rho_{01} & \rho_{02} \\ \rho_{01}^* & \rho_{11} & \rho_{12} \\ \rho_{02}^* & \rho_{12}^* & \rho_{22} \end{pmatrix}, \quad (3.3.11)$$

the output state of  $\Phi_{\Gamma}^{(3)}$  is:

$$\Phi_{\Gamma}^{(3)}(\rho) = \begin{pmatrix} \gamma_{10}\rho_{11} + \gamma_{20}\rho_{22} + \rho_{00} & \sqrt{1-\gamma_{10}}\rho_{01} & \sqrt{1-\gamma_{20}-\gamma_{21}}\rho_{02} \\ \sqrt{1-\gamma_{10}}\rho_{01}^* & (1-\gamma_{10})\rho_{11} + \gamma_{21}\rho_{22} & \sqrt{1-\gamma_{10}}\sqrt{1-\gamma_{20}-\gamma_{21}}\rho_{12} \\ \sqrt{1-\gamma_{20}-\gamma_{21}}\rho_{02}^* & \sqrt{1-\gamma_{10}}\sqrt{1-\gamma_{20}-\gamma_{21}}\rho_{12}^* & (1-\gamma_{20}-\gamma_{21})\rho_{22} \end{pmatrix}, \quad (3.3.12)$$

while the output state of the complementary channel  $\tilde{\Phi}_{\Gamma}^{(3)}$  is

$$\tilde{\Phi}_{\Gamma}^{(3)}(\rho) = \begin{pmatrix} (1-\gamma_{10})\rho_{11} + (1-\gamma_{20}-\gamma_{21})\rho_{22} + \rho_{00} & \sqrt{\gamma_{10}}\rho_{01} & \sqrt{\gamma_{20}}\rho_{02} & \sqrt{1-\gamma_{10}}\sqrt{\gamma_{21}}\rho_{12} \\ \sqrt{\gamma_{10}}\rho_{01}^* & \frac{\gamma_{10}\rho_{11}}{\sqrt{\gamma_{10}}\sqrt{\gamma_{20}}\rho_{12}^*} & \frac{\sqrt{\gamma_{10}}\sqrt{\gamma_{20}}\rho_{12}}{\gamma_{20}\rho_{22}} & 0 \\ \sqrt{\gamma_{20}}\rho_{02}^* & 0 & 0 & \frac{\gamma_{21}\rho_{22}}{\gamma_{21}\rho_{22}} \end{pmatrix}. \quad (3.3.13)$$

Refer to Figure 3.3.1 for a schematic representation of 3-dimensional MAD channels.

### 3.3.c Composition rules

The paper [CG21a] shows that MAD channels in  $d = 3$  are closed under channel composition, which means that the composition of two 3-dimensional MAD channels is itself a 3-dimensional MAD channel. This result can be generalized to an arbitrary dimension  $d$ , as shown in Section 4.2. The composition rules of 3-dimensional MAD channels are:

$$\begin{aligned} \Phi_{\Gamma}^{(3)} &= \Phi_{\Gamma''}^{(3)} \circ \Phi_{\Gamma'}^{(3)}, \\ \begin{cases} \gamma_{10} = \gamma'_{10} + \gamma''_{10}(1 - \gamma'_{10}), \\ \gamma_{20} = \gamma'_{20} + \gamma''_{20}(1 - \gamma'_{20}) + \gamma'_{21}\gamma''_{10}, \\ \gamma_{21} = \gamma'_{21}(1 - \gamma''_{10}) + \gamma''_{21}(1 - \gamma'_{20} - \gamma'_{21}), \end{cases} \end{aligned} \quad (3.3.14)$$

where  $\gamma_{ji} = \langle j|\Gamma|i\rangle, \gamma'_{ji} = \langle j|\Gamma'|i\rangle, \gamma''_{ji} = \langle j|\Gamma''|i\rangle$ . Intuitively, the composition rules (3.3.14) suggest that the transition probability  $\gamma_{ji}$ , resulting from a composition of two MAD channels, is the sum of the probabilities all the possible two-step decay "paths" from  $|j\rangle$  to  $|i\rangle$ . This idea is corroborated in Section 4.2.

### 3.3.d Covariance

Consider a  $d$ -dimensional MAD channel  $\Phi_\Gamma : \sigma(\mathcal{H}) \mapsto \sigma(\mathcal{H})$  and consider the  $d$ -dimensional unitary matrices  $U$  diagonal in the computational basis:

$$U \equiv \sum_{j=0}^{d-1} e^{i\varphi_j} |j\rangle\langle j| \quad \varphi_j \in \mathbb{R} \quad \forall j. \quad (3.3.15)$$

It is possible to verify that  $\Phi_\Gamma$  is covariant under the action of the group of unitary operators whose elements in the representation in  $\mathcal{H}$  are in the form (3.3.15), i.e.:

$$\Phi_\Gamma(U\rho U^\dagger) = U\Phi_\Gamma(\rho)U^\dagger. \quad (3.3.16)$$

### 3.3.e Maximum of coherent information for degradable MAD channels

If a channel  $\Phi$  is covariant under the action of a group  $\mathfrak{G}$ , by employing (2.8.3) and the invariance of the von Neumann entropy under unitary operations, one obtains:

$$\begin{aligned} \Phi : \sigma(\mathcal{H}_A) &\mapsto \sigma(\mathcal{H}_B) \text{ covariant under } \mathfrak{G}, \\ \Rightarrow I_c(U_g^A \rho U_g^{A\dagger}, \Phi) &= I_c(\rho, \Phi). \end{aligned} \quad (3.3.17)$$

Furthermore, consider the state  $\bar{\rho}_{\mathfrak{G}}$  obtained by taking the average over all the applications of elements  $g \in \mathfrak{G}$  upon the input state  $\rho$ :

$$\bar{\rho}_{\mathfrak{G}} \equiv \int d\mu_g U_g^A \rho U_g^{A\dagger}, \quad (3.3.18)$$

where  $\mu_g$  is a probability distribution over the group  $\mathfrak{G}$ ; if  $\Phi$  is degradable, by the property (2.11.13) the coherent information is concave in the input state  $\rho$ , therefore:

$$I_c(\bar{\rho}_{\mathfrak{G}}, \Phi) \geq \int d\mu_g I_c(U_g^A \rho U_g^{A\dagger}, \Phi) \stackrel{(3.3.17)}{=} I_c(\rho, \Phi). \quad (3.3.19)$$

Regarding MAD channels  $\Phi_\Gamma$ , as seen in (3.3.16),  $\mathfrak{G}$  could be replaced by the group of unitary operators diagonal in the computational basis; in this case,  $\bar{\rho}_{\mathfrak{G}}$  corresponds to a diagonal density matrices  $\rho^{(diag)}$ , so that (3.3.19) becomes:

$$I_c(\rho^{(diag)}, \Phi_\Gamma) \geq I_c(\rho, \Phi_\Gamma). \quad (3.3.20)$$

Hence, for degradable MAD channels, the search for the maximum over input states in (2.12.3) can be restricted to diagonal input states:

$$Q(\Phi_\Gamma) = Q^{(1)}(\Phi_\Gamma) \equiv \max_{\rho} I_c(\rho, \Phi_\Gamma) \stackrel{(3.3.20)}{=} \max_{\rho^{(diag)}} I_c(\rho^{(diag)}, \Phi_\Gamma). \quad (3.3.21)$$

### 3.3.f Single decays

Consider the single decay channels  $\Phi_{\Gamma_{10}(\gamma)}^{(3)}, \Phi_{\Gamma_{20}(\gamma)}^{(3)}, \Phi_{\Gamma_{21}(\gamma)}^{(3)}$ , whose transition matrices present the same single transition probability:

$$\Gamma_{10}(\gamma) \equiv \begin{pmatrix} 1 & 0 & 0 \\ \gamma & 1-\gamma & 0 \\ 0 & 0 & 1 \end{pmatrix}, \quad \Gamma_{20}(\gamma) \equiv \begin{pmatrix} 1 & 0 & 0 \\ 0 & 1 & 0 \\ \gamma & 0 & 1-\gamma \end{pmatrix}, \quad \Gamma_{21}(\gamma) \equiv \begin{pmatrix} 1 & 0 & 0 \\ 0 & 1 & 0 \\ 0 & \gamma & 1-\gamma \end{pmatrix}. \quad (3.3.22)$$

Define the swap matrices:

$$U_{10} \equiv \begin{pmatrix} 0 & 1 & 0 \\ 1 & 0 & 0 \\ 0 & 0 & 1 \end{pmatrix}, \quad U_{21} \equiv \begin{pmatrix} 1 & 0 & 0 \\ 0 & 0 & 1 \\ 0 & 1 & 0 \end{pmatrix}; \quad (3.3.23)$$

the channels  $\Phi_{\Gamma_{10}(\gamma)}^{(3)}, \Phi_{\Gamma_{20}(\gamma)}^{(3)}, \Phi_{\Gamma_{21}(\gamma)}^{(3)}$  can be mapped into each other via unitary channels corresponding to (3.3.23):

$$\mathcal{U}_{10}(\bullet) \equiv U_{10} \bullet U_{10}, \quad \mathcal{U}_{21}(\bullet) \equiv U_{21} \bullet U_{21}, \quad (3.3.24)$$

$$\begin{aligned} \mathcal{U}_{21} \circ \Phi_{\Gamma_{10}(\gamma)}^{(3)} \circ \mathcal{U}_{21} &= \Phi_{\Gamma_{20}(\gamma)}^{(3)}, \\ \mathcal{U}_{10} \circ \Phi_{\Gamma_{20}(\gamma)}^{(3)} \circ \mathcal{U}_{10} &= \Phi_{\Gamma_{21}(\gamma)}^{(3)}, \\ \mathcal{U}_{10} \circ \mathcal{U}_{21} \circ \Phi_{\Gamma_{10}(\gamma)}^{(3)} \circ \mathcal{U}_{21} \circ \mathcal{U}_{10} &= \Phi_{\Gamma_{21}(\gamma)}^{(3)}. \end{aligned} \quad (3.3.25)$$

From the bottleneck inequality (2.14.1), (3.3.25) and the invertibility of unitary channels, one can infer that  $\Phi_{\Gamma_{10}(\gamma)}^{(3)}, \Phi_{\Gamma_{20}(\gamma)}^{(3)}, \Phi_{\Gamma_{21}(\gamma)}^{(3)}$  have the same capacity functionals, which means that the capacity of a single decay 3-dimensional MAD channel only depends on the transition probability, not on the specific levels involved in the decay.

The composition rules for  $\Phi_{\Gamma_{10}(\gamma)}^{(3)}, \Phi_{\Gamma_{20}(\gamma)}^{(3)}, \Phi_{\Gamma_{21}(\gamma)}^{(3)}$  are very similar to those found for ADC's (3.1.5):

$$\begin{aligned} \Phi_{\Gamma_{ji}(\gamma)}^{(3)} &= \Phi_{\Gamma_{ji}(\gamma'')}^{(3)} \circ \Phi_{\Gamma_{ji}(\gamma')}, \\ \gamma &= \gamma' + \gamma''(1 - \gamma') \geq \gamma', \gamma'', \end{aligned} \quad (3.3.26)$$

where  $0 \leq i < j \leq 1$ .

### 3.3.g Monotonicity

Exploiting the composition rules derived in Subsection 3.3.c, one can infer monotonicity properties for the capacity functionals of 3-dimensional MAD channels. In fact, the relation (2.14.1), in the context of (3.3.14), becomes:

$$\mathfrak{C}\left(\Phi_{\Gamma}^{(3)}\right) \leq \min \left\{ \mathfrak{C}\left(\Phi_{\Gamma'}^{(3)}\right), \mathfrak{C}\left(\Phi_{\Gamma''}^{(3)}\right) \right\}. \quad (3.3.27)$$

Define a generic 3-dimensional MAD channel:

$$\Phi_{\Gamma}^{(3)} \equiv \Phi_{\Gamma(\gamma_{10}, \gamma_{20}, \gamma_{21})}^{(3)}, \quad (3.3.28)$$

where the dependency of  $\Gamma$  in (3.3.8) on the real parameters  $\gamma_{10}, \gamma_{20}, \gamma_{21}$  has been made explicit; using (3.3.14), one can find decompositions of  $\Phi_{\Gamma(\gamma_{10}, \gamma_{20}, \gamma_{21})}^{(3)}$ , whose composing channels have higher capacity than  $\Phi_{\Gamma(\gamma_{10}, \gamma_{20}, \gamma_{21})}^{(3)}$ . Some of these decompositions are reported below:

$$\Phi_{\Gamma(\gamma_{10}, \gamma_{20}, \gamma_{21})}^{(3)} = \Phi_{\Gamma(0, \gamma_{20}, \gamma_{21})}^{(3)} \circ \Phi_{\Gamma(\gamma_{10}, 0, 0)}^{(3)}, \quad (3.3.29)$$

$$\Phi_{\Gamma(\gamma_{10}, \gamma_{20}, \gamma_{21})}^{(3)} = \Phi_{\Gamma(0, \bar{\gamma}_{20}, 0)}^{(3)} \circ \Phi_{\Gamma(\gamma_{10}, 0, \gamma_{21})}^{(3)} \quad \bar{\gamma}_{20} \equiv \frac{\gamma_{20}}{1 - \gamma_{21}}, \quad (3.3.30)$$

$$\Phi_{\Gamma(\gamma_{10}, \gamma_{20}, \gamma_{21})}^{(3)} = \Phi_{\Gamma(0, 0, \bar{\gamma}_{21})}^{(3)} \circ \Phi_{\Gamma(\gamma_{10}, \gamma_{20}, 0)}^{(3)} \quad \bar{\gamma}_{21} \equiv \frac{\gamma_{21}}{1 - \gamma_{20}}, \quad (3.3.31)$$

Employing (3.3.26) into (3.3.29), (3.3.30) and (3.3.31), each single decay channel found in these decompositions is split into two new single decay channels with transition probabilities  $\gamma'_{ji}, \gamma''_{ji} \leq \gamma_{ji}$ :

$$\Phi_{\Gamma(\gamma_{10}, 0, 0)}^{(3)} = \Phi_{\Gamma(\gamma'_1 0, 0, 0)}^{(3)} \circ \Phi_{\Gamma(\gamma''_{10}, 0, 0)}^{(3)}, \quad (3.3.32)$$

$$\Phi_{\Gamma(0, \bar{\gamma}_{20}, 0)}^{(3)} = \Phi_{\Gamma(0, \bar{\gamma}_{20}'', 0)}^{(3)} \circ \Phi_{\Gamma(0, \bar{\gamma}_{20}', 0)}^{(3)}, \quad (3.3.33)$$

$$\Phi_{\Gamma(0, 0, \bar{\gamma}_{21})}^{(3)} = \Phi_{\Gamma(0, 0, \bar{\gamma}_{21}'')}^{(3)} \circ \Phi_{\Gamma(0, 0, \bar{\gamma}_{21}')}^{(3)}. \quad (3.3.34)$$

where:

$$\bar{\gamma}_{21}'' \equiv \frac{\gamma_{21}''}{1 - \gamma_{20}} \quad \bar{\gamma}_{21}' \equiv \frac{\gamma_{21}'}{1 - \gamma_{20}}, \quad (3.3.35)$$

$$\bar{\gamma}_{20}'' \equiv \frac{\gamma_{20}''}{1 - \gamma_{21}} \quad \bar{\gamma}_{20}' \equiv \frac{\gamma_{20}'}{1 - \gamma_{21}}. \quad (3.3.36)$$

Therefore, (3.3.29), (3.3.30) and (3.3.31) become:

$$\Phi_{\Gamma(\gamma_{10}, \gamma_{20}, \gamma_{21})}^{(3)} = \Phi_{\Gamma(\gamma'_{10}, \gamma_{20}, \gamma_{21})}^{(3)} \circ \Phi_{\Gamma(\gamma''_{10}, 0, 0)}^{(3)} \quad \gamma'_{10} \leq \gamma_{10}, \quad (3.3.37)$$

$$\Phi_{\Gamma(\gamma_{10}, \gamma_{20}, \gamma_{21})}^{(3)} = \Phi_{\Gamma(0, \bar{\gamma}_{20}'', 0)}^{(3)} \circ \Phi_{\Gamma(\gamma_{10}, \gamma'_{20}, \gamma_{21})}^{(3)} \quad \gamma'_{20} \leq \gamma_{20}, \quad (3.3.38)$$

$$\Phi_{\Gamma(\gamma_{10}, \gamma_{20}, \gamma_{21})}^{(3)} = \Phi_{\Gamma(0, 0, \bar{\gamma}_{21}'')}^{(3)} \circ \Phi_{\Gamma(\gamma_{10}, \gamma_{20}, \gamma'_{21})}^{(3)} \quad \gamma'_{21} \leq \gamma_{21}. \quad (3.3.39)$$

Combining (3.3.37), (3.3.38) and (3.3.39) with (3.3.27), the monotonicity rules w.r.t. the transition probabilities for the capacities of 3-dimensional MAD channels are found.

$$\begin{aligned} \mathfrak{C}\left(\Phi_{\Gamma(\gamma_{10}, \gamma_{20}, \gamma_{21})}^{(3)}\right) &\leq \mathfrak{C}\left(\Phi_{\Gamma(\gamma'_{10}, \gamma_{20}, \gamma_{21})}^{(3)}\right) \quad \forall \gamma_{10} \geq \gamma'_{10}, \\ \mathfrak{C}\left(\Phi_{\Gamma(\gamma_{10}, \gamma_{20}, \gamma_{21})}^{(3)}\right) &\leq \mathfrak{C}\left(\Phi_{\Gamma(\gamma_{10}, \gamma'_{20}, \gamma_{21})}^{(3)}\right) \quad \forall \gamma_{20} \geq \gamma'_{20}, \\ \mathfrak{C}\left(\Phi_{\Gamma(\gamma_{10}, \gamma_{20}, \gamma_{21})}^{(3)}\right) &\leq \mathfrak{C}\left(\Phi_{\Gamma(\gamma_{10}, \gamma_{20}, \gamma'_{21})}^{(3)}\right) \quad \forall \gamma_{21} \geq \gamma'_{21}. \end{aligned} \quad (3.3.40)$$

This means that, when any transition probability of a 3-dimensional MAD channel increases, its capacity functionals decrease.

### 3.3.h Quantum capacity and private classical capacity

In Section 2.12 the quantum capacity of quantum channels was introduced; in most cases, it is not possible to compute the exact value of this quantity for a given channel, however, one notable exception to this rule stems from degradable channels, whose quantum capacity corresponds to the maximum over all input states of the coherent information of the channel, as seen in (2.12.3). Another important simplification for degradable MAD channels is provided by (3.3.21), which restricts the search for the maximum of the coherent information over diagonal input states. For degradable 3-dimensional MAD channels, this translates to:

$$\begin{aligned} Q\left(\Phi_{\Gamma}^{(3)}\right) &= \max_{\rho} I_c\left(\rho, \Phi_{\Gamma}^{(3)}\right) = \max_{p_0, p_1} I_c\left(\rho^{(diag)}, \Phi_{\Gamma}^{(3)}\right), \\ \rho^{(diag)} &\equiv \begin{pmatrix} p_0 & 0 & 0 \\ 0 & p_1 & 0 \\ 0 & 0 & 1 - p_0 - p_1 \end{pmatrix}, \quad \begin{cases} 0 \leq p_0, p_1 \leq 1, \\ 0 \leq 1 - p_0 - p_1 \leq 1. \end{cases} \end{aligned} \tag{3.3.41}$$

Equation (3.3.21) (and, particularly for  $d = 3$ , (3.3.41)) allows for the development of a *modus operandi* for the analysis of the quantum capacity of  $d$ -dimensional MAD channels  $\Phi_{\Gamma}$ :

- Find degradability and antidegradability regions for  $\Phi_{\Gamma}$ .
- Compute the quantum capacity in the degradability regions using (3.3.21).
- Try to extend the computation to non-degradable zones.

The last step in this process, in the context of 3, 4-dimensional MAD channels, is to be expanded individually in each degradable zone.

### 3.3.i Degradability regions

A generic algorithm for determining the degradability regions of a  $d$ -dimensional MAD channel is offered in Section 4.6; it consists on finding the right-inverse map for a  $d$ -dimensional MAD channel  $\Phi_{\Gamma}$ , denoted by  $\Phi_{\Gamma}^{(-1)}$  and defined in (4.5.7), and checking the positivity of the Choi matrix  $C_{\Lambda}$  corresponding to the map:

$$\Lambda \equiv \tilde{\Phi}_{\Gamma} \circ \Phi_{\Gamma}^{-1}. \tag{3.3.42}$$

By (2.5.17),  $C_{\Lambda} \geq 0$  if and only if  $\Lambda$  is completely positive; since  $\Lambda$  is linear and trace preserving by construction<sup>1</sup>, its complete positiveness would imply that it is a quantum channel, acting as the degrading channel of  $\Phi_{\Gamma}$ , which, in light of this, would be a degradable channel. To simplify this computation-heavy task, a more heuristic approach

---

<sup>1</sup>This is a consequence of the linearity and trace preservation of both  $\Phi_{\Gamma}^{(-1)}$  (see (4.5.7)) and  $\tilde{\Phi}_{\Gamma}$ .

is needed and provided here for the specific case of  $d = 3$ . Given a 3-dimensional MAD channel  $\Phi_{\Gamma}^{(3)}$ , in order to find a connecting channel  $\Lambda^{(3)}$  such that:

$$\Lambda^{(3)} \circ \Phi_{\Gamma}^{(3)} = \tilde{\Phi}_{\Gamma}^{(3)}, \quad (3.3.43)$$

assume that the rank of the output density matrix is greater or equal than the rank of the density matrix of the environment:

$$\text{rank} \left( \Phi_{\Gamma}^{(3)}(\rho) \right) \geq \text{rank} \left( \tilde{\Phi}_{\Gamma}^{(3)}(\rho) \right) \quad \forall \rho. \quad (3.3.44)$$

For a generic  $\rho$ ,  $\text{rank} \left( \Phi_{\Gamma}^{(3)}(\rho) \right) = 3$ ; given a minimal Kraus set  $\mathcal{K}$  of a channel  $\Phi$ , from (2.6.2) it can be deduced that the rank of  $\tilde{\Phi}(\rho)$  corresponds to the cardinality of  $\mathcal{K}$ , hence,  $\text{rank} \left( \tilde{\Phi}_{\Gamma}^{(3)}(\rho) \right) = 4$ ; the rank of the environment can be reduced to be  $\leq 3$  by "turning off" at least one decay, i.e. by setting at least one  $\gamma_{ji} = 0$  for some  $i \leq j$ . This breaks down the problem to three scenarios:

1.  $\gamma_{10} = 0$ , in which case  $\Phi_{\Gamma}^{(3)}$  is degradable for  $\gamma_{20} + \gamma_{21} \leq 1/2$ , see [below](#).
2.  $\gamma_{20} = 0$ , in which case  $\Phi_{\Gamma}^{(3)}$  is never degradable, see [below](#).
3.  $\gamma_{21} = 0$ , in which case  $\Phi_{\Gamma}^{(3)}$  is degradable for  $\gamma_{10} \leq 1/2 \wedge \gamma_{20} \leq 1/2$ , see [below](#).

### Degradability for $\gamma_{10} = 0$

The output state of  $\Phi_{\Gamma(0,\gamma_{20},\gamma_{21})}^{(3)}$  is:

$$\Phi_{\Gamma(0,\gamma_{20},\gamma_{21})}^{(3)}(\rho) = \begin{pmatrix} \gamma_{20}\rho_{22} + \rho_{00} & \rho_{01} & \sqrt{1 - \gamma_{20} - \gamma_{21}}\rho_{02} \\ \rho_{01}^* & \gamma_{21}\rho_{22} + \rho_{11} & \sqrt{1 - \gamma_{20} - \gamma_{21}}\rho_{12} \\ \sqrt{1 - \gamma_{20} - \gamma_{21}}\rho_{02}^* & \sqrt{1 - \gamma_{20} - \gamma_{21}}\rho_{12}^* & (1 - \gamma_{20} - \gamma_{21})\rho_{22} \end{pmatrix}. \quad (3.3.45)$$

While the state of the environment is:

$$\tilde{\Phi}_{\Gamma(0,\gamma_{20},\gamma_{21})}^{(3)}(\rho) = \begin{pmatrix} (1 - \gamma_{20} - \gamma_{21})\rho_{22} + \rho_{00} + \rho_{11} & \sqrt{\gamma_{20}}\rho_{02} & \sqrt{\gamma_{21}}\rho_{12} \\ \sqrt{\gamma_{20}}\rho_{02}^* & \gamma_{20}\rho_{22} & 0 \\ \sqrt{\gamma_{21}}\rho_{12}^* & 0 & \gamma_{21}\rho_{22} \end{pmatrix}. \quad (3.3.46)$$

Given the degrading map

$$\Lambda_{\Gamma(0,\gamma_{20},\gamma_{21})}^{(3)} \equiv \tilde{\Phi}_{\Gamma(0,\gamma_{20},\gamma_{21})}^{(3)} \circ \Phi_{\Gamma(0,\gamma_{20},\gamma_{21})}^{(3)-1}, \quad (3.3.47)$$

checking the positivity of the associated Choi matrix yields the degradability condition:

$$\gamma_{20} + \gamma_{21} \leq \frac{1}{2}. \quad (3.3.48)$$

### Degradability for $\gamma_{20} = 0$

The output state of  $\Phi_{\Gamma(\gamma_{10}, 0, \gamma_{21})}^{(3)}$  is:

$$\Phi_{\Gamma(\gamma_{10}, 0, \gamma_{21})}^{(3)}(\rho) = \begin{pmatrix} \gamma_{10}\rho_{11} + \rho_{00} & \sqrt{1 - \gamma_{10}}\rho_{01} & \sqrt{1 - \gamma_{21}}\rho_{02} \\ \sqrt{1 - \gamma_{10}}\rho_{01}^* & (1 - \gamma_{10})\rho_{11} + \gamma_{21}\rho_{22} & \sqrt{1 - \gamma_{10}}\sqrt{1 - \gamma_{21}}\rho_{12} \\ \sqrt{1 - \gamma_{21}}\rho_{02}^* & \sqrt{1 - \gamma_{10}}\sqrt{1 - \gamma_{21}}\rho_{12}^* & (1 - \gamma_{21})\rho_{22} \end{pmatrix}, \quad (3.3.49)$$

while the state of the environment is:

$$\tilde{\Phi}_{\Gamma(\gamma_{10}, 0, \gamma_{21})}^{(3)}(\rho) = \begin{pmatrix} (1 - \gamma_{10})\rho_{11} + (1 - \gamma_{21})\rho_{22} + \rho_{00} & \sqrt{\gamma_{10}}\rho_{01} & \sqrt{1 - \gamma_{10}}\sqrt{\gamma_{21}}\rho_{12} \\ \sqrt{\gamma_{10}}\rho_{01}^* & \gamma_{10}\rho_{11} & 0 \\ \sqrt{1 - \gamma_{10}}\sqrt{\gamma_{21}}\rho_{12}^* & 0 & \gamma_{21}\rho_{22} \end{pmatrix}. \quad (3.3.50)$$

Since the Choi matrix associated to

$$\Lambda_{\Gamma(\gamma_{10}, 0, \gamma_{21})}^{(3)} \equiv \tilde{\Phi}_{\Gamma(\gamma_{10}, 0, \gamma_{21})}^{(3)} \circ \Phi_{\Gamma(\gamma_{10}, 0, \gamma_{21})}^{(3)-1} \quad (3.3.51)$$

is positive semi-definite only if either one of  $\gamma_{10}, \gamma_{21}$  is set to 0 (and the other is  $\leq 1/2$ ), the channel  $\Phi_{\Gamma(\gamma_{10} \neq 0, 0, \gamma_{21} \neq 0)}^{(3)}$  is never degradable.

### Degradability for $\gamma_{21} = 0$

The output state of  $\Phi_{\Gamma(\gamma_{10}, \gamma_{20}, 0)}^{(3)}$  is:

$$\Phi_{\Gamma(\gamma_{10}, \gamma_{20}, 0)}^{(3)}(\rho) = \begin{pmatrix} \gamma_{10}\rho_{11} + \gamma_{20}\rho_{22} + \rho_{00} & \sqrt{1 - \gamma_{10}}\rho_{01} & \sqrt{1 - \gamma_{20}}\rho_{02} \\ \sqrt{1 - \gamma_{10}}\rho_{01}^* & (1 - \gamma_{10})\rho_{11} & \sqrt{1 - \gamma_{10}}\sqrt{1 - \gamma_{20}}\rho_{12} \\ \sqrt{1 - \gamma_{20}}\rho_{02}^* & \sqrt{1 - \gamma_{10}}\sqrt{1 - \gamma_{20}}\rho_{12}^* & (1 - \gamma_{20})\rho_{22} \end{pmatrix}, \quad (3.3.52)$$

while the state of the environment is:

$$\tilde{\Phi}_{\Gamma(\gamma_{10}, \gamma_{20}, 0)}^{(3)}(\rho) = \begin{pmatrix} (1 - \gamma_{10})\rho_{11} + (1 - \gamma_{20})\rho_{22} + \rho_{00} & \sqrt{\gamma_{10}}\rho_{01} & \sqrt{\gamma_{20}}\rho_{02} \\ \sqrt{\gamma_{10}}\rho_{01}^* & \gamma_{10}\rho_{11} & \sqrt{\gamma_{10}}\sqrt{\gamma_{20}}\rho_{12} \\ \sqrt{\gamma_{20}}\rho_{02}^* & \sqrt{\gamma_{10}}\sqrt{\gamma_{20}}\rho_{12}^* & \gamma_{20}\rho_{22} \end{pmatrix}. \quad (3.3.53)$$

Given the degrading map

$$\Lambda_{\Gamma(\gamma_{10}, \gamma_{20}, 0)}^{(3)} \equiv \tilde{\Phi}_{\Gamma(\gamma_{10}, \gamma_{20}, 0)}^{(3)} \circ \Phi_{\Gamma(\gamma_{10}, \gamma_{20}, 0)}^{(3)-1}, \quad (3.3.54)$$

checking the positivity of the associated Choi matrix yields the degradability condition:

$$\gamma_{10} \leq \frac{1}{2} \wedge \gamma_{20} \leq \frac{1}{2}. \quad (3.3.55)$$

### Degradability conditions

Compounding the results exposed in this Subsection, the degradability conditions for  $\Phi_{\Gamma(\gamma_{10}, \gamma_{20}, \gamma_{21})}^{(3)}$  are found:

$$\begin{aligned} \Phi_{\Gamma(\gamma_{10}, \gamma_{20}, \gamma_{21})}^{(3)} \text{ is degradable.} \\ \uparrow \\ \left( \gamma_{10} = 0 \wedge \gamma_{20} + \gamma_{21} \leq \frac{1}{2} \right) \vee \left( \gamma_{21} = 0 \wedge \gamma_{10} \leq \frac{1}{2} \wedge \gamma_{20} \leq \frac{1}{2} \right). \end{aligned} \quad (3.3.56)$$

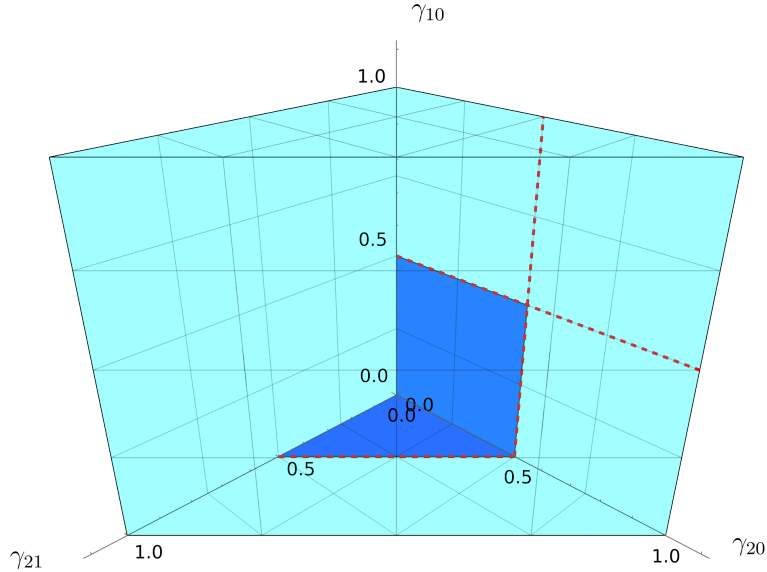


**Figure 3.3.2:** The plot is cast in the parameter space for a 3-dimensional MAD channel; all these channels satisfy the conditions (3.3.10), which are represented in cyan in the plot, while the blue areas correspond to the degradability conditions reported in (3.3.57)

The conditions in (3.3.56) are illustrated in Figure 3.3.2.

### Additional degradable settings

One may wonder if the conditions in (3.3.56) encompass all the degradability regions for  $\Phi_{\Gamma(\gamma_{10}, \gamma_{20}, \gamma_{21})}^{(3)}$ ; particularly, it is not clear whether there exists a configuration of  $\{\gamma_{10}, \gamma_{20}, \gamma_{21}\}$  such that  $\gamma_{10}, \gamma_{20}, \gamma_{21} \neq 0$  and  $\Phi_{\Gamma(\gamma_{10}, \gamma_{20}, \gamma_{21})}^{(3)}$  is degradable. To tackle this question, it is possible to exploit the result in (4.4.2), which states that the channels forming an arbitrary decomposition of a degradable channel must be degradable themselves. The right-most channel in the decomposition (3.3.30) of a generic 3-dimensional MAD channel is only degradable if either one of  $\gamma_{10}, \gamma_{21}$  is set to 0, therefore it is not possible to find a configuration  $\{\gamma_{10}, \gamma_{20}, \gamma_{21}\}$  such that  $\gamma_{10}, \gamma_{20}, \gamma_{21} \neq 0$  and  $\Phi_{\Gamma(\gamma_{10}, \gamma_{20}, \gamma_{21})}^{(3)}$  is degradable. Thus, (3.3.56) can be rewritten in a more strict form:

$$\begin{aligned} \Phi_{\Gamma(\gamma_{10}, \gamma_{20}, \gamma_{21})}^{(3)} \text{ is degradable.} \\ \Updownarrow \\ \left( \gamma_{10} = 0 \wedge \gamma_{20} + \gamma_{21} \leq \frac{1}{2} \right) \vee \left( \gamma_{21} = 0 \wedge \gamma_{10} \leq \frac{1}{2} \wedge \gamma_{20} \leq \frac{1}{2} \right). \end{aligned} \tag{3.3.57}$$

Note that this means that in the case of 3-dimensional MAD channels, the condition  $\text{rank}(\Phi_{\Gamma}^{(3)}(\rho)) \geq \text{rank}(\tilde{\Phi}_{\Gamma}^{(3)}(\rho)) \forall \rho$  is a necessary condition for the degradability of

$\Phi_{\Gamma}^{(3)}$ ; this is not true in general, a counterexample for 4-dimensional MAD's is offered in (4.7.9).

### 3.3.j Quantum capacity of 3-dimensional MAD channels

Using the results illustrated in this Chapter, the quantum capacities of a wide range of settings for 3-dimensional MAD channels were found. Notably, the quantum capacity was obtained even in some non-degradable regions in the parameter space of the channel. The techniques employed in this analysis were used and expanded to derive the results reported in Chapter 5 for the quantum capacities of 4-dimensional MAD channels. For plots and details of the 3-dimensional case, refer to [CG21a].



# Properties of MAD channels

This chapter will center around the exposition of some general properties of Multi-Level Amplitude Damping channels. The main focus of this Thesis work are 4-dimensional MAD channel, therefore special attention was put into this particular case. However, most of the properties reported here hold for any dimension  $d$ , potentially allowing future studies of MAD channels in higher dimensions to be built upon these results.

## 4.1 Settings for $d$ -dimensional MAD channels

The settings for  $d$ -dimensional MAD channels have already been defined in Subsection 3.3.a. The relation (3.3.5), in particular, will turn out to be extremely useful in Section 4.2 for the derivation of the composition rules of MAD channels.

### Settings for 4-dimensional MAD channels

Substituting  $d = 4$  in the definitions given in Subsection 3.3.a, one obtains the settings that describe a 4-dimensional MAD channel  $\Phi_{\Gamma}^{(4)}$ , which is completely identified by the

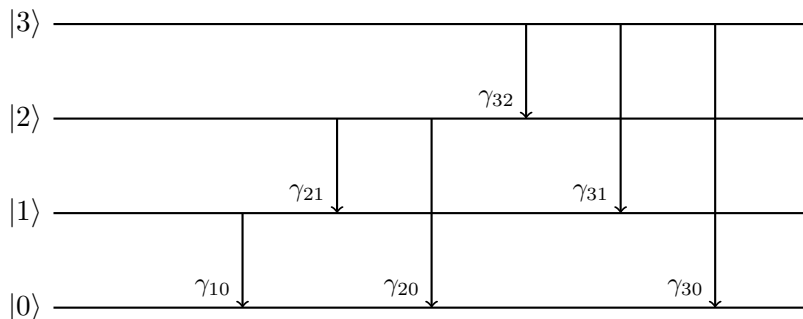


**Figure 4.1.1:** MAD channels represent decay processes, where each level of a system has a fixed probability of decaying onto a lower level. Here, a schematic depiction of a 4-dimensional MAD is reported

transition matrix  $\Gamma$ :

$$\Gamma \equiv \begin{pmatrix} 1 & 0 & 0 & 0 \\ \gamma_{10} & 1 - \gamma_{10} & 0 & 0 \\ \gamma_{20} & \gamma_{21} & 1 - \gamma_{20} - \gamma_{21} & 0 \\ \gamma_{30} & \gamma_{31} & \gamma_{32} & 1 - \gamma_{30} - \gamma_{31} - \gamma_{32} \end{pmatrix}, \quad (4.1.1)$$

whose elements satisfy are real,  $\geq 0$  and  $\leq 1$ , accordingly to (3.3.3). The Kraus set of  $\Phi_{\Gamma}^{(4)}$  is composed by the Kraus operators:

$$K_{00} = \begin{pmatrix} 1 & 0 & 0 & 0 \\ 0 & \sqrt{1 - \gamma_{10}} & 0 & 0 \\ 0 & 0 & \sqrt{1 - \gamma_{20} - \gamma_{21}} & 0 \\ 0 & 0 & 0 & \sqrt{1 - \gamma_{30} - \gamma_{31} - \gamma_{32}} \end{pmatrix},$$

$$K_{01} = \begin{pmatrix} 0 & \sqrt{\gamma_{10}} & 0 & 0 \\ 0 & 0 & 0 & 0 \\ 0 & 0 & 0 & 0 \\ 0 & 0 & 0 & 0 \end{pmatrix}, K_{02} = \begin{pmatrix} 0 & 0 & \sqrt{\gamma_{20}} & 0 \\ 0 & 0 & 0 & 0 \\ 0 & 0 & 0 & 0 \\ 0 & 0 & 0 & 0 \end{pmatrix}, K_{12} = \begin{pmatrix} 0 & 0 & 0 & 0 \\ 0 & 0 & \sqrt{\gamma_{21}} & 0 \\ 0 & 0 & 0 & 0 \\ 0 & 0 & 0 & 0 \end{pmatrix}, \quad (4.1.2)$$

$$K_{03} = \begin{pmatrix} 0 & 0 & 0 & \sqrt{\gamma_{30}} \\ 0 & 0 & 0 & 0 \\ 0 & 0 & 0 & 0 \\ 0 & 0 & 0 & 0 \end{pmatrix}, K_{13} = \begin{pmatrix} 0 & 0 & 0 & 0 \\ 0 & 0 & 0 & \sqrt{\gamma_{31}} \\ 0 & 0 & 0 & 0 \\ 0 & 0 & 0 & 0 \end{pmatrix}, K_{23} = \begin{pmatrix} 0 & 0 & 0 & 0 \\ 0 & 0 & 0 & 0 \\ 0 & 0 & 0 & \sqrt{\gamma_{32}} \\ 0 & 0 & 0 & 0 \end{pmatrix}.$$

Given a generic input  $\rho \in \sigma(\mathcal{H}_4)$ :

$$\rho \equiv \begin{pmatrix} \rho_{00} & \rho_{01} & \rho_{02} & \rho_{03} \\ \rho_{01}^* & \rho_{11} & \rho_{12} & \rho_{13} \\ \rho_{02}^* & \rho_{12}^* & \rho_{22} & \rho_{23} \\ \rho_{03}^* & \rho_{13}^* & \rho_{23}^* & \rho_{33} \end{pmatrix}, \quad (4.1.3)$$

the corresponding output state of the channel  $\Phi_{\Gamma}^{(4)}$  is:

$$\Phi_{\Gamma}^{(4)}(\rho) = \begin{pmatrix} \rho_{00} + \gamma_{10}\rho_{11} + \gamma_{20}\rho_{22} + \gamma_{30}\rho_{33} & \sqrt{1 - \gamma_{10}}\rho_{01} & \sqrt{1 - \gamma_{20} - \gamma_{21}}\rho_{02} & \sqrt{1 - \gamma_{30} - \gamma_{31} - \gamma_{32}}\rho_{03} \\ \rho_{01}^*\sqrt{1 - \gamma_{10}} & (1 - \gamma_{10})\rho_{11} + \gamma_{21}\rho_{22} + \gamma_{31}\rho_{33} & \sqrt{1 - \gamma_{10}}\sqrt{1 - \gamma_{20} - \gamma_{21}}\rho_{12} & \sqrt{1 - \gamma_{10}}\sqrt{1 - \gamma_{30} - \gamma_{31} - \gamma_{32}}\rho_{13} \\ \rho_{02}^*\sqrt{1 - \gamma_{20} - \gamma_{21}} & \rho_{12}^*\sqrt{1 - \gamma_{10}}\sqrt{1 - \gamma_{20} - \gamma_{21}} & (1 - \gamma_{20} - \gamma_{21})\rho_{22} + \gamma_{32}\rho_{33} & \sqrt{1 - \gamma_{20} - \gamma_{21}}\sqrt{1 - \gamma_{30} - \gamma_{31} - \gamma_{32}}\rho_{23} \\ \rho_{03}^*\sqrt{1 - \gamma_{30} - \gamma_{31} - \gamma_{32}} & \rho_{13}^*\sqrt{1 - \gamma_{10}}\sqrt{1 - \gamma_{30} - \gamma_{31} - \gamma_{32}} & \rho_{23}^*\sqrt{1 - \gamma_{20} - \gamma_{21}}\sqrt{1 - \gamma_{30} - \gamma_{31} - \gamma_{32}} & (1 - \gamma_{30} - \gamma_{31} - \gamma_{32})\rho_{33} \end{pmatrix}, \quad (4.1.4)$$

while the output state of the complementary channel  $\tilde{\Phi}_{\Gamma}^{(4)}$  is a  $7 \times 7$  matrix that does not fit within the margins of this document; its form can be nonetheless obtained using [these Mathematica notebooks](#). Refer to Figure 4.1.1 for a schematic representation of 4-dimensional MAD channels.

## 4.2 Composition of MAD channels

As seen in (3.3.14) and (3.1.5), MAD channels in  $d = 2$  (ADC's) and  $d = 3$  are closed under composition, meaning that the composition of two  $d$ -dimensional MAD channels for  $d = 2, 3$  is still a  $d$ -dimensional MAD channel, whose transition probabilities can be

found and depend on the transition probabilities of the starting channels. In this section, a general rule for the composition of  $d$ -dimensional will be derived. The closeness of these channels under composition will be first assumed and then verified *a posteriori* using the composition rules that were found. First, one needs to define three transition matrices  $\Gamma, \Gamma', \Gamma''$ , whose transition probabilities are, respectively,  $\gamma_{ji}, \gamma'_{ji}, \gamma''_{ji}$ ; then, one reminds that, substituting (3.3.1) into (2.5.4), MAD channels assume the form:

$$\Phi_\Gamma(\rho) = \sum_{i=0}^{j-1} \sum_{j=1}^{d-1} \gamma_{ji} \rho_{jj} |i\rangle\langle i| + \sum_{i=0}^{d-1} \sum_{j=1}^{d-1} \sqrt{\gamma_{ii}\gamma_{jj}} \rho_{ij} |i\rangle\langle j|. \quad (4.2.1)$$

One may try to write:

$$\Phi_\Gamma = \Phi_{\Gamma''} \circ \Phi_{\Gamma'} \quad (4.2.2)$$

and try to find a function  $f$  such that:

$$\Gamma = f(\Gamma', \Gamma''). \quad (4.2.3)$$

If one were to write  $\Phi_{\Gamma''} \circ \Phi_{\Gamma'}(\rho)$  in the form (4.2.1), they would obtain:

$$\begin{aligned} \Phi_{\Gamma''} \circ \Phi_{\Gamma'}(\rho) &= \sum_{i=0}^{l-1} \sum_{l=1}^{j-1} \sum_{j=1}^{d-1} \gamma''_{li} \gamma'_{jl} \rho_{jj} |i\rangle\langle i| + \\ &\quad \sum_{i=0}^{j-1} \sum_{j=1}^{d-1} \gamma''_{ii} \gamma'_{ji} \rho_{jj} |i\rangle\langle i| + \\ &\quad \sum_{i=0}^{j-1} \sum_{j=1}^{d-1} \gamma''_{ji} \gamma'_{jj} \rho_{jj} |i\rangle\langle i| + \\ &\quad \sum_{i=0}^{d-1} \sum_{j=1}^{d-1} \sqrt{\gamma''_{ii} \gamma'_{ii} \gamma''_{jj} \gamma'_{jj}} \rho_{ij} |i\rangle\langle j|, \end{aligned} \quad (4.2.4)$$

which, employing the last property in (3.3.3), translates to

$$\Phi_{\Gamma''} \circ \Phi_{\Gamma'}(\rho) = \sum_{i=0}^{j-1} \sum_{j=1}^{d-1} \left( \sum_{l=0}^{d-1} \gamma''_{li} \gamma'_{jl} \right) \rho_{jj} |i\rangle\langle i| + \sum_{i=0}^{d-1} \sum_{j=1}^{d-1} \sqrt{\gamma''_{ii} \gamma'_{ii} \gamma''_{jj} \gamma'_{jj}} \rho_{ij} |i\rangle\langle j|. \quad (4.2.5)$$

This would represent the right hand side of (4.2.2) for a generic input  $\rho$ . By direct computation, it is possible to verify that fixing the composition laws:

$$\gamma_{ji} = \sum_{l=0}^{d-1} \gamma''_{li} \gamma'_{jl} \quad \forall i \leq j \quad (4.2.6)$$

reduces (4.2.5) to (4.2.1). Therefore, it is possible to infer that the composition of two  $d$ -dimensional MAD channels is a  $d$ -dimensional MAD channel, whose transition

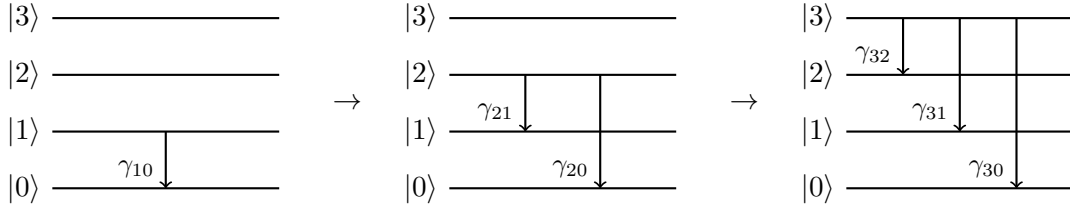


**Figure 4.2.1:** Visual representation of the decomposition of a 4-dimensional MAD channel using (4.2.11), read from left to right in "chronological" order. Thanks to (4.2.11), one could interpret a generic 4-dimensional MAD channel as the action of a single decay from  $|1\rangle$  to  $|0\rangle$ , followed by a double decay from  $|2\rangle$  to  $|1\rangle$  and  $|0\rangle$ , followed by a triple decay from  $|3\rangle$  to  $|2\rangle$ ,  $|1\rangle$  and  $|0\rangle$ .

probabilities depend on those of the initial channels as in (4.2.6). In terms of transition matrices, (4.2.6) can easily be obtained by setting  $f(\Gamma', \Gamma'') \equiv \Gamma'\Gamma''$  in (4.2.3), so that the composition rules of MAD channels can be summarized by:

$$\begin{aligned} \Phi_\Gamma &= \Phi_{\Gamma''} \circ \Phi_{\Gamma'}, \\ \Gamma &= \Gamma'\Gamma''. \end{aligned} \quad (4.2.7)$$

### 4.2.a Useful decompositions of MAD channels

Following (4.2.7), one could find various decompositions of a generic MAD channels which may help to simplify the process of finding the capacity of the channel. In this section, the most intuitive decompositions will be listed.

#### Separated decays from increasing levels

This decomposition is the easiest to derive and also the most useful; it is found by defining the matrices:

$$\begin{aligned} \Gamma_k &\equiv \mathbb{1}_d + \sum_{i=0}^{k-1} \gamma_{ki} |k\rangle\langle i| - \sum_{i=0}^{k-1} \gamma_{ki} |k\rangle\langle k|, \\ \Gamma^{(k)} &\equiv \mathbb{1}_d + \sum_{j=1}^{k-1} \sum_{i=0}^{j-1} \gamma_{ji} |j\rangle\langle i| - \sum_{j=1}^{k-1} \sum_{i=0}^{j-1} \gamma_{ji} |j\rangle\langle j|, \end{aligned} \quad (4.2.8)$$

where  $k < d$  and  $\Gamma_k$  represents a special kind of MAD channel where only the level  $|k\rangle$  is allowed to decay, while  $\Gamma^{(k)}$  represents a MAD channel where the decays from levels  $|k\rangle$  and upwards are forbidden. In this setting, the most generic  $d$ -dimensional transition matrix  $\Gamma$  in (3.3.4) is equal to  $\Gamma^{(d)}$ . By direct computation, setting  $k = d - 1$  in (4.2.8) leads to:

$$\Gamma^{(d)} = \Gamma^{(d-1)} \Gamma_{d-1}, \quad (4.2.9)$$

then, by iterating (4.2.9), one arrives at the decomposition:

$$\Gamma = \Gamma^{(d)} = \Gamma_1 \Gamma_2 \dots \Gamma_{d-1}, \quad (4.2.10)$$

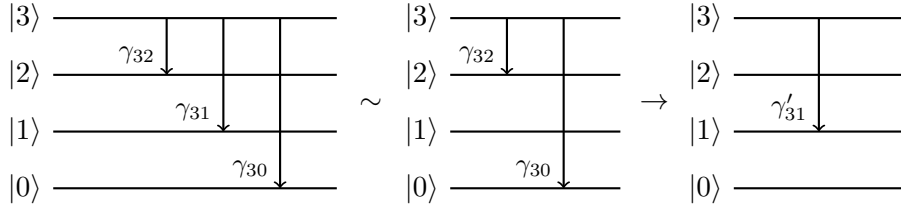


**Figure 4.2.2:** Example of the decomposition in (4.2.13), having fixed  $k = 3, n = 1$  for 4-dimensional MAD channels, read from left to right in "chronological" order. In this case, (4.2.13) implies that the 4-dimensional MAD channel representing decays from level  $|3\rangle$  onto lower levels can be decomposed by isolating a single decay, which is performed after a transition encompassing all the other decays and with a modified transition probability, defined in (4.2.13).

which, by employing (4.2.7), translates to:

$$\Phi_\Gamma = \Phi_{\Gamma_{d-1}} \circ \dots \circ \Phi_{\Gamma_1}. \quad (4.2.11)$$

Intuitively speaking, (4.2.11) means that in a MAD channel, the lower energy levels "have precedence" when decaying, as represented in Figure 4.2.1.

The matrices  $\Gamma_k$  can be decomposed even further: one needs to define the matrices:

$$\begin{aligned} \Gamma_k^{(n)} &\equiv \mathbb{1}_d + \gamma'_{kn} |k\rangle\langle n| - \gamma_{kn} |k\rangle\langle k|, \\ T_k^{(n)} &\equiv \mathbb{1}_d + \sum_{\substack{i=0 \\ i \neq n}}^{k-1} \gamma_{ki} |k\rangle\langle i| - \sum_{\substack{i=0 \\ i \neq n}}^{k-1} \gamma_{ki} |k\rangle\langle k|, \\ T_k^{(n)} &= \Gamma_k - \gamma_{kn} |k\rangle\langle n| + \gamma_{kn} |k\rangle\langle k|, \end{aligned} \quad (4.2.12)$$

where  $n < k$ ; these matrices compose in the following way:

$$\begin{aligned} \gamma'_{kn} &\equiv \gamma_{kn} \left( 1 - \sum_{\substack{i=0 \\ i \neq n}}^{k-1} \gamma_{ki} \right)^{-1}, \\ \Gamma_k &= T_k^{(n)} \Gamma_k^{(n)}. \end{aligned} \quad (4.2.13)$$

The physical interpretation is clear: in this setting, given the decays from the level  $|k\rangle$ , the decay onto the level  $|n\rangle$  needs to be performed at the end of the process. In order to achieve this, one needs to modify the amplitude  $\gamma_{kn}$  as in (4.2.13); a schematic graph of this decomposition is reported in Figure 4.2.2. Note that the denominator of  $\gamma'_{kn}$  in (4.2.13) does not depend on  $\gamma_{kn}$ .

### MAD channel as composition of single decays

One may want to expand on the idea behind (4.2.13) in order to create a composition of single transition matrices. This can be achieved by a slight redefinition of the matrices

in (4.2.12):

$$\begin{aligned}\Xi_k^{(n)} &\equiv \mathbb{1}_d + \gamma_{kn}^{(n+1)} |k\rangle\langle n| - \gamma_{kn}^{(n+1)} |k\rangle\langle k|, \\ H_k^{(n)} &\equiv \mathbb{1}_d + \sum_{i=n}^{k-1} \gamma_{ki} |k\rangle\langle i| - \sum_{i=n}^{k-1} \gamma_{ki} |k\rangle\langle k|,\end{aligned}\quad (4.2.14)$$

where  $n < k$ . The  $\Xi_k^{(n)}$ 's represent single decay MAD channels with modified amplitudes w.r.t. the original channel, while the  $H_k^{(n)}$ 's represent MAD channels where only the  $|k\rangle$  level can decay, with the same amplitudes as the original channel and having the transitions onto the lowest  $n$  levels forbidden. One can verify that:

$$H_k^{(0)} = \Gamma_k, \quad (4.2.15)$$

which matches the descriptive definition given above. In order to find the values of  $\gamma_{kn}^{(n+1)}$  in terms of the original amplitudes, one must try to solve the iterative equation:

$$H_k^{(n)} = H_k^{(n+1)} \Xi_k^{(n)}. \quad (4.2.16)$$

The (4.2.16) fixes the values of  $\gamma_{kn}^{(n+1)}$ :

$$\gamma_{kn}^{(n+1)} \equiv \frac{\gamma_{kn}}{1 - \sum_{i=n+1}^{k-1} \gamma_{ki}}, \quad (4.2.17)$$

which also implies that:

$$H_k^{(k-1)} = \Xi_k^{(k-1)}. \quad (4.2.18)$$

Using the iterative (4.2.16) and employing (4.2.15), (4.2.18) allows for the decomposition of  $\Gamma_k$  in single level transition matrices:

$$\Gamma_k = H_k^{(0)} = H_k^{(1)} \Xi_k^{(0)} = H_k^{(2)} \Xi_k^{(1)} \Xi_k^{(0)} = \dots = \Xi_k^{(k-1)} \dots \Xi_k^{(0)}. \quad (4.2.19)$$

Combining (4.2.10) and (4.2.19), it is possible to consider a generic MAD channel as a composition of single-decay MAD channels, with appropriately modified amplitudes:

$$\Gamma = \prod_{\substack{k=1 \\ \rightarrow}}^{d-1} \left( \Xi_k^{(k-1)} \dots \Xi_k^{(0)} \right), \quad (4.2.20)$$

where  $\prod_{\rightarrow}$  indicates that the product is meant to be expanded from left to right for increasing  $k$ 's. The (4.2.20) translates to:

$$\Phi_\Gamma = \bigodot_{\substack{k=1 \\ \leftarrow}}^{d-1} \left( \Phi_{\Xi_k^{(0)}} \circ \dots \circ \Phi_{\Xi_k^{(k-1)}} \right), \quad (4.2.21)$$

where  $\bigodot_{\leftarrow}$  indicates a composition of channels that is meant to be expanded from right to left for increasing  $k$ 's.

## 4.3 Equivalence of single decay MAD channels

Expanding on the ideas introduced in Subsection 3.3.f, it is possible to prove that the capacity functionals of any single decay  $d$ -dimensional MAD channel only depend on the single transition probability, not on the levels involved in the decay. Consider the swap unitaries:

$$U_{mn} \equiv \mathbb{1}_d - |m\rangle\langle m| - |n\rangle\langle n| + |m\rangle\langle n| + |n\rangle\langle m| \quad m, n \in \{0, \dots, d-1\}, \quad (4.3.1)$$

and the associated unitary quantum channels:

$$\mathcal{U}_{mn}(\bullet) \equiv U_{mn} \bullet U_{mn}; \quad (4.3.2)$$

note that, if  $m = n$ , then  $\mathcal{U}_{mn} = \text{Id}_{\sigma(\mathcal{H}_d)}$ . Let  $\Gamma_{ji}(\gamma)$ ,  $j > i$ , be a single decay transition matrix of transition probability  $\gamma$ :

$$\Gamma_{ji}(\gamma) \equiv \mathbb{1}_d + \gamma |j\rangle\langle i| - \gamma |i\rangle\langle j|, \quad (4.3.3)$$

It can be shown that:

$$\begin{aligned} \mathcal{U}_{kj} \circ \Phi_{\Gamma_{ji}(\gamma)} \circ \mathcal{U}_{kj} &= \Phi_{\Gamma_{ki}(\gamma)} \quad k > i, \\ \mathcal{U}_{ki} \circ \Phi_{\Gamma_{ji}(\gamma)} \circ \mathcal{U}_{ki} &= \Phi_{\Gamma_{jk}(\gamma)} \quad k < j. \end{aligned} \quad (4.3.4)$$

Utilizing the relations (4.3.4), it is possible to transform  $\Phi_{\Gamma_{ji}(\gamma)}$  into another single decay MAD channel  $\Phi_{\Gamma_{j'i'}(\gamma)}$ ,  $j' > i'$ . In order to achieve this, one needs to distinguish the two cases where  $j' \geq j$  or  $j' < j$ :

$$\begin{aligned} j' \geq j \Rightarrow \Phi_{\Gamma_{j'i'}(\gamma)} &= \mathcal{U}_{i'i} \circ \mathcal{U}_{j'j} \circ \Phi_{\Gamma_{ji}(\gamma)} \circ \mathcal{U}_{j'j} \circ \mathcal{U}_{i'i}, \\ j' < j \Rightarrow \Phi_{\Gamma_{j'i'}(\gamma)} &= \mathcal{U}_{j'j} \circ \mathcal{U}_{i'i} \circ \Phi_{\Gamma_{ji}(\gamma)} \circ \mathcal{U}_{i'i} \circ \mathcal{U}_{j'j}. \end{aligned} \quad (4.3.5)$$

Employing (4.3.5) and the pipeline inequalities (2.14.1), one can conclude that the capacity functionals of single decay MAD channels depend only on their transition probability, not on the levels involved in the decay. These covariance relations were to be expected, as the unitaries involved represent a swap in the "labels" of the levels upon which they act. As long as changing the labels does not require modifying the nature of the channel (e.g. swapping the labels  $|2\rangle$  and  $|1\rangle$  for  $\Phi_{\Gamma_{21}(\gamma)}$  implies that the channel is no longer a MAD channel, as the decay becomes a transition from a lower to a higher energy level), those operations are always permitted.

## 4.4 Composition of degradable channels

The topic of this section is not strictly related to MAD channels; however, its usefulness in the derivation of the degradability zone of MAD's will become apparent in Section

[4.7.](#) Given two LCPT maps  $\Psi_1, \Psi_2$  and their composition  $\Psi \equiv \Psi_2 \circ \Psi_1$ , it will be shown that:

$$\begin{aligned} \Psi &= \Psi_2 \circ \Psi_1, \\ \Psi \text{ degradable} &\Rightarrow \Psi_1, \Psi_2 \text{ degradable}, \end{aligned} \quad (4.4.1)$$

or, more eloquently:

$$\begin{aligned} \Psi &= \Psi_2 \circ \Psi_1, \\ \exists \Lambda \text{ LCPT} : \Lambda \circ \Psi = \tilde{\Psi} &\Rightarrow \begin{cases} \exists \Lambda_1 \text{ LCPT} : \Lambda_1 \circ \Psi_1 = \tilde{\Psi}_1, \\ \exists \Lambda_2 \text{ LCPT} : \Lambda_2 \circ \Psi_2 = \tilde{\Psi}_2. \end{cases} \end{aligned} \quad (4.4.2)$$

### Complementary channels equivalence

The complementary channel  $\tilde{\Psi}$  is unitarily equivalent to its counterpart written in terms of the channels  $\Psi_{1,2}$ :

$$\tilde{\Psi}'(\rho) = \tilde{\Psi}_1(\rho)_{E1} \otimes \tilde{\Psi}_2(\Psi_1(\rho))_{E2}, \quad (4.4.3)$$

i.e. the output of the complementary channel of  $\Psi$ , in this representation, corresponds to the tensor product of two environment states in the systems  $E1, E2$ . By [\(2.6.4\)](#), there must exist a unitary transformation  $\mathfrak{V}$  such that:

$$\tilde{\Psi}'(\rho) = \mathfrak{V} \left( \tilde{\Psi}(\rho) \right) = V \tilde{\Psi}(\rho) V^\dagger. \quad (4.4.4)$$

### $\Psi_2$ is degradable

Define  $\rho_1 \equiv \Psi_1(\rho)$ ; using this definition, the degradability hypothesis of  $\Psi$  reads:

$$\tilde{\Psi}(\rho) = \Lambda \circ \Psi_2(\rho_1). \quad (4.4.5)$$

One can then build the LCPT channel  $\Omega_2$ :

$$\Omega_2 \equiv \text{tr}_{E1} \circ \mathfrak{V}, \quad (4.4.6)$$

where  $\text{tr}_{E1}$  is the LCPT channel describing the partial trace over the  $E1$  environment. Applying  $\Omega_2$  to [\(4.4.5\)](#) leads to:

$$\tilde{\Psi}_2(\rho_1) = \Omega_2 \circ \Lambda \circ \Psi_2(\rho_1). \quad (4.4.7)$$

Therefore, if one thought of  $\Psi_1$  as a state preparation device, by defining the LCPT  $\Lambda_2 \equiv \Omega_2 \circ \Lambda$  one would obtain:

$$\tilde{\Psi}_2 = \Lambda_2 \circ \Psi_2, \quad (4.4.8)$$

proving the degradability of  $\Phi_2$ .

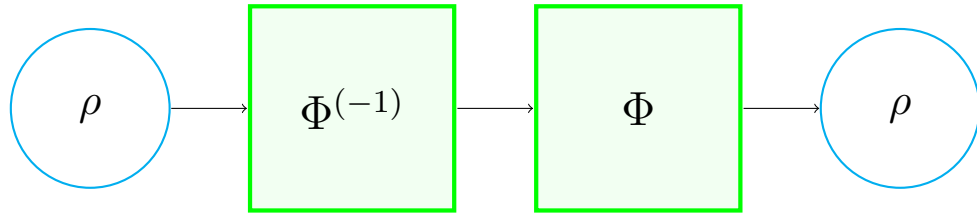


**Figure 4.5.1:** The map  $\Phi^{(-1)}$  acts as the right inverse of the MAD channel  $\Phi$

### $\Psi_1$ is degradable

Define the LCPT map:

$$\Omega_1 \equiv \text{tr}_{E2} \circ \mathfrak{V}. \quad (4.4.9)$$

Starting from  $\tilde{\Psi} = \Lambda \circ \Psi$ , apply  $\Omega_1$  to both sides, which yields:

$$\tilde{\Psi}_1 = \Omega_1 \circ \Lambda \circ \Psi_2 \circ \Psi_1. \quad (4.4.10)$$

Then, one could define the LCPT

$$\Lambda_1 = \Omega_1 \circ \Lambda \circ \Psi_2, \quad (4.4.11)$$

which can be substituted into (4.4.10):

$$\tilde{\Psi}_1 = \Lambda_1 \circ \Psi_1. \quad (4.4.12)$$

(4.4.12) and (4.4.8) together prove (4.4.2).

## 4.5 Inverse maps of MAD channels

It is not always possible to find the (left or right) inverse map of a LCPT channel, a clear example of this fact are the channels which send a  $D$ -dimensional system into a  $d$ -dimensional system, where  $d < D$ . This is not the case for MAD channels; in fact it turns out that their inverse maps has a rather intuitive, albeit convoluted, definition. In the following, the right inverse map (represented in Figure 4.5.1) of a generic MAD channel will be derived.

### 4.5.a Inverse maps of ADC's

The inverse map of an ADC provides a valuable guide for the derivation of the inverse of a MAD channel. The reader can find a description of ADC's in Section 3.1. The scope of this subsection is to find the right inverse map of an ADC:

$$\begin{aligned} A_\gamma^{-1} : \sigma(\mathcal{H}_2) &\mapsto \sigma(\mathcal{H}_2), \\ A_\gamma \circ A_\gamma^{-1}(\rho) &= \rho. \end{aligned} \quad (4.5.1)$$

The map  $A_\gamma^{-1}$ , while trace preserving and linear, is not expected to be completely positive, therefore it is not expected to be a quantum channel. In fact it could be cast in a "pseudo-Kraus" representation:

$$A_\gamma^{-1}(\theta) = \tilde{K}_0(\gamma)\theta\tilde{K}_0(\gamma)^\dagger - \tilde{K}_1(\gamma)\theta\tilde{K}_1(\gamma)^\dagger,$$

$$\tilde{K}_0(\gamma) = \begin{pmatrix} 1 & 0 \\ 0 & \frac{1}{\sqrt{1-\gamma}} \end{pmatrix} \quad \tilde{K}_1(\gamma) = \begin{pmatrix} 0 & \sqrt{\frac{\gamma}{1-\gamma}} \\ 0 & 0 \end{pmatrix}. \quad (4.5.2)$$

Notice that, while  $\tilde{K}_0(\gamma)$  and  $\tilde{K}_1(\gamma)$  form a Kraus set, the " $-$ " sign in (4.5.2) implies that  $A_\gamma^{-1}$  is **not** necessarily a quantum channel, as it is not written in the Kraus representation. One could also write (4.5.2) in matrix form:

$$A_\gamma^{-1}(\theta) = \begin{pmatrix} \theta_{00} - \frac{\gamma}{1-\gamma}\theta_{11} & \frac{1}{\sqrt{1-\gamma}}\theta_{01} \\ \frac{1}{\sqrt{1-\gamma}}\theta_{01}^* & \frac{1}{(1-\gamma)}\theta_{11} \end{pmatrix}. \quad (4.5.3)$$

The map defined in (4.5.1) is also the left-inverse of  $A_\gamma$ , which can be verified by direct computation.

#### 4.5.b Inverse of single decay MAD channels

Consider the MAD channel  $\Phi_{\Xi_k^{(n)}}$ , where  $\Xi_k^{(n)}$  is defined in (4.2.14) and the associated transition probability can be found in (4.2.17). This is a single decay MAD channel, which acts on the subspace spanned by  $|k\rangle$  and  $|n\rangle$  as an ADC with the same transition probability. Therefore, one might be tempted to define the right-inverse of  $\Phi_{\Xi_k^{(n)}}$  as the embedding onto  $\mathcal{H}_d$  of the right-inverse of an ADC. Let  $\Phi_{\Xi_k^{(n)}}^{-1}$  be the right inverse of  $\Phi_{\Xi_k^{(n)}}$ . Given  $\theta \in \sigma(\text{span}\{|k\rangle, |n\rangle\})$ ,  $\Phi_{\Xi_k^{(n)}}^{-1}$  needs to satisfy:

$$\Phi_{\Xi_k^{(n)}}^{-1}(\theta) = \begin{pmatrix} \theta_{nn} - \gamma_{kn}^{(n+1)} \left(1 - \gamma_{kn}^{(n+1)}\right)^{-1} \theta_{kk} & \left(1 - \gamma_{kn}^{(n+1)}\right)^{-1/2} \theta_{nk} \\ \left(1 - \gamma_{kn}^{(n+1)}\right)^{-1/2} \theta_{nk}^* & \left(1 - \gamma_{kn}^{(n+1)}\right)^{-1} \theta_{kk} \end{pmatrix}. \quad (4.5.4)$$

This can be achieved by defining  $\Phi_{\Xi_k^{(n)}}^{-1}$  as:

$$\Phi_{\Xi_k^{(n)}}^{(-1)}(\rho) \equiv \tilde{K}_0\left(\Xi_k^{(n)}\right) \rho \tilde{K}_0\left(\Xi_k^{(n)}\right)^\dagger - \tilde{K}_1\left(\Xi_k^{(n)}\right) \rho \tilde{K}_1\left(\Xi_k^{(n)}\right)^\dagger,$$

$$\tilde{K}_0\left(\Xi_k^{(n)}\right) \equiv \mathbb{1}_d - \left(1 - \left(1 - \gamma_{kn}^{(n+1)}\right)^{-1/2}\right) |k\rangle\langle k|, \quad (4.5.5)$$

$$\tilde{K}_1\left(\Xi_k^{(n)}\right) \equiv \left(\frac{\gamma_{kn}^{(n+1)}}{1 - \gamma_{kn}^{(n+1)}}\right)^{1/2} |n\rangle\langle k|,$$

where  $\rho \in \sigma(\mathcal{H}_d)$ . It is possible to show, by direct computation, that:

$$\Phi_{\Xi_k^{(n)}} \circ \Phi_{\Xi_k^{(n)}}^{-1}(\rho) = \rho \quad \forall \rho \in \sigma(\mathcal{H}_d). \quad (4.5.6)$$

Notice that the map  $\Phi_{\Xi_k^{(n)}}^{-1}$  is linear and trace preserving and is also the left-inverse of  $\Phi_{\Xi_k^{(n)}}$ .

### 4.5.c Inverse map as composition of inverse maps of single decays

The importance of (4.5.6) lies in the fact that it can be composed to generate the right-inverse map of a general MAD channel. In fact, recall that in (4.2.21) it was shown that a MAD channel can be seen as a composition of single decay MAD channels. Then, by "inverting" those single decay transitions one by one, the resulting channel must be the identity channel. This line of reasoning results in the definition:

$$\Phi_{\Gamma}^{-1} = \bigodot_{k=1}^{d-1} \left( \Phi_{\Xi_k^{(k-1)}}^{-1} \circ \dots \circ \Phi_{\Xi_k^{(0)}}^{-1} \right) \quad (4.5.7)$$

which, by construction, satisfies:

$$\Phi_{\Gamma} \circ \Phi_{\Gamma}^{-1} = \text{Id}. \quad (4.5.8)$$

Since each of the  $\Phi_{\Xi_k^{(n)}}^{-1}$ 's is linear and trace preserving, and a generic composition of such maps holds those same properties, then  $\Phi_{\Gamma}^{-1}$  must also be linear and trace preserving.

Notice, finally, that  $\Phi_{\Gamma}^{-1}$ , again, by construction, is also the left inverse of  $\Phi_{\Gamma}$ .

## 4.6 Degradability of MAD channels

As seen in Section 2.12, the quantum capacity of degradable channels is computable and corresponds to the maximum (calculated over all possible inputs) of the coherent information (2.12.3). Therefore, it is important to find a complete characterization of the degradability conditions of MAD channels.

Since MAD channels admit a right inverse map, starting from (2.7.1), verifying the degradability of  $\Phi_{\Gamma}$  reduces to verifying that  $\Lambda_{\Gamma}$  in:

$$\Lambda_{\Gamma} \equiv \tilde{\Phi}_{\Gamma} \circ \Phi_{\Gamma}^{-1} \quad (4.6.1)$$

is LCPT. The map  $\Lambda_{\Gamma}$  is linear and trace preserving by construction, while the complete positiveness is not guaranteed; using Choi's theorem (2.5.17), it is possible to verify whether or not  $\Lambda_{\Gamma}$  satisfies that last property:

$$\Lambda_{\Gamma} \text{ is completely positive} \Leftrightarrow C_{\Lambda_{\Gamma}} \text{ is positive}, \quad (4.6.2)$$

where  $C_{\Lambda_\Gamma}$  is the Choi matrix of the map  $\Lambda_\Gamma$ , defined as in (2.5.12)<sup>1</sup>.

$$C_{\Lambda_\Gamma} \equiv \frac{1}{d} [\Lambda_\Gamma \otimes \text{Id}] (|\Omega\rangle\langle\Omega|), \quad (4.6.3)$$

$|\Omega\rangle\langle\Omega|$  maximally entangled state.

The computation of the eigenvalues of  $C_{\Lambda_\Gamma}$  for a generic 4-dimensional  $\Gamma$  turns out to be relatively demanding for a desktop computer (see Section 7.2 for details on computation methods), but all degradability regions can be found regardless by means of lateral thinking that simplifies the computation tasks, as demonstrated in Section 4.7.

## 4.7 Degradability of 4-dimensional MAD channels

In Subsection 3.3.i, the degradability regions for 3-dimensional MAD channels were determined by ensuring that the rank of the output state of the channel was not smaller than the rank of the state of the environment (3.3.44), which implied reducing the number of decays in the channel, and checking *a posteriori* whether or not less strict degradability conditions could be found by introducing additional decays to those regions. In the case of 4-dimensional MAD channels  $\Phi_\Gamma^{(4)}$ , (3.3.44) becomes:

$$\text{rank}(\Phi_\Gamma^{(4)}(\rho)) \geq \text{rank}(\tilde{\Phi}_\Gamma^{(4)}(\rho)) \quad \forall \rho, \quad (4.7.1)$$

which implies that the number of decays in the channel needs to not exceed 3. The number of 4-dimensional MAD channels with 3 decays can be found by counting the number of ways one can select 3 different couples  $(j, i)$ , where  $j < i$ ; the number of such couples is  $\binom{4}{2} = 6$ , which means that the number of 3-decay configurations is  $\binom{6}{3} = 20$ ; many of these configurations are unitarily equivalent.

In what follows, 4-dimensional MAD channels connected by unitary transformations of the form (4.3.2) will be grouped in **Classes**; one can identify 9 Classes of 3-decay channels, 4 Classes of 2-decay channels and 1 Class of single decay channels.

### 4.7.a Class 1A

This class identifies the single decay MAD channels; as seen in Section 4.3, if the transition probability is fixed, all possible configurations of single decay MAD's are unitarily equivalent. Let  $\Phi_{\Gamma_{1A}(\gamma)}$  be a generic channel belonging to Class 1A, with transition probability  $\gamma$ . This class presents the PCDS structure (3.2.1), where  $\Phi_{BB} =$

---

<sup>1</sup>the factor  $1/d$  is kept here for the sake of consistency, but is obviously not necessary when checking for positiveness

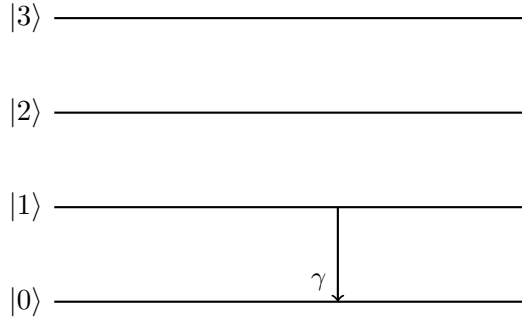


**Figure 4.7.1:** Class 1A consists of an ADC embedded into the higher dimensional  $\mathcal{H}_4$

$\text{Id}_{\sigma(\mathcal{H}_2)}$  and  $\Phi_{\text{AA}} = \text{ADC}_\gamma$  an amplitude damping channel; therefore, following (3.2.2), the degradability conditions of  $\Phi_{\Gamma_{1A}(\gamma)}$  are the same as those given in (3.1.15):

$$\Phi_{\Gamma_{1A}(\gamma)} \text{ degradable} \Leftrightarrow \gamma \leq \frac{1}{2}. \quad (4.7.2)$$

The existence of a noiseless subspace guarantees that  $\Phi_{\Gamma_{1A}(\gamma)}$  is never antidegradable.

#### 4.7.b Class 2A

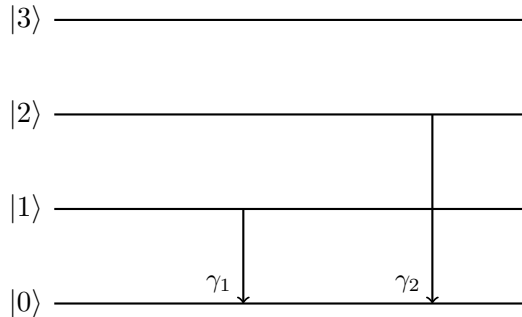


**Figure 4.7.2:** An example of channel belonging in Class 2A is provided by the embedding of  $\Phi_{\Gamma(\gamma_1, \gamma_2, 0)}^{(3)}$  in  $\mathcal{H}_4$ .

Channels belonging to this class are unitarily equivalent to the MAD channel identified by the transition matrix  $\Gamma = \mathbf{1}_4 + \gamma_1 |1\rangle\langle 0| - \gamma_1 |1\rangle\langle 1| + \gamma_2 |2\rangle\langle 0| - \gamma_2 |2\rangle\langle 2|$ , depicted in Figure 4.7.2. Let a generic channel in this class be called  $\Phi_{\Gamma_{2A}(\gamma_1, \gamma_2)}$ ; this channel presents the PCDS structure (3.2.1), where  $\Phi_{\text{BB}} = \text{Id}_{\sigma(\mathcal{H}_1)}$  and  $\Phi_{\text{AA}} = \Phi_{\Gamma(\gamma_1, \gamma_2, 0)}^{(3)}$ , where  $\Phi_{\Gamma(\gamma_1, \gamma_2, 0)}^{(3)}$  is the 3-dimensional MAD channel defined in (3.3.28). Following (3.2.2), the degradability conditions of  $\Phi_{\Gamma_{2A}(\gamma_1, \gamma_2)}$  are the same as those given in (3.3.55):

$$\Phi_{\Gamma_{2A}(\gamma_1, \gamma_2)} \text{ degradable} \Leftrightarrow \gamma_1 \leq \frac{1}{2} \wedge \gamma_2 \leq \frac{1}{2}. \quad (4.7.3)$$

The existence of a noiseless subspace guarantees that  $\Phi_{\Gamma_{2A}(\gamma_1, \gamma_2)}$  is never antidegradable.

### 4.7.c Class 2B

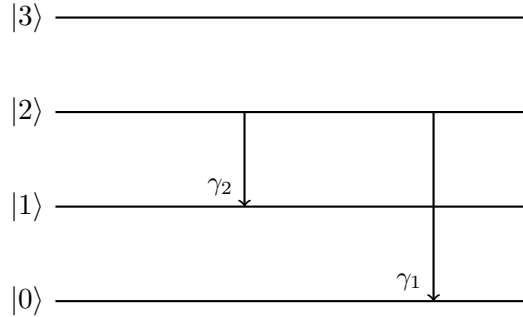


**Figure 4.7.3:** An example of channel belonging in **Class 2B** is provided by the embedding of  $\Phi_{\Gamma(0,\gamma_1,\gamma_2)}^{(3)}$  in  $\mathcal{H}_4$ .

Channels belonging to this class are unitarily equivalent to the MAD channel identified by the transition matrix  $\Gamma = \mathbb{1}_4 + \gamma_1 |2\rangle\langle 0| + \gamma_2 |2\rangle\langle 1| - (\gamma_1 + \gamma_2) |2\rangle\langle 2|$ , depicted in Figure 4.7.3. Let a generic channel in this class be called  $\Phi_{\Gamma_{2B}(\gamma_1,\gamma_2)}$ ; this channel presents the PCDS structure (3.2.1), where  $\Phi_{BB} = \text{Id}_{\sigma(\mathcal{H}_1)}$  and  $\Phi_{AA} = \Phi_{\Gamma(0,\gamma_1,\gamma_2)}^{(3)}$ . Following (3.2.2), the degradability conditions of  $\Phi_{\Gamma_{2B}(\gamma_1,\gamma_2)}$  are the same as those given in (3.3.48):

$$\Phi_{\Gamma_{2B}(\gamma_1,\gamma_2)} \text{ degradable} \Leftrightarrow \gamma_1 + \gamma_2 \leq \frac{1}{2}. \quad (4.7.4)$$

The existence of a noiseless subspace guarantees that  $\Phi_{\Gamma_{2B}(\gamma_1,\gamma_2)}$  is never antidegradable.

### 4.7.d Class 2C

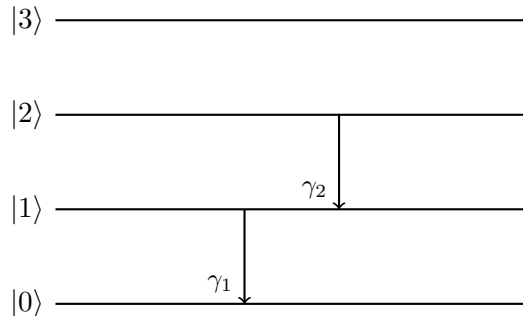


**Figure 4.7.4:** An example of channel belonging in **Class 2C** is provided by the embedding of  $\Phi_{\Gamma(\gamma_1,0,\gamma_2)}^{(3)}$  in  $\mathcal{H}_4$ .

Channels belonging to this class are unitarily equivalent to the MAD channel identified by the transition matrix  $\Gamma = \mathbb{1}_4 + \gamma_1 |1\rangle\langle 0| - \gamma_1 |1\rangle\langle 1| + \gamma_2 |2\rangle\langle 1| - \gamma_2 |2\rangle\langle 2|$ , depicted in Figure 4.7.4. Let a generic channel in this class be called  $\Phi_{\Gamma_{2C}(\gamma_1,\gamma_2)}$ ; this

channel presents the PCDS structure (3.2.1), where  $\Phi_{BB} = \text{Id}_{\sigma(\mathcal{H}_1)}$  and  $\Phi_{AA} = \Phi_{\Gamma(\gamma_1, 0, \gamma_2)}^{(3)}$ . Following (3.2.2) and Subsection 3.3.i, it can be inferred that  $\Phi_{\Gamma_{2C}(\gamma_1, \gamma_2)}$  is never degradable. The existence of a noiseless subspace guarantees that  $\Phi_{\Gamma_{2C}(\gamma_1, \gamma_2)}$  is never antidegradable.

#### 4.7.e Class 2D

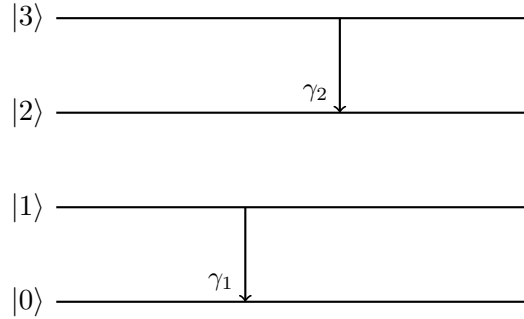


**Figure 4.7.5:** Class 2D is comprised of PCDS channels whose subchannels are ADC's

Channels belonging to this class are unitarily equivalent to the MAD channel identified by the transition matrix  $\Gamma = \mathbb{1}_4 + \gamma_1 |1\rangle\langle 0| - \gamma_1 |1\rangle\langle 1| + \gamma_2 |3\rangle\langle 2| - \gamma_2 |3\rangle\langle 3|$ , depicted in Figure 4.7.4. Let a generic channel in this class be called  $\Phi_{\Gamma_{2D}(\gamma_1, \gamma_2)}$ ; this channel presents the PCDS structure (3.2.1), where  $\Phi_{AA} = ADC_{\gamma_1}$  and  $\Phi_{BB} = ADC_{\gamma_2}$ . Following (3.2.2) and (3.1.15), the degradability conditions of  $\Phi_{\Gamma_{2D}(\gamma_1, \gamma_2)}$  are:

$$\Phi_{\Gamma_{2D}(\gamma_1, \gamma_2)} \text{ degradable} \Leftrightarrow \gamma_1 \leq \frac{1}{2} \wedge \gamma_2 \leq \frac{1}{2}. \quad (4.7.5)$$

The existence of a noiseless subspace guarantees that  $\Phi_{\Gamma_{2D}(\gamma_1, \gamma_2)}$  is never antidegradable.

#### 4.7.f Class 3A

This class of channels consists PCDS channels whose subchannels are the identity channel  $\Phi_{BB} = \text{Id}_{\sigma(\mathcal{H}_1)}$  and a 3-dimensional MAD channel  $\Phi_{AA} = \Phi_{\Gamma(\gamma_1, \gamma_2, \gamma_3)}^{(3)}$ . Turning off one of the decays reduces this class to one of the 2-decay classes:

- $\gamma_1 = 0 \Rightarrow \text{Class 3A} \sim \text{Class 2B};$
- $\gamma_2 = 0 \Rightarrow \text{Class 3A} \sim \text{Class 2C};$
- $\gamma_3 = 0 \Rightarrow \text{Class 3A} \sim \text{Class 2A}.$

Let a generic channel belonging to this class be called  $\Phi_{\Gamma_{3A}(\gamma_1, \gamma_2, \gamma_3)}$ ; following (3.2.2) and (3.3.57),  $\Phi_{\Gamma(\gamma_1, \gamma_2, \gamma_3)}^{(3)}$  is never degradable if  $\gamma_1, \gamma_2, \gamma_3 \neq 0$ . This also implies, as a consequence of (4.4.2), that it is not possible to build a 4-decay degradable MAD channel starting from a MAD channel belonging to Class 3A. The existence of a noiseless subspace guarantees that  $\Phi_{\Gamma_{3A}(\gamma_1, \gamma_2, \gamma_3)}$  is never antidegradable.

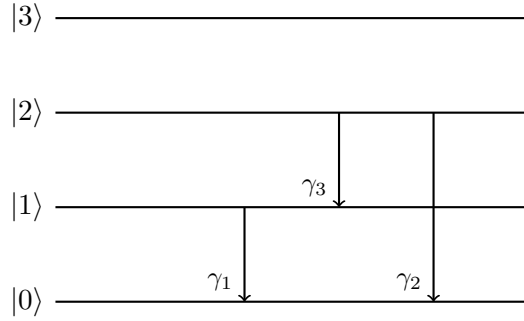


**Figure 4.7.6:** Class 3A consists of 3-dimensional MAD channels embedded into the higher dimensional  $\mathcal{H}_4$

#### 4.7.g Class 3B

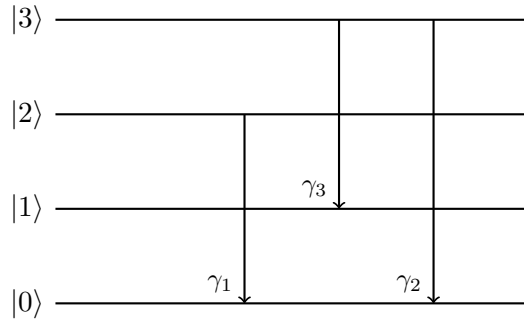


**Figure 4.7.7:** Class 3B

Consider the transition matrix:

$$\Gamma_{3B}(\gamma_1, \gamma_2, \gamma_3) = \mathbb{1}_4 + \gamma_1 |2\rangle\langle 0| + \gamma_2 |3\rangle\langle 0| + \gamma_3 |3\rangle\langle 1| - \gamma_1 |2\rangle\langle 2| - (\gamma_2 + \gamma_3) |3\rangle\langle 3|; \quad (4.7.6)$$

Class 3B is comprised of all the channels unitarily equivalent to  $\Phi_{\Gamma_{3B}(\gamma_1, \gamma_2, \gamma_3)}$ , depicted in Figure 4.7.7. Turning off one of the decays reduces this class to one of the 2-decay classes:

- $\gamma_1 = 0 \Rightarrow$  Class 3A  $\sim$  Class 2B;
- $\gamma_2 = 0 \Rightarrow$  Class 3A  $\sim$  Class 2D;
- $\gamma_3 = 0 \Rightarrow$  Class 3A  $\sim$  Class 2A.

The degradability conditions for this channel are:

$$\Phi_{\Gamma_{3B}(\gamma_1, \gamma_2, \gamma_3)} \text{ degradable} \Leftrightarrow \gamma_1 \leq \frac{1}{2} \wedge \gamma_2 + \gamma_3 \leq \frac{1}{2}. \quad (4.7.7)$$

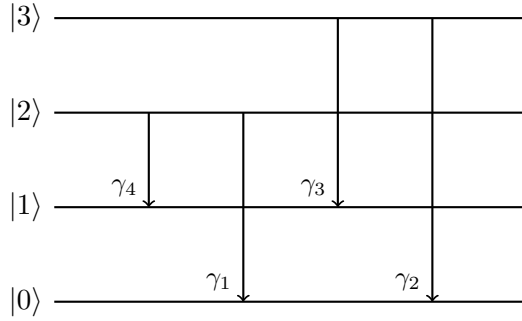


Figure 4.7.8: Class 4A

Starting from a channel in Class 3B, it is possible to build a degradable 4-decay MAD channel: consider the transition matrix:

$$\Gamma_{4A}(\gamma_1, \gamma_2, \gamma_3, \gamma_4) \equiv \Gamma_{3B}(\gamma_1, \gamma_2, \gamma_3) + \gamma_4 |2\rangle\langle 1| - \gamma_4 |2\rangle\langle 2|. \quad (4.7.8)$$

The degradability conditions for  $\Phi_{\Gamma_{4A}(\gamma_1, \gamma_2, \gamma_3, \gamma_4)}$  are:

$$\Phi_{\Gamma_{4A}(\gamma_1, \gamma_2, \gamma_3, \gamma_4)} \text{ degradable} \Leftrightarrow \gamma_1 + \gamma_4 \leq \frac{1}{2} \wedge \gamma_2 + \gamma_3 \leq \frac{1}{2}. \quad (4.7.9)$$

This channel provides a counterexample to (4.7.1), proving that the relation is not a necessary condition for the degradability of a channel. The existence of a noiseless subspace for  $\Phi_{\Gamma_{3B}(\gamma_1, \gamma_2, \gamma_3)}$  guarantees that the channel is never antidegradable.

#### 4.7.h Class 3C

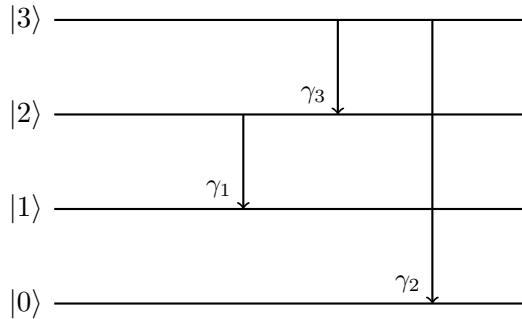


Figure 4.7.9: Class 3C

Consider the transition matrix:

$$\Gamma_{3C}(\gamma_1, \gamma_2, \gamma_3) = \mathbb{1}_4 + \gamma_1 |2\rangle\langle 1| + \gamma_2 |3\rangle\langle 0| + \gamma_3 |3\rangle\langle 2| - \gamma_1 |2\rangle\langle 2| - (\gamma_2 + \gamma_3) |3\rangle\langle 3|; \quad (4.7.10)$$

Class 3C is comprised of all the channels unitarily equivalent to  $\Phi_{\Gamma_{3C}(\gamma_1, \gamma_2, \gamma_3)}$ , depicted in Figure 4.7.9. Turning off one of the decays reduces this class to one of the 2-decay classes:

- $\gamma_1 = 0 \Rightarrow \text{Class 3C} \sim \text{Class 2B};$
- $\gamma_2 = 0 \Rightarrow \text{Class 3C} \sim \text{Class 2C};$
- $\gamma_3 = 0 \Rightarrow \text{Class 3C} \sim \text{Class 2D}.$

$\Phi_{\Gamma_{3C}(\gamma_1, \gamma_2, \gamma_3)}$  is never degradable when  $\gamma_1, \gamma_2, \gamma_3 \neq 0$ . The existence of a noiseless subspace guarantees that  $\Phi_{\Gamma_{3C}(\gamma_1, \gamma_2, \gamma_3)}$  is never antidegradable.

#### 4.7.i Class 3D

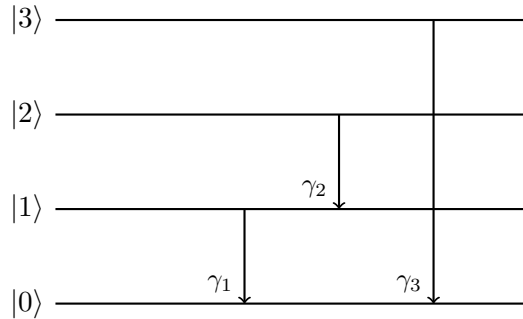


Figure 4.7.10: Class 3D

Consider the transition matrix:

$$\Gamma_{3D}(\gamma_1, \gamma_2, \gamma_3) = \mathbb{1}_4 + \gamma_1 |1\rangle\langle 0| + \gamma_2 |2\rangle\langle 1| + \gamma_3 |3\rangle\langle 0| - \gamma_1 |1\rangle\langle 1| - \gamma_2 |2\rangle\langle 2| - \gamma_3 |3\rangle\langle 3|; \quad (4.7.11)$$

Class 3D is comprised of all the channels unitarily equivalent to  $\Phi_{\Gamma_{3D}(\gamma_1, \gamma_2, \gamma_3)}$ , depicted in Figure 4.7.10. Turning off one of the decays reduces this class to one of the 2-decay classes:

- $\gamma_1 = 0 \Rightarrow \text{Class 3D} \sim \text{Class 2D};$
- $\gamma_2 = 0 \Rightarrow \text{Class 3D} \sim \text{Class 2A};$
- $\gamma_3 = 0 \Rightarrow \text{Class 3D} \sim \text{Class 2C}.$

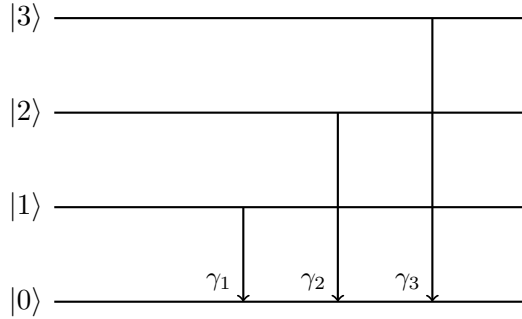
$\Phi_{\Gamma_{3D}(\gamma_1, \gamma_2, \gamma_3)}$  is never degradable when  $\gamma_1, \gamma_2, \gamma_3 \neq 0$ .

#### 4.7.j Class 3E

Consider the transition matrix:

$$\Gamma_{3E}(\gamma_1, \gamma_2, \gamma_3) = \mathbb{1}_4 + \gamma_1 |1\rangle\langle 0| + \gamma_2 |2\rangle\langle 0| + \gamma_3 |3\rangle\langle 0| - \gamma_1 |1\rangle\langle 1| - \gamma_2 |2\rangle\langle 2| - \gamma_3 |3\rangle\langle 3|; \quad (4.7.12)$$

$\Phi_{\Gamma_{3E}(\gamma_1, \gamma_2, \gamma_3)}$  is the only channel in Class 3E, depicted in Figure 4.7.11. Turning off one of the decays reduces this class to one of the 2-decay classes:

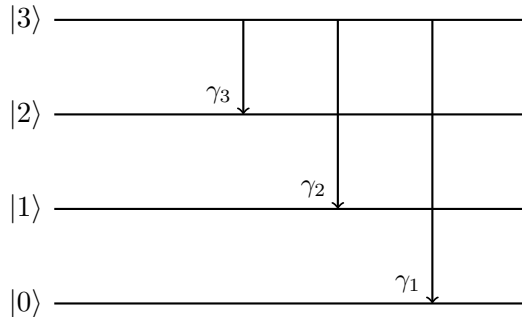
**Figure 4.7.11: Class 3E**

- $\gamma_1 = 0 \Rightarrow \text{Class 3E} \sim \text{Class 2A};$
- $\gamma_2 = 0 \Rightarrow \text{Class 3E} \sim \text{Class 2A};$
- $\gamma_3 = 0 \Rightarrow \text{Class 3E} \sim \text{Class 2A}.$

The degradability conditions for  $\Phi_{\Gamma_{3E}(\gamma_1, \gamma_2, \gamma_3)}$  are:

$$\Phi_{\Gamma_{3E}(\gamma_1, \gamma_2, \gamma_3)} \text{ degradable} \Leftrightarrow \gamma_1 \leq \frac{1}{2} \wedge \gamma_2 \leq \frac{1}{2} \wedge \gamma_3 \leq \frac{1}{2}. \quad (4.7.13)$$

#### 4.7.k Class 3F

**Figure 4.7.12: Class 3F**

Consider the transition matrix:

$$\Gamma_{3E}(\gamma_1, \gamma_2, \gamma_3) = \mathbb{1}_4 + \gamma_1 |3\rangle\langle 0| + \gamma_2 |3\rangle\langle 1| + \gamma_3 |3\rangle\langle 2| - (\gamma_1 + \gamma_2 + \gamma_3) |3\rangle\langle 3|; \quad (4.7.14)$$

$\Phi_{\Gamma_{3F}(\gamma_1, \gamma_2, \gamma_3)}$  is the only channel in Class 3F, depicted in Figure 4.7.12. Turning off one of the decays reduces this class to one of the 2-decay classes:

- $\gamma_1 = 0 \Rightarrow \text{Class 3F} \sim \text{Class 2B};$
- $\gamma_2 = 0 \Rightarrow \text{Class 3F} \sim \text{Class 2B};$

- $\gamma_3 = 0 \Rightarrow \text{Class 3F} \sim \text{Class 2B}.$

The degradability conditions for  $\Phi_{\Gamma_{3F}(\gamma_1, \gamma_2, \gamma_3)}$  are:

$$\Phi_{\Gamma_{3F}(\gamma_1, \gamma_2, \gamma_3)} \text{ degradable} \Leftrightarrow \gamma_1 \leq \frac{1}{2} \wedge \gamma_2 \leq \frac{1}{2} \wedge \gamma_3 \leq \frac{1}{2}. \quad (4.7.15)$$

The existence of a noiseless subspace guarantees that  $\Phi_{\Gamma_{3F}(\gamma_1, \gamma_2, \gamma_3)}$  is never antidegradable.

#### 4.7.1 Class 3G

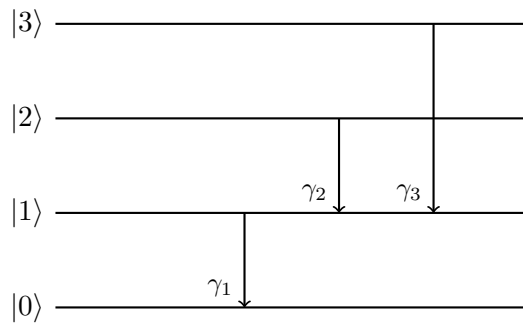


**Figure 4.7.13: Class 3G**

Consider the transition matrix:

$$\Gamma_{3G}(\gamma_1, \gamma_2, \gamma_3) = \mathbb{1}_4 + \gamma_1 |1\rangle\langle 0| + \gamma_2 |2\rangle\langle 1| + \gamma_3 |3\rangle\langle 1| - \gamma_1 |1\rangle\langle 1| - \gamma_2 |2\rangle\langle 2| - \gamma_3 |3\rangle\langle 3|; \quad (4.7.16)$$

$\Phi_{\Gamma_{3G}(\gamma_1, \gamma_2, \gamma_3)}$  is the only channel in Class 3G, depicted in Figure 4.7.13. Turning off one of the decays reduces this class to one of the 2-decay classes:

- $\gamma_1 = 0 \Rightarrow \text{Class 3G} \sim \text{Class 2A};$
- $\gamma_2 = 0 \Rightarrow \text{Class 3G} \sim \text{Class 2C};$
- $\gamma_3 = 0 \Rightarrow \text{Class 3G} \sim \text{Class 2C}.$

$\Phi_{\Gamma_{3G}(\gamma_1, \gamma_2, \gamma_3)}$  is never degradable when  $\gamma_1, \gamma_2, \gamma_3 \neq 0$ .

#### 4.7.m Class 3H

Consider the transition matrix:

$$\Gamma_{3H}(\gamma_1, \gamma_2, \gamma_3) = \mathbb{1}_4 + \gamma_1 |2\rangle\langle 0| + \gamma_2 |2\rangle\langle 1| + \gamma_3 |3\rangle\langle 2| - (\gamma_1 + \gamma_2) |2\rangle\langle 2| - \gamma_3 |3\rangle\langle 3|; \quad (4.7.17)$$

$\Phi_{\Gamma_{3H}(\gamma_1, \gamma_2, \gamma_3)}$  is the only channel in Class 3H, depicted in Figure 4.7.14. Turning off one of the decays reduces this class to one of the 2-decay classes:

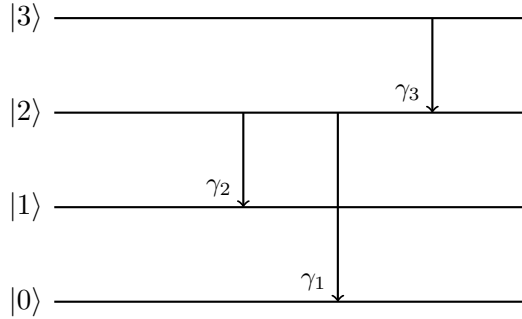


Figure 4.7.14: Class 3H

- $\gamma_1 = 0 \Rightarrow$  Class 3H  $\sim$  Class 2C;
- $\gamma_2 = 0 \Rightarrow$  Class 3H  $\sim$  Class 2C;
- $\gamma_3 = 0 \Rightarrow$  Class 3H  $\sim$  Class 2B.

$\Phi_{\Gamma_{3H}(\gamma_1, \gamma_2, \gamma_3)}$  is never degradable when  $\gamma_1, \gamma_2, \gamma_3 \neq 0$ .

#### 4.7.n Class 3I

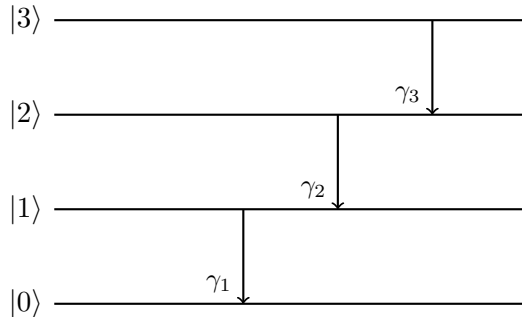


Figure 4.7.15: Class 3I

Consider the transition matrix:

$$\Gamma_{3I}(\gamma_1, \gamma_2, \gamma_3) = \mathbb{1}_4 + \gamma_1 |1\rangle\langle 0| + \gamma_2 |2\rangle\langle 1| + \gamma_3 |3\rangle\langle 2| - \gamma_1 |1\rangle\langle 1| - \gamma_2 |2\rangle\langle 2| - \gamma_3 |3\rangle\langle 3|; \quad (4.7.18)$$

$\Phi_{\Gamma_{3I}(\gamma_1, \gamma_2, \gamma_3)}$  is the only channel in Class 3I, depicted in Figure 4.7.15. Turning off one of the decays reduces this class to one of the 2-decay classes:

- $\gamma_1 = 0 \Rightarrow$  Class 3I  $\sim$  Class 2C;
- $\gamma_2 = 0 \Rightarrow$  Class 3I  $\sim$  Class 2D;
- $\gamma_3 = 0 \Rightarrow$  Class 3I  $\sim$  Class 2C.

$\Phi_{\Gamma_{3I}(\gamma_1, \gamma_2, \gamma_3)}$  is never degradable when  $\gamma_1, \gamma_2, \gamma_3 \neq 0$ .

## 4.8 Degradability of a MAD channel embedded in a higher dimensional system

The structure defined in (3.2.1) lends itself very well to the case of MAD channels; in fact, given a  $d$ -dimensional MAD channel  $\Phi_\Gamma : \sigma(\mathcal{H}_d) \mapsto \sigma(\mathcal{H}_d)$ , one may consider another MAD channel  $\Phi_{\bar{\Gamma}} : \sigma(\mathcal{H}_{d+1}) \mapsto \sigma(\mathcal{H}_{d+1})$  whose transition probabilities are:

$$\bar{\gamma}_{ji} = \begin{cases} \gamma_{ji} & \text{if } 0 \leq i < j \leq d-1, \\ 0 & \text{if } 0 \leq i < j = d. \end{cases} \quad (4.8.1)$$

In the context of (3.2.1), the  $\Phi_{AA}$  and  $\Phi_{BB}$  channels of  $\Phi_{\bar{\Gamma}}$  are  $\Phi_\Gamma$  and  $\text{Id}_{\sigma(\mathcal{H}_1)}$ . Then, (3.2.2) implies that  $\Phi_{\bar{\Gamma}}$  is degradable if and only if  $\Phi_\Gamma$  is degradable.

## 4.9 Monotonicity properties

In [CG21a], using the pipeline inequalities (2.14.1) and the monotonicity of the 3-dimensional MAD channels in their parameters, proven in Subsection 3.3.g, the authors were able to compute some capacity functionals for certain configurations of the channels that were not degradable nor anti-degradable. In order to generalize the property of monotonicity of the capacity functionals to the  $d$ -dimensional case, one needs to consider two transition matrices,  $\Gamma, \Gamma'$ , whose elements  $\gamma_{ji}, \gamma'_{ji}$  differ only for a single pair of indices  $(j_0, i_0)$ , so that:

$$\gamma'_{j_0, i_0} \geq \gamma_{j_0, i_0}. \quad (4.9.1)$$

Then, on account of the pipeline inequalities (2.14.1), one could conclude that the capacities MAD channels are non increasing in the parameter  $\gamma'_{j_0, i_0} \geq \gamma_{j_0, i_0}$  if one were able to find two LCPT maps  $\Lambda_L, \Lambda_R$  such that:

$$\Lambda_L \circ \Phi_\Gamma \circ \Lambda_R = \Phi_{\Gamma'}. \quad (4.9.2)$$

Finding  $\Lambda_L, \Lambda_R$  is not an easy task and generally one has to resort to heuristic methods to simplify the problem. Recalling the property of closure under composition for MAD channels, one might assume that  $\Lambda_L, \Lambda_R$  are MAD's themselves; however, for  $d > 3$ , this line of reasoning only allows to derive monotonicity properties under the transition probabilities  $\gamma_{d-1, i_0}$ ,  $\forall 0 \leq i_0 < d-1$  and  $\gamma_{10}$ :

- **Monotonicity under  $\gamma_{d-1, i_0}$ :** Consider  $\Lambda_R = \text{Id}_{\sigma(\mathcal{H}_d)}$  the identity channel and  $\Lambda_L = \Phi_{\Gamma_{\lambda_{d-1, i_0}}}$  a single decay MAD channel from  $|d-1\rangle$  to  $|i_0\rangle$  with transition probability  $\lambda_{d-1, i_0}$ . From (4.2.7), the resulting channel in (4.9.2),  $\Phi_{\Gamma'} = \Phi_{\Gamma_{\lambda_{d-1, i_0}}} \circ \Phi_\Gamma$  has the same transition probabilities  $\gamma'_{ji}$  of  $\Phi_\Gamma$  aside from  $\gamma'_{d-1, i_0} \geq \gamma_{d-1, i_0}$ .
- **Monotonicity under  $\gamma_{10}$ :** Consider  $\Lambda_L = \text{Id}_{\sigma(\mathcal{H}_d)}$  the identity channel and  $\Lambda_R = \Phi_{\Gamma_{\lambda_{10}}}$  a single decay MAD channel from  $|1\rangle$  to  $|0\rangle$  with transition probability  $\lambda_{10}$ . From (4.2.7), the resulting channel in (4.9.2),  $\Phi_{\Gamma'} = \Phi_\Gamma \circ \Phi_{\Gamma_{\lambda_{10}}}$  has the same transition probabilities  $\gamma'_{ji}$  of  $\Phi_\Gamma$  aside from  $\gamma'_{10} \geq \gamma_{10}$ .

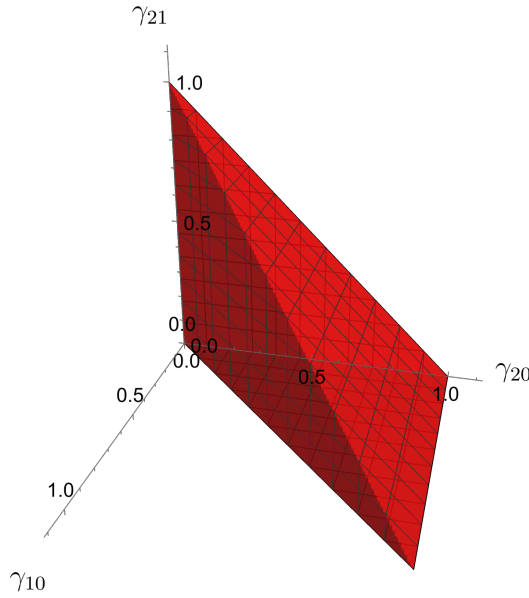


**Figure 4.9.1:** Monotonicity region under  $\gamma_{21}$  (4.9.7). Note that  $\gamma_{21}, \gamma_{20}$  are still bounded by (3.3.3), meaning that  $0 \leq \gamma_{20} + \gamma_{21} \leq 1$ .

### Monotonicity properties in $d = 4$

It is unclear whether a 4-dimensional MAD channel presents monotonous capacities under the transition probabilities  $\gamma_{20}, \gamma_{21}$ . As stated above, resorting to (4.9.2) is only useful if additional assumptions are made. Assume that either one of  $\Lambda_L, \Lambda_R = \text{Id}_{\sigma(\mathcal{H}_d)}$ , then, utilizing the inverse map (4.5.7), from (4.9.2):

$$\Lambda_R = \text{Id}_{\sigma(\mathcal{H}_d)} \Rightarrow \Lambda_L = \Phi_{\Gamma'} \circ \Phi_{\Gamma}^{(-1)}, \quad (4.9.3)$$

$$\Lambda_L = \text{Id}_{\sigma(\mathcal{H}_d)} \Rightarrow \Lambda_R = \Phi_{\Gamma}^{(-1)} \circ \Phi_{\Gamma'}. \quad (4.9.4)$$

Note that, by construction, both of these maps are linear and trace preserving; verifying their complete positiveness would imply that they are quantum channels, which can be done by verifying the positive semi-definiteness of their Choi matrices, due to (2.5.17).

#### Case $\gamma'_{21} \geq \gamma_{21}$

Assume that  $\Gamma'$  and  $\Gamma$  only differ in the  $|2\rangle\langle 1|$  element, so that:

$$\begin{aligned} \gamma'_{21} &\equiv \gamma_{21} + \varepsilon_{21} \geq \gamma_{21}, \\ 0 &\leq \varepsilon_{21} \leq \gamma_{22}, \end{aligned} \quad (4.9.5)$$

where the last condition is needed in order for  $\gamma_{22}' = \gamma_{22} - \varepsilon_{21} \geq 0$  to be satisfied. Computing the eigenvalues of the Choi matrices of  $\Lambda_L, \Lambda_R$  in (4.9.3) and (4.9.4), one finds that the former is only positive semi-definite if:

$$\gamma_{32} = 0, \quad (4.9.6)$$

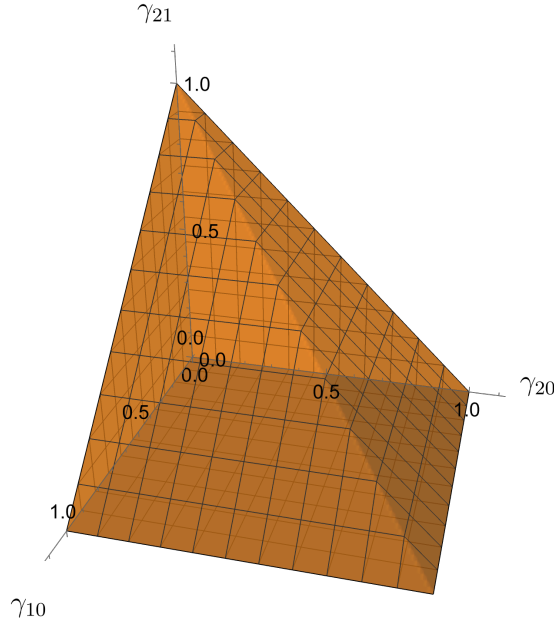


**Figure 4.9.2:** Monotonicity region under  $\gamma_{20}$  (4.9.10). Note that  $\gamma_{21}, \gamma_{20}$  are still bounded by (3.3.3), meaning that  $0 \leq \gamma_{20} + \gamma_{21} \leq 1$ .

while the latter is positive semi-definite under the following condition:

$$\gamma_{20} - \gamma_{10} \geq 0, \quad (4.9.7)$$

which means that the capacity functionals of a 4-dimensional MAD channel are monotonous under  $\gamma_{21}$  if  $\gamma_{32} = 0$  or  $\gamma_{20} \geq \gamma_{10}$ . The region described by (4.9.7) is illustrated in Figure 4.9.1.

### Case $\gamma'_{20} \geq \gamma_{20}$

Assume that  $\Gamma'$  and  $\Gamma$  only differ in the  $|2\rangle\langle 0|$  element, so that:

$$\begin{aligned} \gamma'_{20} &\equiv \gamma_{20} + \varepsilon_{20} \geq \gamma_{20}, \\ 0 &\leq \varepsilon_{20} \leq \gamma_{22}, \end{aligned} \quad (4.9.8)$$

where the last condition is needed in order for  $\gamma_{22}' = \gamma_{22} - \varepsilon_{20} \geq 0$  to be satisfied. Computing the eigenvalues of the Choi matrices of  $\Lambda_L, \Lambda_R$  in (4.9.3) and (4.9.4), one finds that the former is only positive semi-definite if:

$$\gamma_{32} = 0, \quad (4.9.9)$$

while the latter is positive semi-definite under the following condition:

$$1 - \gamma_{21} - \gamma_{10} \geq 0, \quad (4.9.10)$$

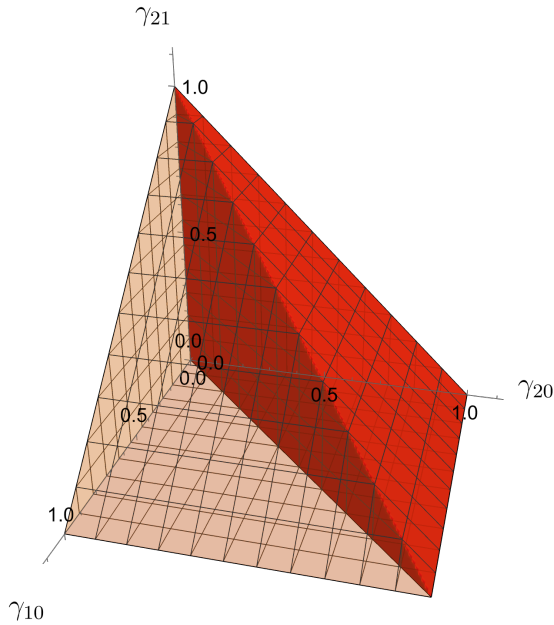


**Figure 4.9.3:** The monotonicity region under  $\gamma_{21}$  (4.9.7) is completely contained within the monotonicity region under  $\gamma_{20}$  (4.9.10).

which means that the capacity functionals of a 4-dimensional MAD channel are monotonous under  $\gamma_{20}$  if  $\gamma_{32} = 0$  or  $\gamma_{21} \leq 1 - \gamma_{10}$ . The region described by (4.9.10) is illustrated in Figure 4.9.2. Note that the region described by (4.9.7) is completely contained within the region described by (4.9.10), as can be seen in Figure 4.9.3.

## 4.10 Complete damping of level $|3\rangle$ in 4-dimensional MAD's

Consider the 4-dimensional MAD channel  $\Phi_{\Gamma_{CD3}}$  identified by the transition matrix:

$$\Gamma_{CD3} = \mathbb{1}_4 + \sum_{j=1}^3 \sum_{i=0}^{j-1} \gamma_{ji} |j\rangle\langle i| - \sum_{j=1}^3 \sum_{i=0}^{j-1} \gamma_{ji} |j\rangle\langle j|, \quad (4.10.1)$$

$$\text{where } \gamma_{33} = 1 - \gamma_{30} - \gamma_{31} - \gamma_{32} = 0.$$

The quantum capacity of this channel can be shown to be equivalent to the quantum capacity of a 3-dimensional MAD channel  $\Phi_{\Gamma_{MAD3}}^{(3)}$ , whose transition matrix is:

$$\Gamma_{MAD3} = \mathbb{1}_3 + \sum_{j=1}^2 \sum_{i=0}^{j-1} \gamma_{ji} |j\rangle\langle i| - \sum_{j=1}^2 \sum_{i=0}^{j-1} \gamma_{ji} |j\rangle\langle j|. \quad (4.10.2)$$

In order to reach this result, one needs to find coinciding upper and lower bounds on  $Q(\Phi_{\Gamma_{CD3}})$ .

### Lower bound

The lower bound on  $Q(\Phi_{\Gamma_{CD3}})$  is trivial: if one were to encode information only on the subspace spanned by  $\{|0\rangle, |1\rangle, |2\rangle\}$ , the channel  $\Phi_{\Gamma_{CD3}}$  would be equivalent to  $\Phi_{\Gamma_{MAD3}}^{(3)}$ ; of course, this choice of encoding is not guaranteed to be optimal, therefore:

$$Q(\Phi_{\Gamma_{CD3}}) \geq Q\left(\Phi_{\Gamma_{MAD3}}^{(3)}\right). \quad (4.10.3)$$

### Upper bound

The upper bound on  $Q(\Phi_{\Gamma_{CD3}})$  can be obtained using the pipeline inequalities (2.14.1) and the Direct Sum channels' property (3.2.8); consider the DS channel:

$$\begin{aligned} \Phi_{\Gamma_{MAD3}}^{DS}(\theta) &\equiv \left[ \begin{array}{c|c} \Phi_{\Gamma_{MAD3}}^{(3)}(p\theta^{(3)}) & 0 \\ \hline 0 & 1-p \end{array} \right], \\ \theta &\equiv \left[ \begin{array}{c|c} p\theta^{(3)} & \theta_{j3} \\ \hline \theta_{j3}^* & 1-p \end{array} \right], \\ \theta &\in \sigma(\mathcal{H}_4), \theta^{(3)} \in \sigma(\mathcal{H}_3), \\ 0 &\leq p \leq 1, \end{aligned} \quad (4.10.4)$$

and the Level Erasure channel:

$$\begin{aligned} LE_{\Gamma_{CD3}}(\rho) &\equiv \begin{pmatrix} \rho_{00} + \gamma_{30}\rho_{33} & \rho_{01} & \rho_{02} & 0 \\ \rho_{01}^* & \rho_{11} + \gamma_{31}\rho_{33} & \rho_{12} & 0 \\ \rho_{02}^* & \rho_{12}^* & \rho_{22} + \gamma_{32}\rho_{33} & 0 \\ 0 & 0 & 0 & 0 \end{pmatrix}, \\ \rho &\equiv \begin{pmatrix} \rho_{00} & \rho_{01} & \rho_{02} & \rho_{03} \\ \rho_{01}^* & \rho_{11} & \rho_{12} & \rho_{13} \\ \rho_{02}^* & \rho_{12}^* & \rho_{22} & \rho_{23} \\ \rho_{03}^* & \rho_{13}^* & \rho_{23}^* & \rho_{33} \end{pmatrix}. \end{aligned} \quad (4.10.5)$$

The composition of these two channel is equal to  $\Phi_{\Gamma_{CD3}}$ :

$$\Phi_{\Gamma_{CD3}} = LE_{\Gamma_{CD3}} \circ \Phi_{\Gamma_{MAD3}}^{DS}. \quad (4.10.6)$$

The quantum capacity of  $\Phi_{\Gamma_{MAD3}}^{DS}$  is given in (3.2.8), which in this case translates to:

$$Q\left(\Phi_{\Gamma_{MAD3}}^{DS}\right) = Q\left(\Phi_{\Gamma_{MAD3}}^{(3)}\right). \quad (4.10.7)$$

The pipeline inequalities (2.14.1) ensure that (4.10.7) is an upper bound for  $Q(\Phi_{\Gamma_{CD3}})$ :

$$Q\left(\Phi_{\Gamma_{CD3}}\right) \leq Q\left(\Phi_{\Gamma_{MAD3}}^{(3)}\right). \quad (4.10.8)$$

Combining (4.10.3) and (4.10.8) leads to the conclusion:

$$Q\left(\Phi_{\Gamma_{CD3}}\right) = Q\left(\Phi_{\Gamma_{MAD3}}^{(3)}\right). \quad (4.10.9)$$

## 5

# Capacity computations for MAD channels in $d = 4$

Building upon the results in Chapters 2, 3 and 4, applying the techniques described in Section 7.2, an analysis of the quantum, private classical and two-way capacities 4-dimensional MAD channel becomes feasible. This analysis was performed and the consequent results are reported in this chapter.

## 5.1 Single decay 4-dimensional MAD channel

All single decay 4-dimensional MAD channel are unitarily equivalent, all belonging to Class 1A defined in Subsection 4.7.a.

### 5.1.a Class 1A

In order to compute the capacities of single decay 4-dimensional MAD channels, consider the sample channel  $\Phi_{\Gamma_{1A}(\gamma_{10})}$  identified by the transition matrix:

$$\Gamma_{1A}(\gamma_{10}) \equiv \mathbb{1}_4 + \gamma_{10} |1\rangle\langle 0| - \gamma_{10} |1\rangle\langle 1|. \quad (5.1.1)$$

As stated in Subsection 4.7.a,  $\Phi_{\Gamma_{1A}(\gamma_{10})}$  obeys the PCDS structure (3.2.1), with  $\Phi_{BB} = \text{Id}_{\sigma(\mathcal{H}_2)}$  and  $\Phi_{AA} = ADC_{\gamma_{10}}$ , and is degradable if and only if  $\gamma_{10} \leq 1/2$ ; in this region, the quantum capacity can be computed directly using (3.3.21):

$$Q(\Phi_{\Gamma_{1A}(\gamma_{10})}) = \max_{\rho^{(diag)}} I_c(\rho^{(diag)}, \Phi_{\Gamma_{1A}(\gamma_{10})}) \quad \forall \gamma_{10} \leq \frac{1}{2}. \quad (5.1.2)$$

For  $\gamma_{10} = 1/2$ ,  $ADC_{\gamma_{10}}$  has null quantum capacity, therefore the capacity of  $\Phi_{\Gamma_{1A}(\gamma_{10})}$  corresponds to its lower bound provided by (3.2.5), which in this case is  $\log_2 3$ . Using the monotonicity properties exposed in Section 4.9, it can be inferred that:

$$Q(\Phi_{\Gamma_{1A}(\gamma_{10})}) = C_P(\Phi_{\Gamma_{1A}(\gamma_{10})}) = \log_2 3 \quad \forall \frac{1}{2} \leq \gamma_{10} \leq 1. \quad (5.1.3)$$

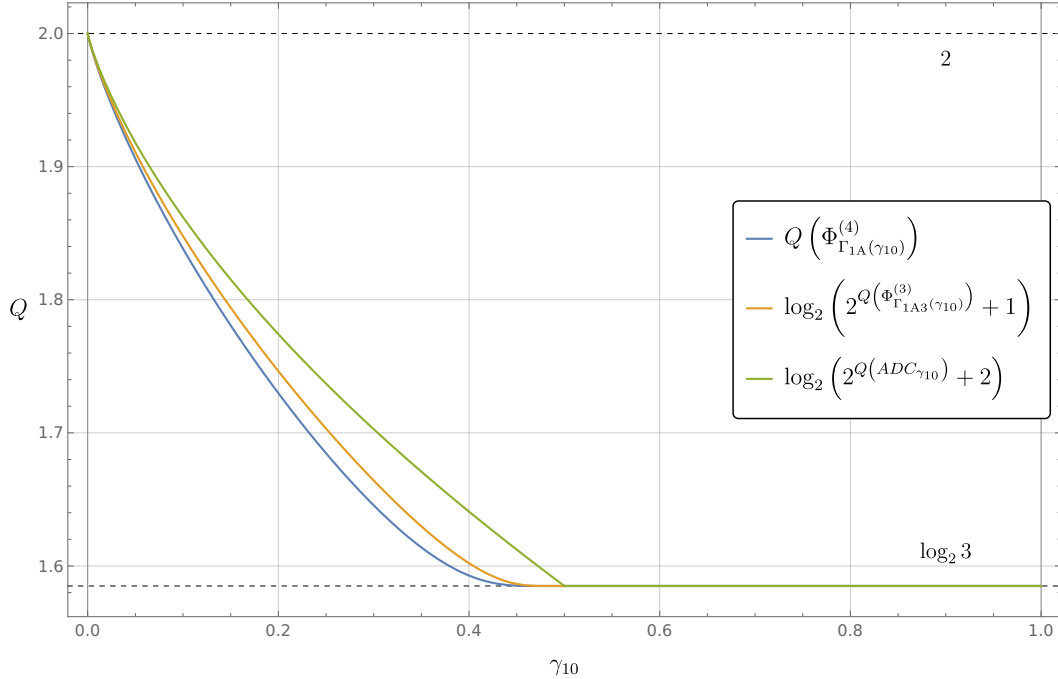


**Figure 5.1.1:** Quantum capacity of  $\Phi_{\Gamma_{1A}(\gamma_{10})}$ , compared with its upper bounds (3.2.4) given by the PCDS structure of the channel.

These results are plotted in Figure 5.1.1, alongside the upper bounds on the quantum capacity of PCDS channels (3.2.4), which are computed starting from the quantum capacity of an ADC and the quantum capacity of a 3-dimensional MAD channel  $\Phi_{\Gamma_{1A3}(\gamma_{10})}^{(3)}$ , identified by the transition matrix:

$$\Gamma_{1A3}(\gamma_{10}) \equiv \mathbb{1}_3 + \gamma_{10} |1\rangle\langle 0| - \gamma_{10} |1\rangle\langle 1|. \quad (5.1.4)$$

## 5.2 2-decay 4-dimensional MAD channels

There are 4 classes of 2-decay 4-dimensional MAD channels, whose capacities are reported in this section.

### 5.2.a Class 2A

Consider the sample channel  $\Phi_{\Gamma_{2A}(\gamma_{10}, \gamma_{20})}$  belonging in Class 2A, identified by the transition matrix:

$$\Gamma_{2A}(\gamma_{10}, \gamma_{20}) = \mathbb{1}_4 + \gamma_{10} |1\rangle\langle 0| + \gamma_{20} |2\rangle\langle 0| - \gamma_{10} |1\rangle\langle 1| - \gamma_{20} |2\rangle\langle 2|. \quad (5.2.1)$$

As stated in Subsection 4.7.a,  $\Phi_{\Gamma_{2A}(\gamma_{10}, \gamma_{20})}$  obeys the PCDS structure (3.2.1), with  $\Phi_{BB} = \text{Id}_{\sigma(\mathcal{H}_1)}$  and  $\Phi_{AA} = \Phi_{\Gamma_{2A3}(\gamma_{10}, \gamma_{20})}^{(3)}$  is a 3-dimensional MAD channel identified by

the transition matrix:

$$\Gamma_{2A3}(\gamma_{10}, \gamma_{20}) = \mathbb{1}_3 + \gamma_{10} |1\rangle\langle 0| + \gamma_{20} |2\rangle\langle 0| - \gamma_{10} |1\rangle\langle 1| - \gamma_{20} |2\rangle\langle 2|. \quad (5.2.2)$$

The degradability conditions for  $\Phi_{\Gamma_{2A}(\gamma_{10}, \gamma_{20})}$  are given in (4.7.3), which in this case translate to:

$$\Phi_{\Gamma_{2A}(\gamma_{10}, \gamma_{20})} \text{ degradable} \Leftrightarrow \gamma_{10} \leq \frac{1}{2} \wedge \gamma_{20} \leq \frac{1}{2}. \quad (5.2.3)$$

In this region, the quantum and classical private capacities can be computed using (3.3.21):

$$\begin{aligned} Q(\Phi_{\Gamma_{2A}(\gamma_{10}, \gamma_{20})}) &= \max_{\rho^{(diag)}} I_c(\rho^{(diag)}, \Phi_{\Gamma_{2A}(\gamma_{10}, \gamma_{20})}), \\ &\forall \gamma_{10}, \gamma_{20} : \gamma_{10} \leq \frac{1}{2} \wedge \gamma_{20} \leq \frac{1}{2}. \end{aligned} \quad (5.2.4)$$

$Q(\Phi_{\Gamma_{2A}(\gamma_{10}, \gamma_{20})})$  presents a symmetry under swap of  $(\gamma_{10}, \gamma_{20})$ , which is a consequence of the relation:

$$\Phi_{\Gamma_{2A}(\gamma_{10}, \gamma_{20})} = \mathcal{U}_{21} \circ \Phi_{\Gamma_{2A}(\gamma_{20}, \gamma_{10})} \circ \mathcal{U}_{21}, \quad (5.2.5)$$

where  $\mathcal{U}_{21}$  is defined in (4.3.2).

It is possible to extend the computation of the quantum capacity of  $\Phi_{\Gamma_{2A}(\gamma_{10}, \gamma_{20})}$  to the whole region  $0 \leq \gamma_{10} \leq 1 \wedge 0 \leq \gamma_{20} \leq 1$ .

**Extension to  $\frac{1}{2} \leq \gamma_{20} \leq 1$**

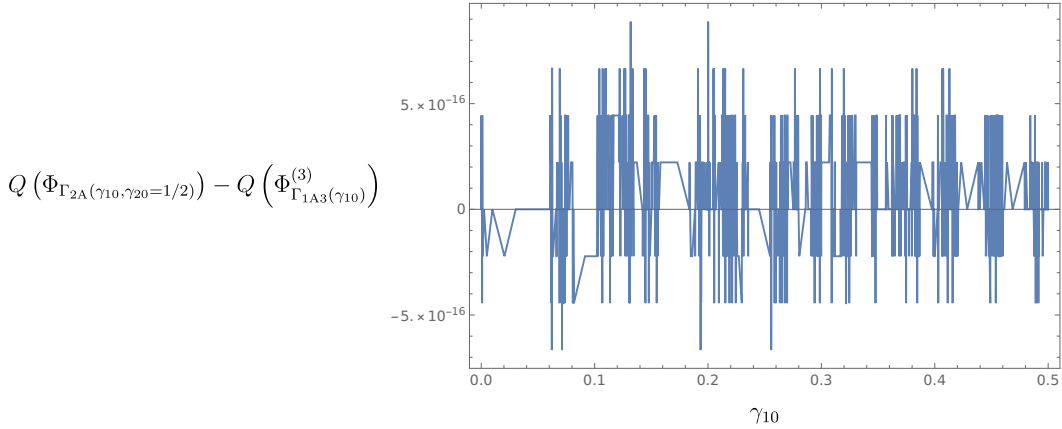


**Figure 5.2.1:** Difference between  $Q(\Phi_{\Gamma_{2A}(\gamma_{10}, \gamma_{20}=1)})$  and  $Q(\Phi_{\Gamma_{2A}(\gamma_{10}, \gamma_{20}=1/2)})$  for  $0 \leq \gamma_{10} \leq 1/2$ ; it is reasonable to assume, due to their very low values, that the discrepancies from 0 in the plot are due to the computational resolution of the machine used for the evaluation.

The channel  $\Phi_{\Gamma_{2A}(\gamma_{10}, \gamma_{20})}$  is covariant to  $\Phi_{\Gamma'_{2A}(\gamma_{10}, \gamma_{20})}$ :

$$\begin{aligned} \Gamma'_{2A}(\gamma_{10}, \gamma_{20}) &\equiv \mathbb{1}_4 + \gamma_{10} |1\rangle\langle 0| + \gamma_{20} |3\rangle\langle 0| - \gamma_{10} |1\rangle\langle 1| - \gamma_{20} |3\rangle\langle 3|, \\ \Phi_{\Gamma'_{2A}(\gamma_{10}, \gamma_{20})} &= \mathcal{U}_{23} \circ \Phi_{\Gamma_{2A}(\gamma_{10}, \gamma_{20})} \circ \mathcal{U}_{23}. \end{aligned} \quad (5.2.6)$$

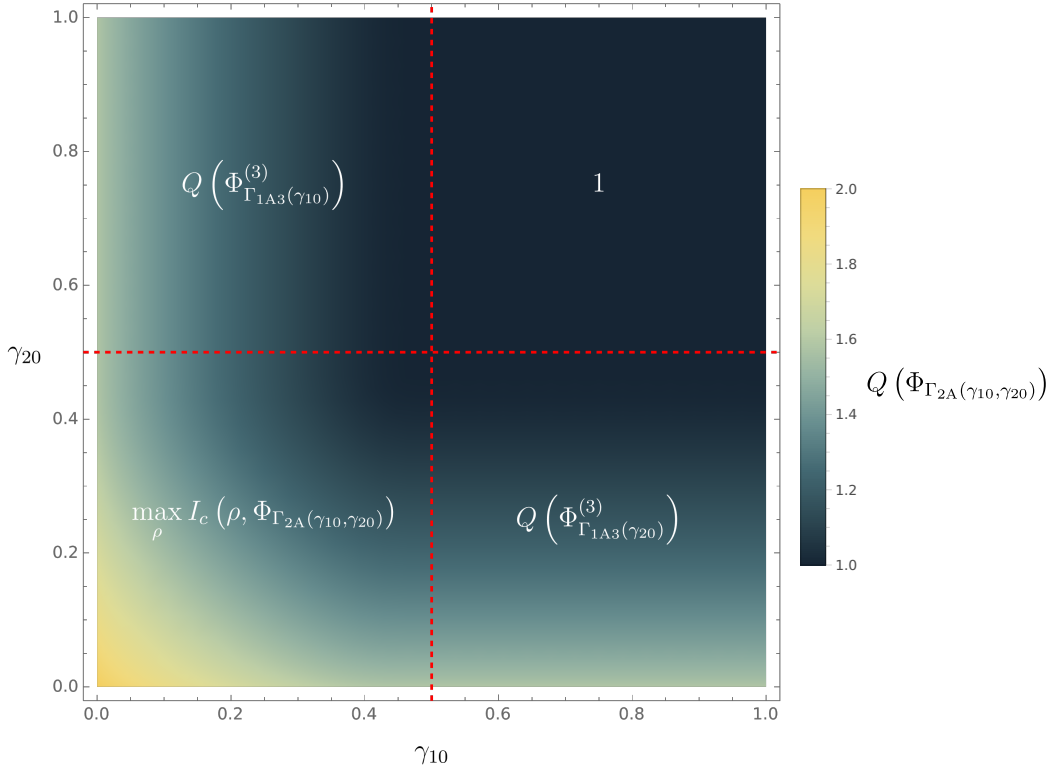


**Figure 5.2.2:** Density plot representing the quantum capacity of  $\Phi_{\Gamma_{2A}(\gamma_{10}, \gamma_{20})}$ .

When  $\gamma_{20} = 1$ , applying (5.2.6) and (4.10.9), one finds that:

$$\begin{aligned} Q(\Phi_{\Gamma_{2A}(\gamma_{10}, \gamma_{20}=1)}) &= Q(\Phi_{\Gamma_{1A3}(\gamma_{10})}^{(3)}), \\ \Gamma_{1A3}(\gamma_{10}) &\equiv \mathbb{1}_3 + \gamma_{10} |1\rangle\langle 0| - \gamma_{10} |1\rangle\langle 1|, \end{aligned} \quad (5.2.7)$$

where  $\Phi_{\Gamma_{1A3}(\gamma_{10})}^{(3)}$  is a 3-dimensional single decay MAD channel. Furthermore, computing the difference between  $Q(\Phi_{\Gamma_{2A}(\gamma_{10}, \gamma_{20}=1)})$  and  $Q(\Phi_{\Gamma_{2A}(\gamma_{10}, \gamma_{20}=1/2)})$  yields the plot reported in Figure 5.2.1. The discrepancies from 0 in the plot are likely due to the computational resolution of the machine used for the calculation. This result, coupled with the monotonicity of the capacities in  $\gamma_{10}$  for MAD channels, as seen in Section 4.9, implies that:

$$Q(\Phi_{\Gamma_{2A}(\gamma_{10}, \gamma_{20})}) = Q(\Phi_{\Gamma_{1A3}(\gamma_{10})}^{(3)}), \quad \forall 0 \leq \gamma_{10} \leq \frac{1}{2}, \frac{1}{2} \leq \gamma_{20} \leq 1. \quad (5.2.8)$$

$Q(\Phi_{\Gamma_{1A3}(\gamma_{10})}^{(3)})$  itself is computable in  $0 \leq \gamma_{10} \leq 1$  following the results of [CG21a].

### Quantum capacity in $\frac{1}{2} \leq \gamma_{20}, \gamma_{10} \leq 1$

When  $\gamma_{20}, \gamma_{10} = 1/2$  the computation of the quantum capacity of  $\Phi_{\Gamma_{2A}(\gamma_{10}, \gamma_{20})}$  is equal to the  $\log_2$  of the dimension of the noiseless subspace of the channel:

$$\Phi_{\Gamma_{2A}(\gamma_{10}=1/2, \gamma_{20}=1/2)} = 1. \quad (5.2.9)$$

This value is a lower bound on the capacity of the channel; hence, given the monotonicity of the channel w.r.t.  $\gamma_{10}, \gamma_{20}$  implies that:

$$Q(\Phi_{\Gamma_{2A}(\gamma_{10}, \gamma_{20})}) = 1, \quad \forall \frac{1}{2} \leq \gamma_{10}, \gamma_{20} \leq 1. \quad (5.2.10)$$

### Quantum capacity plot

The results in (5.2.10), (5.2.8), (5.2.5) and (5.2.4) combine to shape the plot of the quantum capacity for channels belonging in Class 2A reported in Figure 5.2.2.

## 5.2.b Class 2B

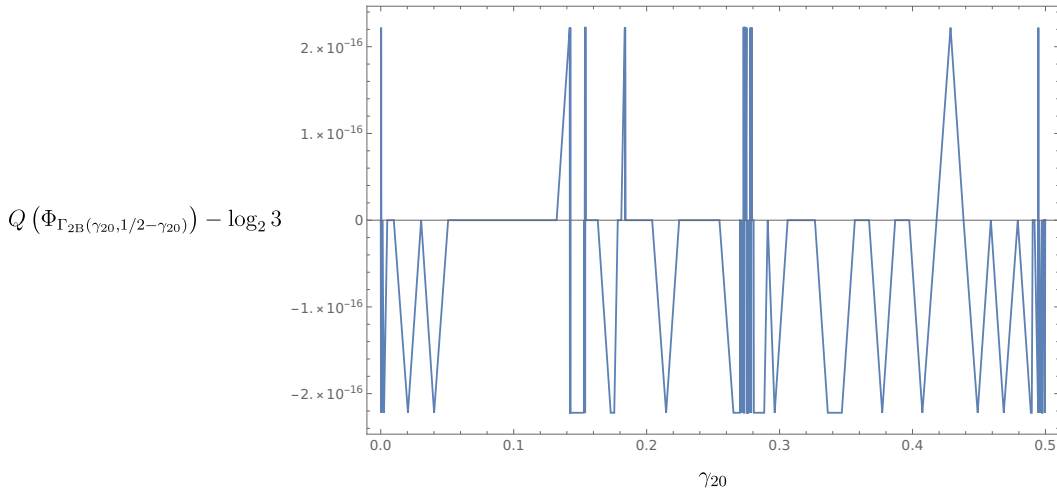


**Figure 5.2.3:** Difference between  $Q(\Phi_{\Gamma_{2B}(\gamma_{20}, \gamma_{21}=1-\gamma_{20})}) = \log_2 3$  and  $Q(\Phi_{\Gamma_{2B}(\gamma_{20}, \gamma_{21}=1/2-\gamma_{20})})$  for  $0 \leq \gamma_{20} \leq 1/2$ ; it is reasonable to assume, due to their very low values, that the discrepancies from 0 in the plot are due to the computational resolution of the machine used for the evaluation.

Consider the sample channel  $\Phi_{\Gamma_{2B}(\gamma_{20}, \gamma_{21})}$  belonging in Class 2B, identified by the transition matrix:

$$\Gamma_{2A}(\gamma_{20}, \gamma_{21}) = \mathbb{1}_4 + \gamma_{20} |2\rangle\langle 0| + \gamma_{21} |2\rangle\langle 1| - (\gamma_{20} + \gamma_{21}) |2\rangle\langle 2|. \quad (5.2.11)$$

The channel  $\Phi_{\Gamma_{2B}(\gamma_{20}, \gamma_{21})}$  obeys the PCDS structure (3.2.1); its degradability conditions are reported in (4.7.4), which in this case translate to:

$$\Phi_{\Gamma_{2B}(\gamma_{20}, \gamma_{21})} \text{ degradable} \Leftrightarrow \gamma_{20} + \gamma_{21} \leq \frac{1}{2}. \quad (5.2.12)$$

In this region, the quantum capacity of  $\Phi_{\Gamma_{2B}(\gamma_{20}, \gamma_{21})}$  can be computed using (3.3.21):

$$\begin{aligned} Q(\Phi_{\Gamma_{2B}(\gamma_{20}, \gamma_{21})}) &= \max_{\rho^{(diag)}} I_c(\rho^{(diag)}, \Phi_{\Gamma_{2B}(\gamma_{20}, \gamma_{21})}), \\ \forall \gamma_{20}, \gamma_{21} : \gamma_{20} + \gamma_{21} &\leq \frac{1}{2}. \end{aligned} \quad (5.2.13)$$

$Q(\Phi_{\Gamma_{2B}(\gamma_{20}, \gamma_{21})})$  is symmetric in the pair  $(\gamma_{20}, \gamma_{21})$  due to the covariance of the channel under the unitary transformation  $\mathcal{U}_{10}$ . It is possible to extend the computation of the quantum capacity performed in  $0 \leq \gamma_{20} + \gamma_{21} \leq \frac{1}{2}$  to the region  $\frac{1}{2} \leq \gamma_{20} + \gamma_{21} \leq 1$ .

**Extension to  $\frac{1}{2} \leq \gamma_{20} + \gamma_{21} \leq 1$**

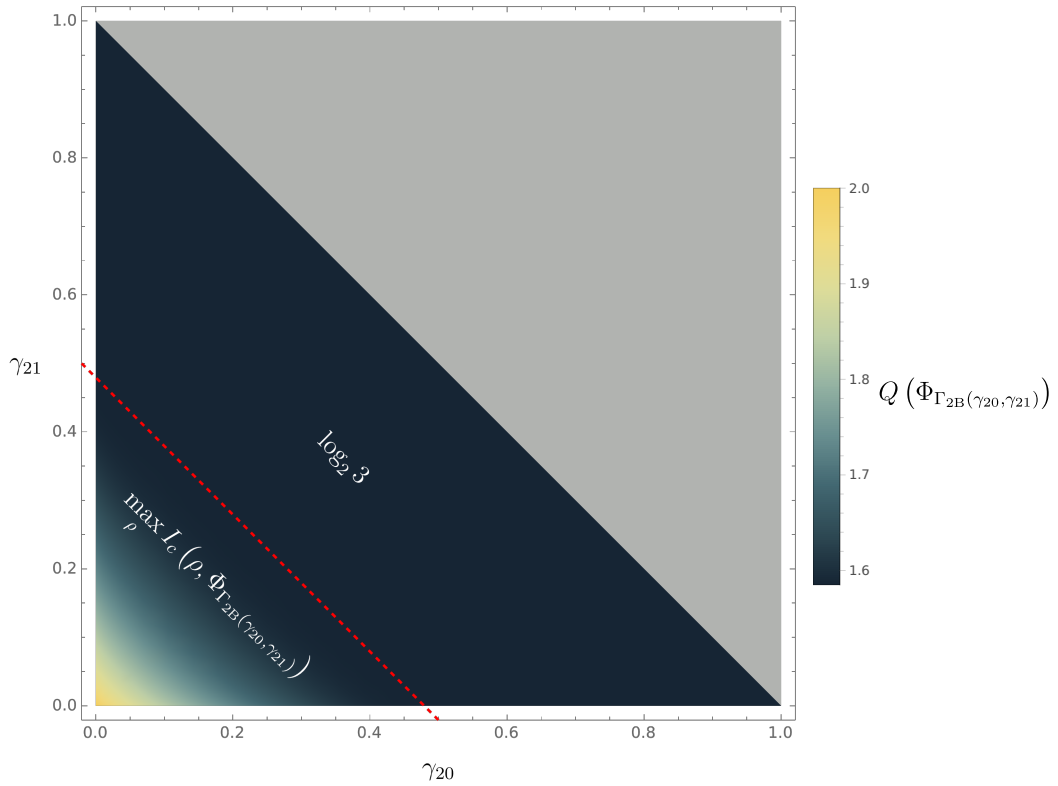


**Figure 5.2.4:** Density plot representing the quantum capacity of  $\Phi_{\Gamma_{2B}(\gamma_{20}, \gamma_{21})}$ .

The channel  $\Phi_{\Gamma_{2B}(\gamma_{20}, \gamma_{21})}$  is covariant to  $\Phi_{\Gamma'_{2B}(\gamma_{20}, \gamma_{21})}$ :

$$\begin{aligned} \Gamma'_{2B}(\gamma_{20}, \gamma_{21}) &\equiv \mathbb{1}_4 + \gamma_{20} |3\rangle\langle 0| + \gamma_{21} |3\rangle\langle 1| - (\gamma_{20} + \gamma_{21}) |3\rangle\langle 3|, \\ \Phi_{\Gamma'_{2B}(\gamma_{20}, \gamma_{21})} &= \mathcal{U}_{23} \circ \Phi_{\Gamma_{2B}(\gamma_{20}, \gamma_{21})} \circ \mathcal{U}_{23}. \end{aligned} \quad (5.2.14)$$

When  $\gamma_{20} + \gamma_{21} = 1$  applying (5.2.14) and (4.10.9), one finds that:

$$Q(\Phi_{\Gamma_{2B}(\gamma_{20}, \gamma_{21}=1-\gamma_{20})}) = Q(\text{Id}_{\sigma(\mathcal{H}_3)}) = \log_2 3. \quad (5.2.15)$$

Furthermore, computing the difference between  $Q(\Phi_{\Gamma_{2B}(\gamma_{20}, \gamma_{21}=1-\gamma_{20})})$  and  $Q(\Phi_{\Gamma_{2B}(\gamma_{20}, \gamma_{20}=1/2-\gamma_{20})})$  yields the plot reported in Figure 5.2.3, from which one could infer that:

$$Q(\Phi_{\Gamma_{2B}(\gamma_{20}, \gamma_{21})}) = \log_2 3, \quad \forall \frac{1}{2} \leq \gamma_{20} + \gamma_{21} \leq 1. \quad (5.2.16)$$

### Quantum capacity plot

The results in (5.2.16) and (5.2.13) combine to shape the plot of the quantum capacity for channels belonging in Class 2B, reported in Figure 5.2.4.

### 5.2.c Class 2C

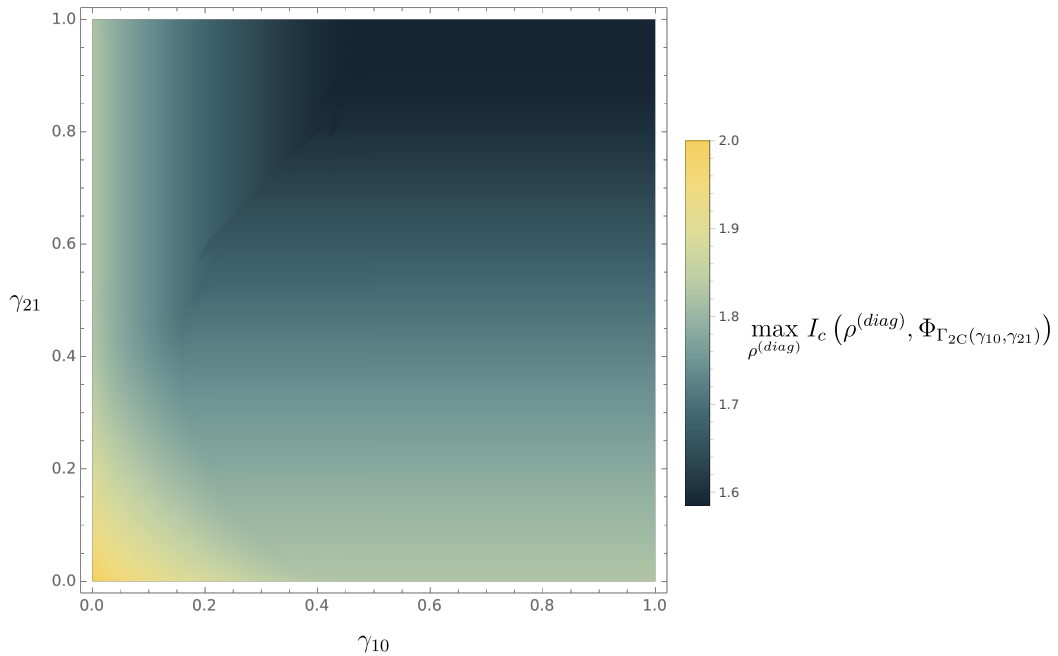


**Figure 5.2.5:** Density plot of the lower bound on the quantum capacity of  $\Phi_{\Gamma_{2C}(\gamma_{10}, \gamma_{21})}$ , obtained from the maximization of the coherent information for a single use on the channel over all possible diagonal input matrices.

Consider the sample channel  $\Phi_{\Gamma_{2C}(\gamma_{10}, \gamma_{21})}$  belonging in Class 2C, identified by the transition matrix:

$$\Gamma_{2C}(\gamma_{10}, \gamma_{21}) = \mathbb{1}_4 + \gamma_{10} |1\rangle\langle 0| + \gamma_{21} |2\rangle\langle 1| - \gamma_{10} |1\rangle\langle 1| - \gamma_{21} |2\rangle\langle 2|. \quad (5.2.17)$$

This channel is never degradable. One needs to settle for computing a lower bound on the quantum capacity, provided by the maximization over all possible diagonal input matrices of the coherent information:

$$\max_{\rho^{(diag)}} I_c(\rho^{(diag)}, \Phi_{\Gamma_{2C}(\gamma_{10}, \gamma_{21})}) \leq Q^{(1)}(\Phi_{\Gamma_{2C}(\gamma_{10}, \gamma_{21})}) \leq Q(\Phi_{\Gamma_{2C}(\gamma_{10}, \gamma_{21})}). \quad (5.2.18)$$

The lower bound in (5.2.18) is plotted in Figure 5.2.5.

### 5.2.d Class 2D

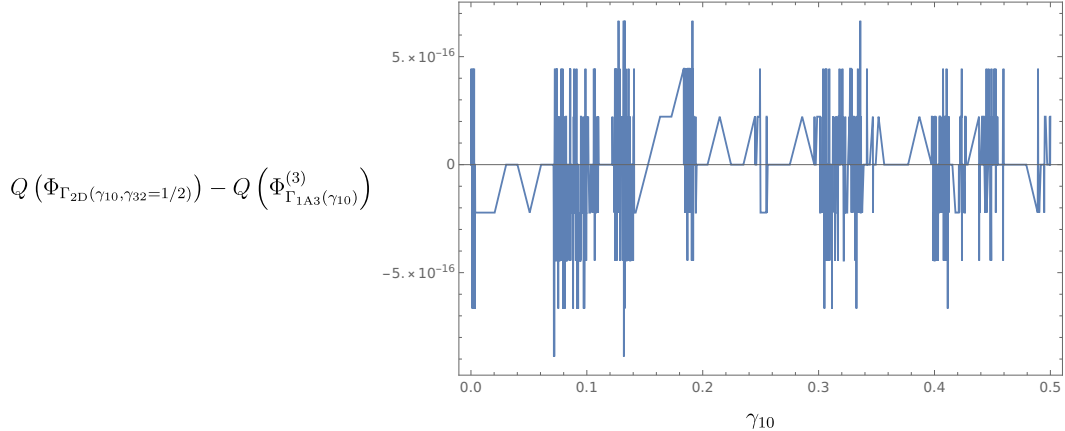


**Figure 5.2.6:** Difference between  $Q(\Phi_{\Gamma_{2D}(\gamma_{10}, \gamma_{32}=1/2)})$  and  $Q(\Phi_{\Gamma_{2D}(\gamma_{10}, \gamma_{32}=1)})$  for  $0 \leq \gamma_{10} \leq 1/2$ ; it is reasonable to assume, due to their very low values, that the discrepancies from 0 in the plot are due to the computational resolution of the machine used for the evaluation.

Consider the sample channel  $\Phi_{\Gamma_{2D}(\gamma_{10}, \gamma_{32})}$  belonging in Class 2D, identified by the transition matrix:

$$\Gamma_{2D}(\gamma_{10}, \gamma_{32}) = \mathbb{1}_4 + \gamma_{10}|1\rangle\langle 0| + \gamma_{32}|3\rangle\langle 2| - \gamma_{10}|1\rangle\langle 1| - \gamma_{32}|3\rangle\langle 3|. \quad (5.2.19)$$

Following (4.7.5), the channel  $\Phi_{\Gamma_{2D}(\gamma_{10}, \gamma_{32})}$  has degradability conditions:

$$\Phi_{\Gamma_{2D}(\gamma_{10}, \gamma_{32})} \text{ degradable} \Leftrightarrow \gamma_{10} \leq \frac{1}{2} \wedge \gamma_{32} \leq \frac{1}{2}. \quad (5.2.20)$$

In this region, the quantum capacity can be computed using (3.3.21):

$$\begin{aligned} Q(\Phi_{\Gamma_{2D}(\gamma_{10}, \gamma_{32})}) &= \max_{\rho^{(diag)}} I_c(\rho^{(diag)}, \Phi_{\Gamma_{2D}(\gamma_{10}, \gamma_{32})}), \\ \forall \gamma_{10}, \gamma_{32} : \gamma_{10} &\leq \frac{1}{2} \wedge \gamma_{32} \leq \frac{1}{2}. \end{aligned} \quad (5.2.21)$$

The quantum capacity  $Q(\Phi_{\Gamma_{2D}(\gamma_{10}, \gamma_{32})})$  is invariant under swap of  $(\gamma_{10}, \gamma_{32})$  as a consequence of the covariance of the channel under the unitary transformation  $\mathcal{U}_{21} \circ \mathcal{U}_{10} \circ \mathcal{U}_{32} \circ \mathcal{U}_{21}$ . It is possible to extend the computation of the quantum capacity performed in the degradability region to rest of the surface  $0 \leq \gamma_{10} \leq 1 \wedge 0 \leq \gamma_{32} \leq 1$ .

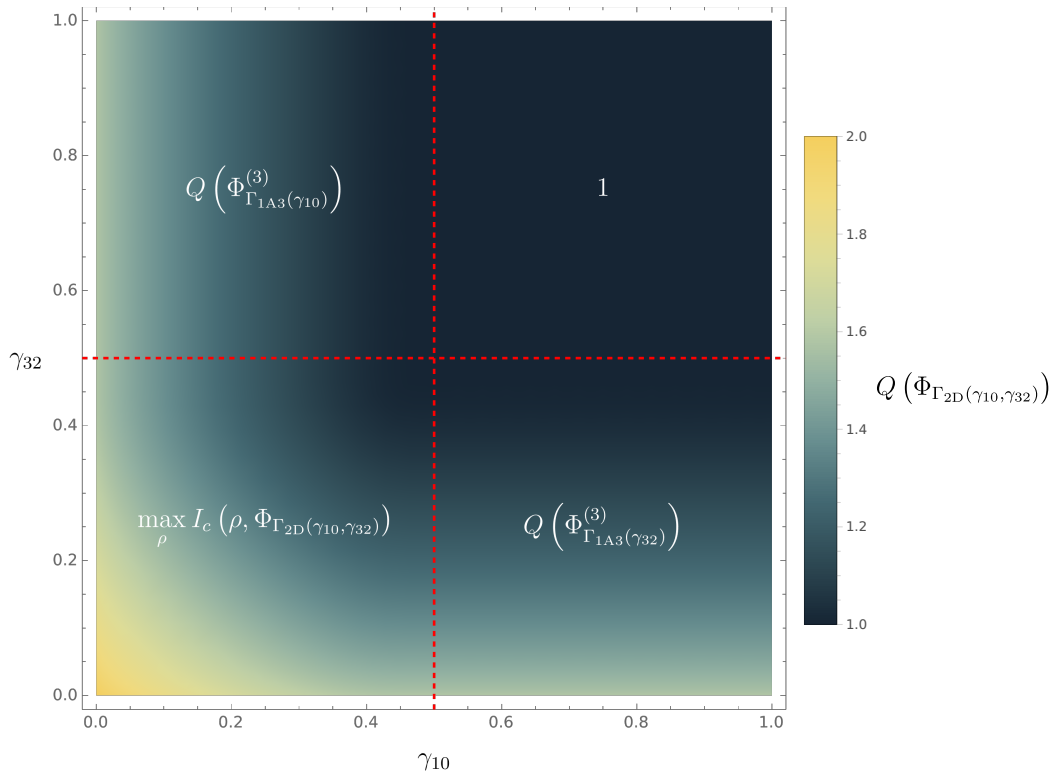


**Figure 5.2.7:** Density plot representing the quantum capacity of  $\Phi_{\Gamma_{2D}(\gamma_{10}, \gamma_{32})}$ .

**Extension to**  $\frac{1}{2} \leq \gamma_{32} \leq 1$

When  $\gamma_{32} = 1$ , applying (4.10.9), one finds that:

$$Q(\Phi_{\Gamma_{2D}(\gamma_{10}, \gamma_{32}=1)}) = Q(\Phi_{\Gamma_{1A3}(\gamma_{10})}^{(3)}), \quad (5.2.22)$$

where  $\Phi_{\Gamma_{1A3}(\gamma_{10})}^{(3)}$  is the 3-dimensional MAD channel identified by the transition matrix defined in (5.2.7). One can verify that  $Q(\Phi_{\Gamma_{2D}(\gamma_{10}, \gamma_{32}=1/2)}) = Q(\Phi_{\Gamma_{2D}(\gamma_{10}, \gamma_{32}=1)})$  by computing their difference; the results are reported in Figure 5.2.6. By employing the monotonicity of  $Q(\Phi_{\Gamma_{2D}(\gamma_{10}, \gamma_{32})})$  in its parameters, it is possible to infer that:

$$Q(\Phi_{\Gamma_{2D}(\gamma_{10}, \gamma_{32})}) = Q(\Phi_{\Gamma_{1A3}(\gamma_{10})}^{(3)}), \quad \forall 0 \leq \gamma_{10} \leq \frac{1}{2}, \frac{1}{2} \leq \gamma_{32} \leq 1. \quad (5.2.23)$$

**Quantum capacity in**  $\frac{1}{2} \leq \gamma_{10}, \gamma_{32} \leq 1$

From the fact that  $Q(\Phi_{\Gamma_{2D}(\gamma_{10}=1/2, \gamma_{32}=1/2)}) = 1$ , 1 being a natural lower bound of  $Q(\Phi_{\Gamma_{2D}(\gamma_{10}, \gamma_{32})})$ , as it is the  $\log_2$  of the noiseless subspace of the channel, and the non-increasing behavior of  $Q(\Phi_{\Gamma_{2D}(\gamma_{10}, \gamma_{32})})$  in the transition probabilities, one can infer that:

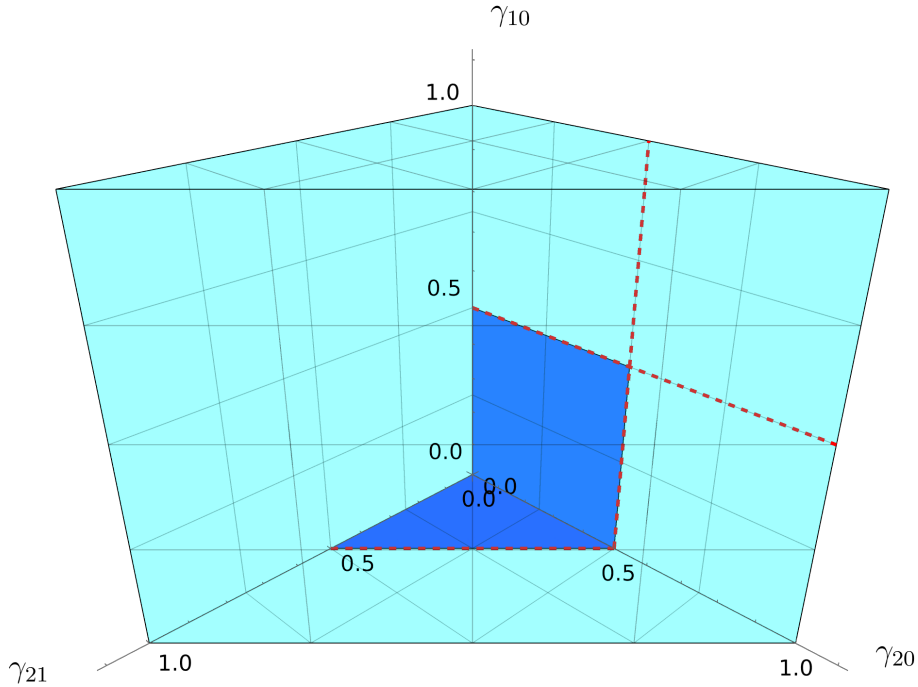


**Figure 5.3.1:** The graph represents the parameter region (cyan) of  $\Phi_{\Gamma_{3A}}(\gamma_{10}, \gamma_{20}, \gamma_{21})$  and its degradability regions (blue).

$$Q(\Phi_{\Gamma_{2D}(\gamma_{10}, \gamma_{32})}) = 1 \quad \forall \frac{1}{2} \leq \gamma_{10}, \gamma_{32} \leq 1. \quad (5.2.24)$$

### Quantum capacity plot

Combining (5.2.24), (5.2.23) and (5.2.21) and the symmetry of  $Q(\Phi_{\Gamma_{2D}(\gamma_{10}, \gamma_{32})})$  in the transition probabilities, the quantum capacity of  $\Phi_{\Gamma_{2D}(\gamma_{10}, \gamma_{32})}$  can be found on the whole surface  $0 \leq \gamma_{10}, \gamma_{32} \leq 1$ . The plot of  $Q(\Phi_{\Gamma_{2D}(\gamma_{10}, \gamma_{32})})$  is reported in Figure 5.2.7.

## 5.3 3-decay 4-dimensional MAD channels

There are 9 classes of 3-decay 4-dimensional MAD channels, whose capacities are reported in this section.

### 5.3.a Class 3A

MAD channels belonging to Class 3A present the PCDS structure (3.2.1), with one of the channels forming the structure being a 3-dimensional MAD channel. Consider the sample channel  $\Phi_{\Gamma_{3A}}(\gamma_{10}, \gamma_{20}, \gamma_{21})$  in class 3A, where the identifying transition matrix is:

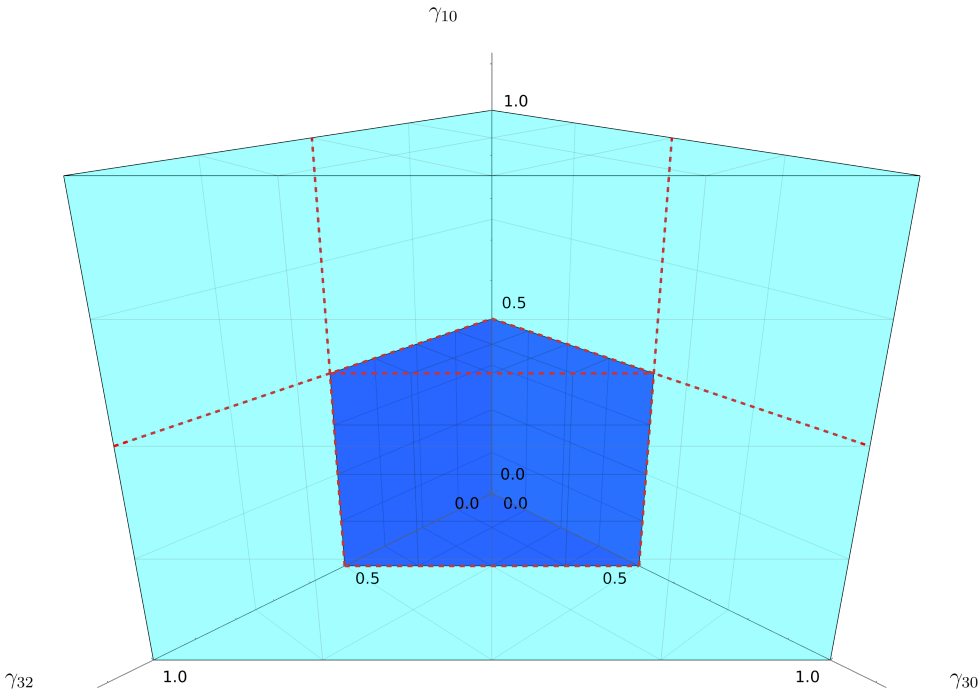


**Figure 5.3.2:** The graph represents the parameter region (cyan) of  $\Phi_{\Gamma_{3B}(\gamma_{20}, \gamma_{30}, \gamma_{31})}$  and its degradability regions (blue).

$$\begin{aligned} \Gamma_{3A}(\gamma_{10}, \gamma_{20}, \gamma_{21}) = & \mathbb{1}_4 + \gamma_{10} |1\rangle\langle 0| + \gamma_{20} |2\rangle\langle 0| + \gamma_{21} |2\rangle\langle 1| \\ & - \gamma_{10} |1\rangle\langle 1| - (\gamma_{20} + \gamma_{21}) |2\rangle\langle 2|. \end{aligned} \quad (5.3.1)$$

The results in Subsection 4.7.f indicate that a necessary condition for the degradability of  $\Phi_{\Gamma_{3A}(\gamma_{10}, \gamma_{20}, \gamma_{21})}$  is  $\gamma_{10} = 0 \vee \gamma_{21} = 0$ , at which point the channel reduces to Class 2B and Class 2A respectively. A graph representing the parameter space of  $\Phi_{\Gamma_{3A}(\gamma_{10}, \gamma_{20}, \gamma_{21})}$ , together with its degradability regions, is reported in Figure 5.3.1.

### 5.3.b Class 3B

Consider the sample channel  $\Phi_{\Gamma_{3B}(\gamma_{20}, \gamma_{30}, \gamma_{31})}$  belonging in class 3B; this channel is identified by the transition matrix:

$$\begin{aligned} \Gamma_{3B}(\gamma_{10}, \gamma_{30}, \gamma_{32}) = & \mathbb{1}_4 + \gamma_{10} |1\rangle\langle 0| + \gamma_{30} |3\rangle\langle 0| + \gamma_{32} |3\rangle\langle 2| \\ & - \gamma_{10} |1\rangle\langle 1| - (\gamma_{30} + \gamma_{32}) |3\rangle\langle 3|. \end{aligned} \quad (5.3.2)$$

The degradability conditions for class 3B, reported in (4.7.7), translate to :

$$\Phi_{\Gamma_{3B}(\gamma_{10}, \gamma_{30}, \gamma_{32})} \text{ degradable} \Leftrightarrow 0 \leq \gamma_{10} \leq \frac{1}{2} \wedge 0 \leq \gamma_{32} + \gamma_{30} \leq \frac{1}{2}; \quad (5.3.3)$$

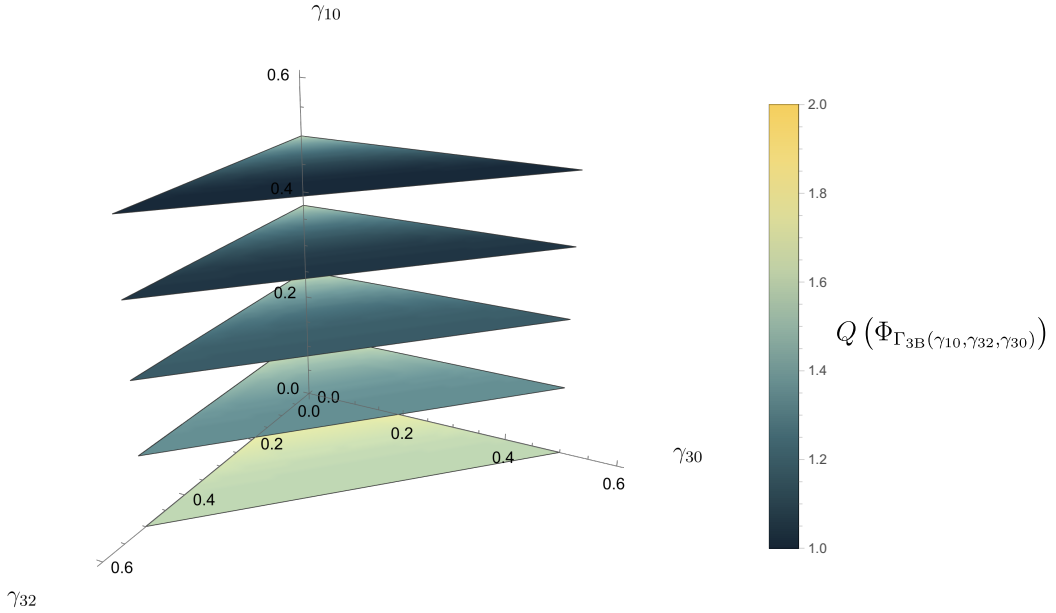


**Figure 5.3.3:** Slices of the quantum capacity in the 3-dimensional degradable region of  $\Phi_{\Gamma_{3B}(\gamma_{10}, \gamma_{30}, \gamma_{32})}$ .

this conditions are rendered in Figure 5.3.2. It is possible to extend the computation performed in the degradability zones to the remainder of the parameter region.

### Quantum capacity in degradability region

One can directly compute the quantum capacity of  $\Phi_{\Gamma_{3B}(\gamma_{10}, \gamma_{30}, \gamma_{32})}$  in the blue region rendered in Figure 5.3.2 using the result (3.3.21).

$$\begin{aligned} Q(\Phi_{\Gamma_{3B}(\gamma_{10}, \gamma_{30}, \gamma_{32})}) &= \max_{\rho^{(diag)}} I_c(\rho^{(diag)}, \Phi_{\Gamma_{3B}(\gamma_{10}, \gamma_{30}, \gamma_{32})}), \\ &\forall \gamma_{10}, \gamma_{30}, \gamma_{32} : 0 \leq \gamma_{30} + \gamma_{32} \leq \frac{1}{2} \wedge 0 \leq \gamma_{10} \leq \frac{1}{2}. \end{aligned} \quad (5.3.4)$$

This computation was performed for 5 choices of  $\gamma_{10}$  in that region and plotted in Figure 5.3.3.

### Quantum capacity on borders of the parameter region

Consider the 2-dimensional surfaces of Figure 5.3.2; it is possible to compute the quantum capacity of  $\Phi_{\Gamma_{3B}(\gamma_{10}, \gamma_{30}, \gamma_{32})}$  on any of these surfaces.

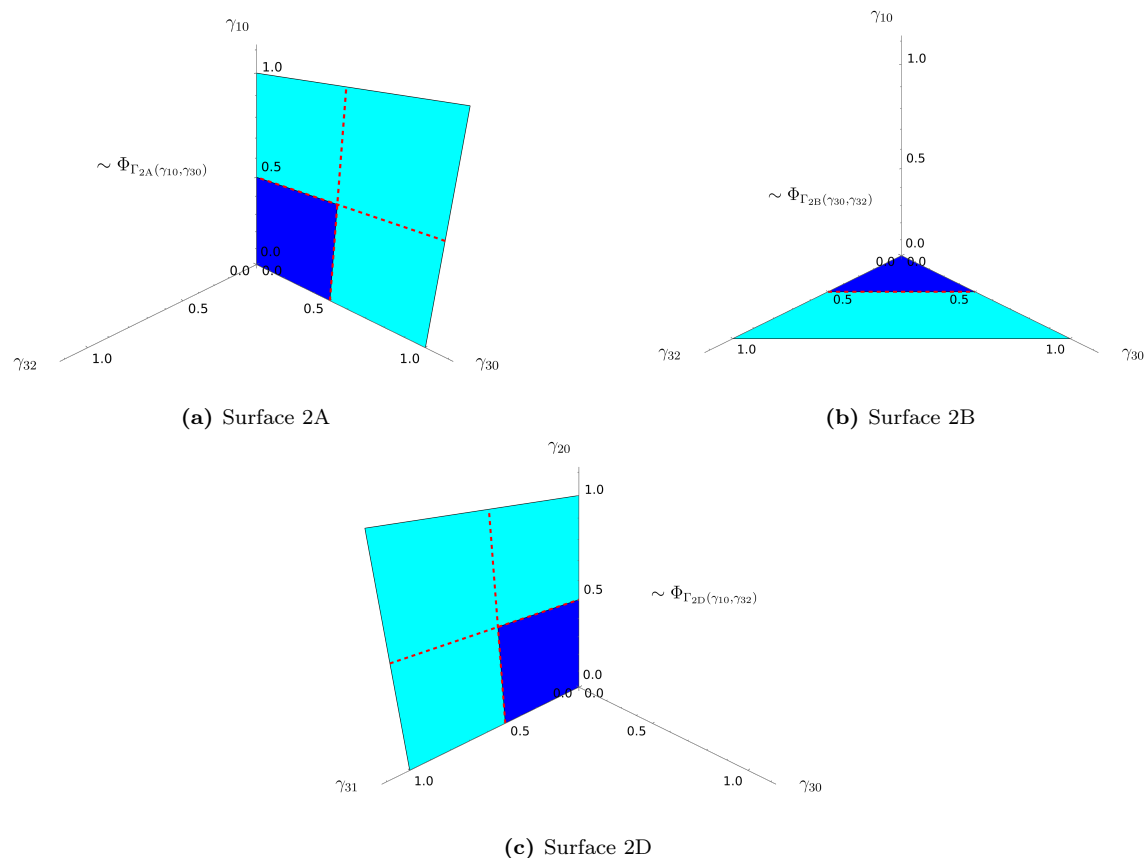


**Figure 5.3.4:** Surfaces in the parameter space of  $\Phi_{\Gamma_{3B}(\gamma_{10}, \gamma_{30}, \gamma_{32})}$  corresponding to setting one of the transition probabilities  $\gamma_{10}, \gamma_{30}, \gamma_{32}$  to 0.

When either  $\gamma_{10}, \gamma_{30}, \gamma_{32}$  is 0 (these surfaces are represented in Figure 5.3.4) the channel reduces to channels belonging to, respectively, Class 2B (Figure 5.3.4b), Class 2D (Figure 5.3.4c) and Class 2A (Figure 5.3.4a). The results in Subsection 5.2.a, Subsection 5.2.b, Subsection 5.2.d allow for the computation of the quantum capacity on those surfaces.

When  $\gamma_{30} + \gamma_{32} = 1$ , the quantum capacity of  $\Phi_{\Gamma_{3B}(\gamma_{10}, \gamma_{30}, \gamma_{32})}$  is computable thanks to the result in (4.10.9), which implies that:

$$Q(\Phi_{\Gamma_{3B}(\gamma_{10}, \gamma_{30}, 1-\gamma_{30})}) = Q(\Phi_{\Gamma_{1A3}(\gamma_{10})}^{(3)}), \quad (5.3.5)$$

where  $\Phi_{\Gamma_{1A3}(\gamma_{10})}^{(3)}$  is defined in (5.2.7).

When  $\gamma_{10} = 1$ , it can be useful to work with another channel belonging in Class 3B, identified by the transition matrix:

$$\begin{aligned} \Gamma'_{3B}(\gamma_{10}, \gamma_{30}, \gamma_{32}) = & \mathbb{1}_4 + \gamma_{10} |3\rangle\langle 0| + \gamma_{30} |2\rangle\langle 0| + \gamma_{32} |2\rangle\langle 1| \\ & - \gamma_{10} |3\rangle\langle 3| - (\gamma_{30} + \gamma_{32}) |2\rangle\langle 2|. \end{aligned} \quad (5.3.6)$$

For a fixed choice of the transition probabilities,  $\Phi_{\Gamma_{3B}(\gamma_{10}, \gamma_{30}, \gamma_{32})}$  and  $\Phi_{\Gamma'_{3B}(\gamma_{10}, \gamma_{30}, \gamma_{32})}$  are unitarily covariant. The quantum capacity of  $\Phi_{\Gamma'_{3B}(\gamma_{10}=1, \gamma_{30}, \gamma_{32})}$  can be found using (4.10.9):

$$Q(\Phi_{\Gamma_{3B}(\gamma_{10}=1, \gamma_{30}, \gamma_{32})}) = Q(\Phi_{\Gamma'_{3B}(\gamma_{10}=1, \gamma_{30}, \gamma_{32})}) = Q(\Phi_{\Gamma_{2B3}(\gamma_{30}, \gamma_{32})}^{(3)}), \quad (5.3.7)$$

where  $\Phi_{\Gamma_{2B3}(\gamma_{30}, \gamma_{32})}^{(3)}$  is a 3-dimensional MAD channel identified by the transition matrix:

$$\Gamma_{2B3}(\gamma_{30}, \gamma_{32}) = \mathbb{1}_3 + \gamma_{30} |2\rangle\langle 0| + \gamma_{32} |2\rangle\langle 1| - (\gamma_{30} + \gamma_{32}) |2\rangle\langle 2|. \quad (5.3.8)$$

The quantum capacity of  $\Phi_{\Gamma_{2B3}(\gamma_{30}, \gamma_{32})}^{(3)}$  can be obtained using the results in [CG21a].

**Extension to  $\frac{1}{2} \leq \gamma_{10} \leq 1$  and  $0 \leq \gamma_{30} + \gamma_{32} \leq \frac{1}{2}$**

$Q(\Phi_{\Gamma_{2B3}(\gamma_{30}, \gamma_{32})}^{(3)})$  is a lower bound on  $Q(\Phi_{\Gamma_{3B}(\gamma_{10}, \gamma_{30}, \gamma_{32})})$ , as it is the emergent quantum capacity from a fixed choice of encoding. Furthermore, numerically computing the difference between these values at  $\gamma_{10} = \frac{1}{2}$  and  $0 \leq \gamma_{30} + \gamma_{32} \leq \frac{1}{2}$ , one finds that (refer to Figure 5.3.5):

$$\begin{aligned} Q(\Phi_{\Gamma_{3B}(\gamma_{10}=1/2, \gamma_{30}, \gamma_{32})}) &= Q(\Phi_{\Gamma_{3B}(\gamma_{10}=1, \gamma_{30}, \gamma_{32})}) \stackrel{(5.3.7)}{=} Q(\Phi_{\Gamma_{2B3}(\gamma_{30}, \gamma_{32})}^{(3)}), \\ \forall \gamma_{30}, \gamma_{32} : 0 &\leq \gamma_{30} + \gamma_{32} \leq \frac{1}{2}. \end{aligned} \quad (5.3.9)$$

The Equation (5.3.9), together with the non-increasing monotonous property of  $Q(\Phi_{\Gamma_{3B}(\gamma_{10}, \gamma_{30}, \gamma_{32})})$  in its parameters, allow to infer the value of the latter quantity in the region  $0 \leq \gamma_{30} + \gamma_{32} \leq \frac{1}{2}, \frac{1}{2} \leq \gamma_{10} \leq 1$ , plotted in Figure 5.3.6.

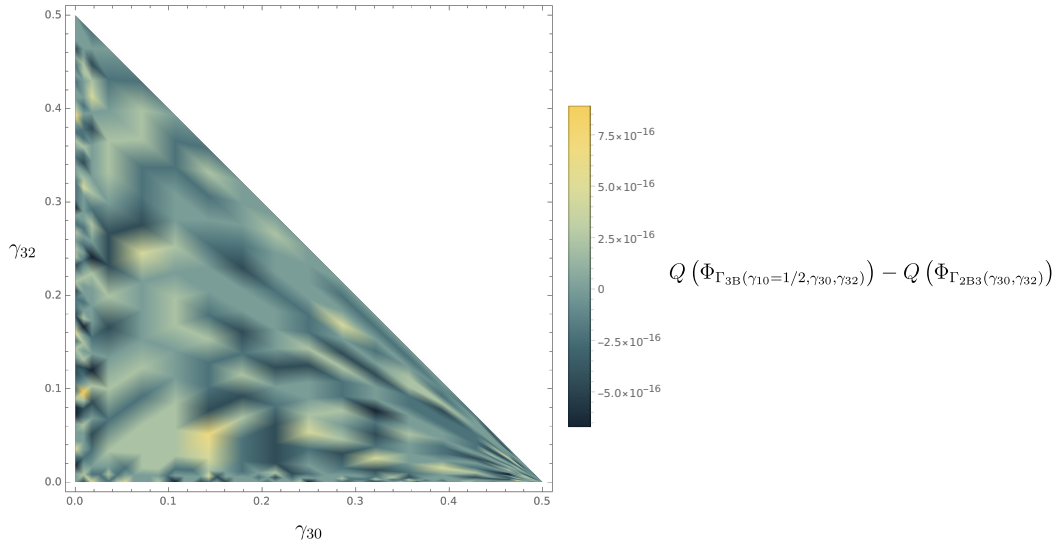


**Figure 5.3.5:** Density plot of the difference between  $Q(\Phi_{\Gamma_{3B}(1/2, \gamma_{30}, \gamma_{32})})$  and  $Q(\Phi_{\Gamma_{2B3}(\gamma_{30}, \gamma_{32})}^{(3)})$ . The discrepancies from 0 are to be attributed to the precision of the machine used for the computation.

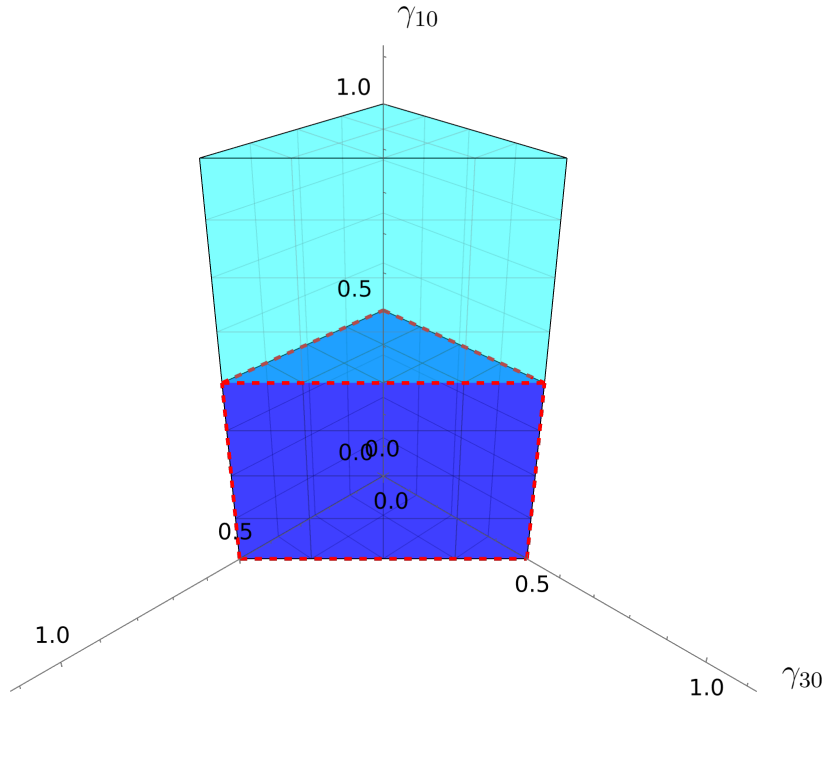


**Figure 5.3.6:** (5.3.10) permits the calculation of the quantum capacity in the cyan region, extending the computation performed in the degradable (blue) region

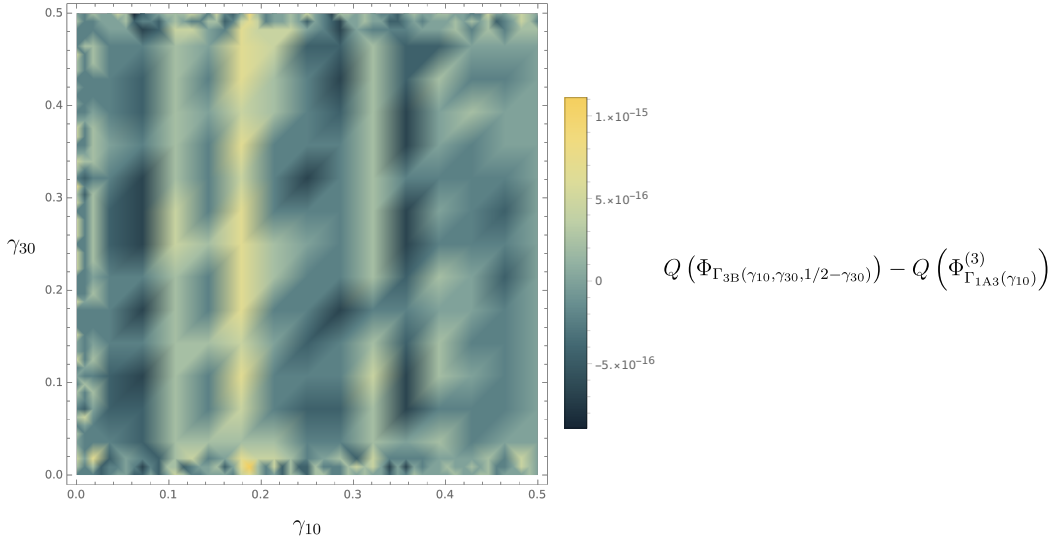


**Figure 5.3.7:** Density plot of the difference between  $Q(\Phi_{\Gamma_{3B}(\gamma_{10}, \gamma_{30}, 1/2 - \gamma_{30})})$  and  $Q(\Phi_{\Gamma_{1A3}(\gamma_{10})}^{(3)})$ . The discrepancies from 0 are to be attributed to the precision of the machine used for the computation.

$$\begin{aligned} Q(\Phi_{\Gamma_{3B}(\gamma_{10}, \gamma_{30}, \gamma_{32})}) &= Q(\Phi_{\Gamma_{2B3}(\gamma_{30}, \gamma_{32})}^{(3)}), \\ \forall \gamma_{10}, \gamma_{30}, \gamma_{32} : 0 \leq \gamma_{30} + \gamma_{32} \leq \frac{1}{2} \wedge \frac{1}{2} \leq \gamma_{10} \leq 1. \end{aligned} \quad (5.3.10)$$

**Extension to**  $\frac{1}{2} \leq \gamma_{30} + \gamma_{32} \leq 1, 0 \leq \gamma_{10} \leq \frac{1}{2}$

Following along the previous line of reasoning, one could calculate the difference between  $Q(\Phi_{\Gamma_{3B}(\gamma_{10}, \gamma_{30}, 1 - \gamma_{30})}) \stackrel{(5.3.5)}{=} Q(\Phi_{\Gamma_{1A3}(\gamma_{10})}^{(3)})$  and  $Q(\Phi_{\Gamma_{3B}(\gamma_{10}, \gamma_{30}, 1/2 - \gamma_{30})})$ , which is plotted in Figure 5.3.7.

$$Q(\Phi_{\Gamma_{3B}(\gamma_{10}, \gamma_{30}, 1/2 - \gamma_{30})}) = Q(\Phi_{\Gamma_{3B}(\gamma_{10}, \gamma_{30}, 1 - \gamma_{30})}) \stackrel{(5.3.5)}{=} Q(\Phi_{\Gamma_{1A3}(\gamma_{10})}^{(3)}). \quad (5.3.11)$$

The monotonicity properties of  $Q(\Phi_{\Gamma_{3B}(\gamma_{10}, \gamma_{30}, \gamma_{32})})$ , together with (5.3.11) allow to obtain the quantum capacity of  $\Phi_{\Gamma_{3B}(\gamma_{10}, \gamma_{30}, \gamma_{32})}$  in the region  $\frac{1}{2} \leq \gamma_{30} + \gamma_{32} \leq 1, 0 \leq \gamma_{10} \leq \frac{1}{2}$ , represented in Figure 5.3.8.

$$\begin{aligned} Q(\Phi_{\Gamma_{3B}(\gamma_{10}, \gamma_{30}, \gamma_{32})}) &= Q(\Phi_{\Gamma_{1A3}(\gamma_{10})}^{(3)}), \\ \forall \gamma_{10}, \gamma_{30}, \gamma_{32} : \frac{1}{2} \leq \gamma_{30} + \gamma_{32} \leq 1 \wedge 0 \leq \gamma_{10} \leq \frac{1}{2}. \end{aligned} \quad (5.3.12)$$

**Extension to**  $\frac{1}{2} \leq \gamma_{30} + \gamma_{32} \leq 1, \frac{1}{2} \leq \gamma_{10} \leq 1$

The remaining region in which the quantum capacity of  $\Phi_{\Gamma_{3B}(\gamma_{10}, \gamma_{30}, \gamma_{32})}$  is yet to be found is  $\frac{1}{2} \leq \gamma_{30} + \gamma_{32} \leq 1, \frac{1}{2} \leq \gamma_{10} \leq 1$ . One could compute this quantum capacity on

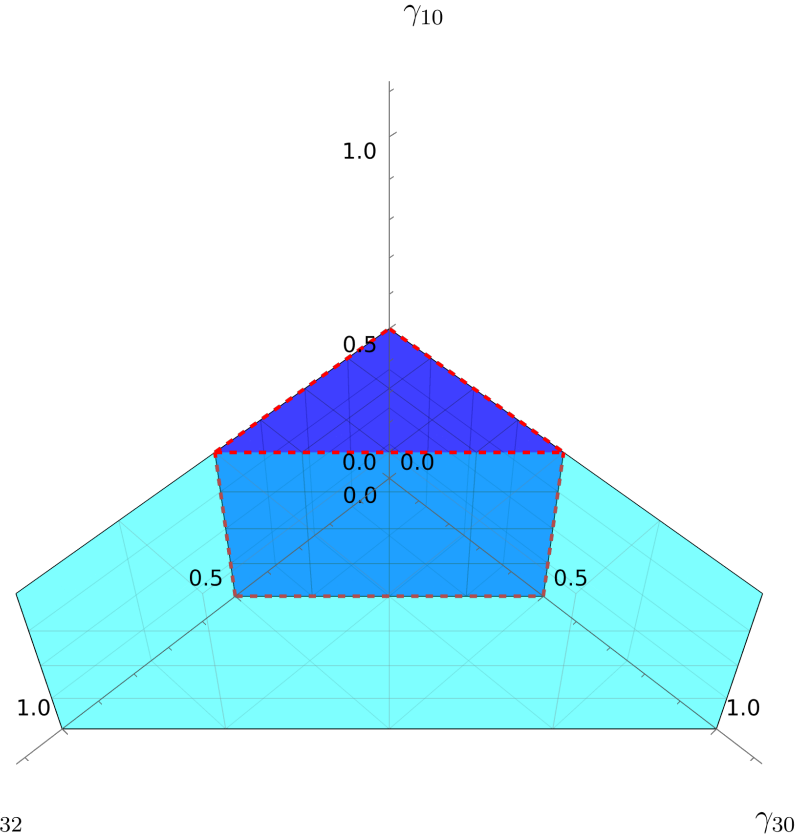


**Figure 5.3.8:** (5.3.10) permits the calculation of the quantum capacity in the cyan region, extending the computation performed in the degradable (blue) region

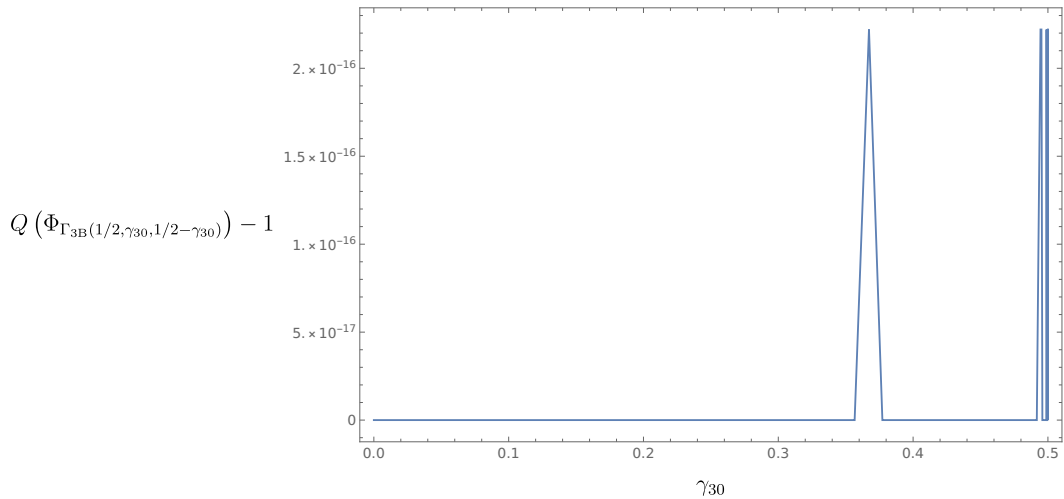


**Figure 5.3.9:** Plot of the difference between  $Q(\Phi_{\Gamma_{3B}(1/2, \gamma_{30}, 1/2 - \gamma_{30})})$  and 1. The discrepancies from 0 are to be attributed to the precision of the machine used for the computation.

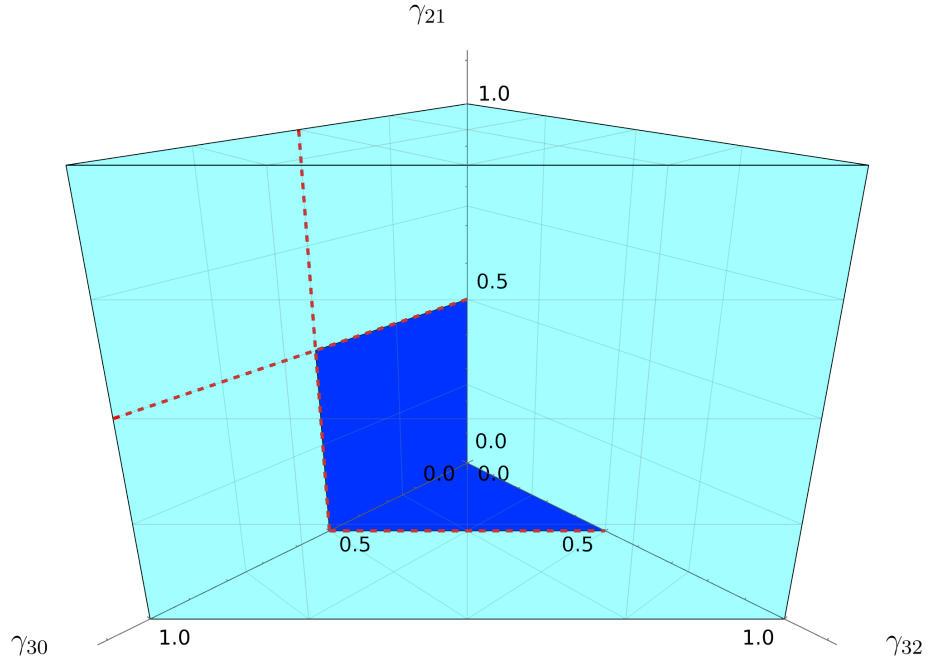


**Figure 5.3.10:** The graph represents the parameter region (cyan) of  $\Phi_{\Gamma_{3C}(\gamma_{21}, \gamma_{30}, \gamma_{32})}$  and its degradability regions (blue).

$\gamma_{10} = \frac{1}{2}$ ,  $\gamma_{30} + \gamma_{32} = \frac{1}{2}$  and verify that it is equal to 1 (see Figure 5.3.9), with 1 being a lower bound on the quantum capacity as its the  $\log_2$  of the noiseless subspace of the channel. Since  $Q(\Phi_{\Gamma_{3B}(\gamma_{10}, \gamma_{30}, \gamma_{32})})$  is non-increasing in its arguments, it is equal to 1 in the whole region  $\frac{1}{2} \leq \gamma_{30} + \gamma_{32} \leq 1$ ,  $\frac{1}{2} \leq \gamma_{10} \leq 1$ :

$$\begin{aligned} Q(\Phi_{\Gamma_{3B}(\gamma_{10}, \gamma_{30}, \gamma_{32})}) &= 1, \\ \forall \gamma_{10}, \gamma_{30}, \gamma_{32} : \frac{1}{2} \leq \gamma_{30} + \gamma_{32} \leq 1 \wedge \frac{1}{2} \leq \gamma_{10} \leq 1. \end{aligned} \tag{5.3.13}$$

Combining (5.3.13), (5.3.12), (5.3.10), and (5.3.4) one is able to find the quantum capacity of  $\Phi_{\Gamma_{3B}(\gamma_{10}, \gamma_{30}, \gamma_{32})}$  in its whole parameter space.

### 5.3.c Class 3C

Consider the sample channel  $\Phi_{\Gamma_{3C}(\gamma_{21}, \gamma_{30}, \gamma_{32})}$  belonging in Class 3C, identified by the transition matrix:

$$\begin{aligned} \Gamma_{3C}(\gamma_{21}, \gamma_{30}, \gamma_{32}) &= \mathbf{1}_4 + \gamma_{21} |2\rangle\langle 1| + \gamma_{30} |3\rangle\langle 0| + \gamma_{32} |3\rangle\langle 2| \\ &\quad - \gamma_{21} |2\rangle\langle 2| - (\gamma_{30} + \gamma_{32}) |3\rangle\langle 3|. \end{aligned} \tag{5.3.14}$$

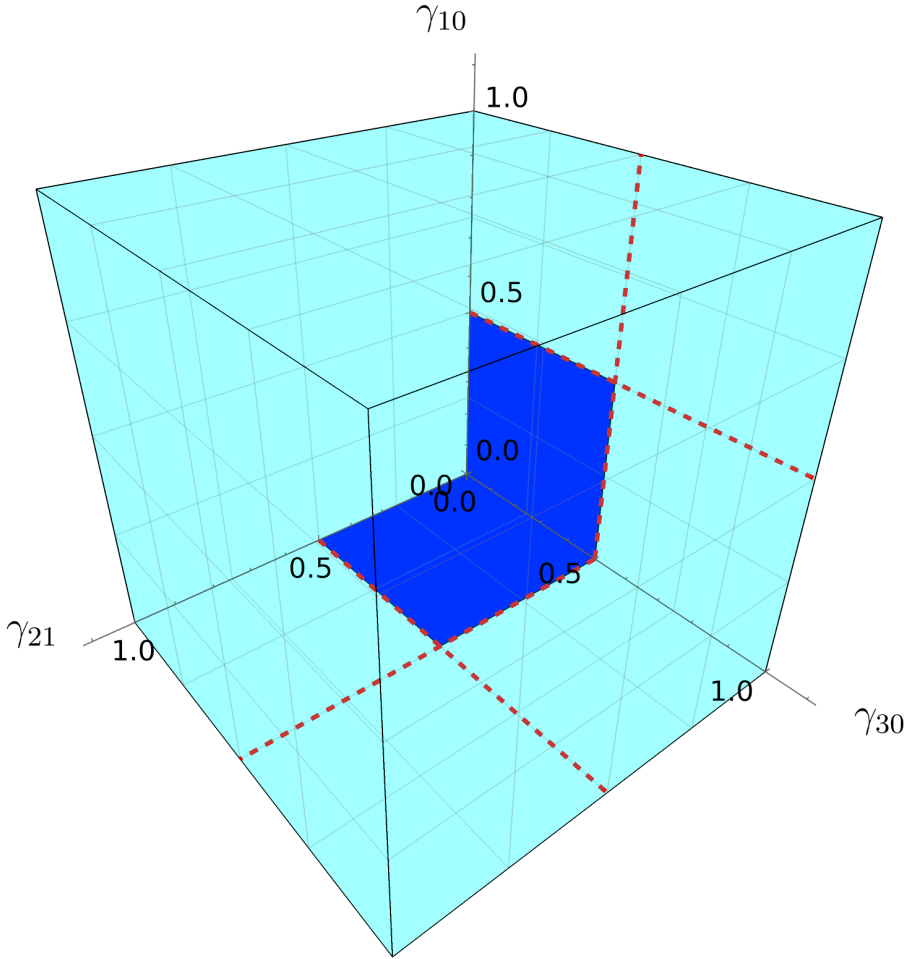


**Figure 5.3.11:** The graph represents the parameter region (cyan) of  $\Phi_{\Gamma_{3D}(\gamma_{10}, \gamma_{21}, \gamma_{30})}$  and its degradability regions (blue).

As a consequence of the results of Subsection 4.7.h,  $\Phi_{\Gamma_{3C}(\gamma_{21}, \gamma_{30}, \gamma_{32})}$  is never degradable unless either one of  $\gamma_{21}$ ,  $\gamma_{32}$  is 0, at which point the channel reduces, respectively, to a channel belonging in Class 2B and Class 2D. The degradability regions in the parameter space of  $\Phi_{\Gamma_{3C}(\gamma_{21}, \gamma_{30}, \gamma_{32})}$  are plotted in Figure 5.3.10.

### 5.3.d Class 3D

Consider the sample channel  $\Phi_{\Gamma_{3D}(\gamma_{10}, \gamma_{21}, \gamma_{30})}$  belonging in Class 3D, identified by the transition matrix:

$$\begin{aligned} \Gamma_{3D}(\gamma_{10}, \gamma_{21}, \gamma_{30}) = & \mathbb{1}_4 + \gamma_{10} |1\rangle\langle 0| + \gamma_{21} |2\rangle\langle 1| + \gamma_{30} |3\rangle\langle 0| \\ & - \gamma_{10} |1\rangle\langle 1| - \gamma_{21} |2\rangle\langle 2| - \gamma_{30} |3\rangle\langle 3|. \end{aligned} \quad (5.3.15)$$

As a consequence of the results of Subsection 4.7.i,  $\Phi_{\Gamma_{3D}(\gamma_{10}, \gamma_{21}, \gamma_{30})}$  is never degradable

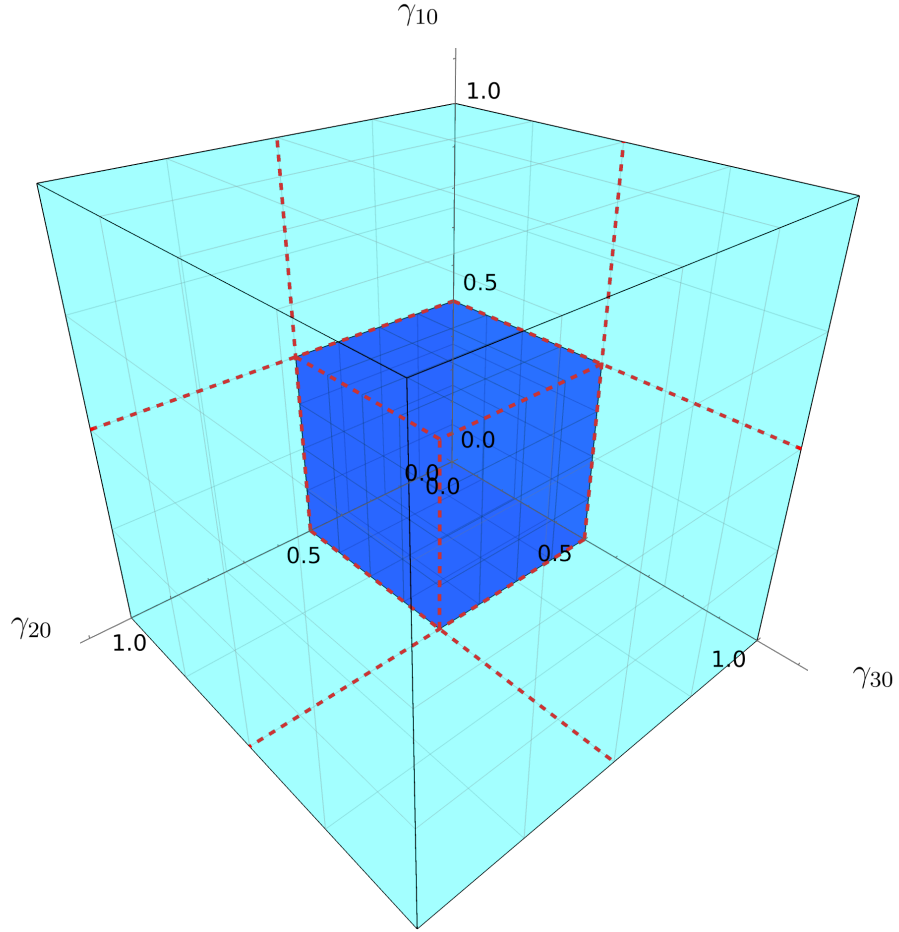


**Figure 5.3.12:** The graph represents the parameter region (cyan) of  $\Phi_{\Gamma_{3D}(\gamma_{10}, \gamma_{21}, \gamma_{30})}$  and its degradability regions (blue).

unless either one of  $\gamma_{10}$ ,  $\gamma_{21}$  is 0, at which point the channel reduces, respectively, to a channel belonging in Class 2D and Class 2A. The degradability regions in the parameter space of  $\Phi_{\Gamma_{3D}(\gamma_{10}, \gamma_{21}, \gamma_{30})}$  are plotted in Figure 5.3.11.

### 5.3.e Class 3E

Consider the sample channel  $\Phi_{\Gamma_{3E}(\gamma_{10}, \gamma_{20}, \gamma_{30})}$  belonging in Class 3E, identified by the transition matrix:

$$\begin{aligned} \Gamma_{3E(\gamma_{10}, \gamma_{20}, \gamma_{30})} = & \mathbb{1}_4 + \gamma_{10} |1\rangle\langle 0| + \gamma_{20} |2\rangle\langle 0| + \gamma_{30} |3\rangle\langle 0| \\ & - \gamma_{10} |1\rangle\langle 1| - \gamma_{20} |2\rangle\langle 2| - \gamma_{30} |3\rangle\langle 3|. \end{aligned} \quad (5.3.16)$$

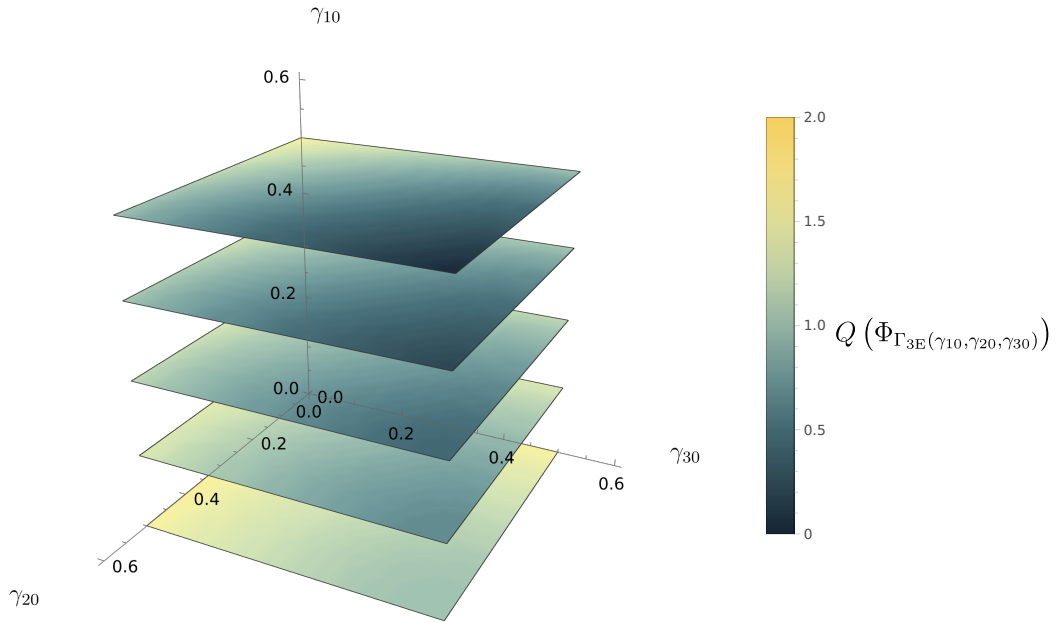


**Figure 5.3.13:** Slices of the quantum capacity in the 3-dimensional degradable region of  $\Phi_{\Gamma_{3E}(\gamma_{10}, \gamma_{20}, \gamma_{30})}$ .

The degradability conditions for class 3E, reported in (4.7.13), translate to :

$$\Phi_{\Gamma_{3E}(\gamma_{10}, \gamma_{20}, \gamma_{30})} \text{ degradable} \Leftrightarrow 0 \leq \gamma_{10} \leq \frac{1}{2} \wedge 0 \leq \gamma_{20} \leq \frac{1}{2} \wedge 0 \leq \gamma_{30} \leq \frac{1}{2}; \quad (5.3.17)$$

these conditions are rendered in Figure 5.3.12. Note that the quantum capacity of  $\Phi_{\Gamma_{3E}(\gamma_{10}, \gamma_{20}, \gamma_{30})}$  is left invariant under any permutation of  $(\gamma_{10}, \gamma_{20}, \gamma_{30})$ . It is possible to extend the computation performed in the degradability zones to the remainder of the parameter region.

### Quantum capacity in degradability region

One can directly compute the quantum capacity of  $\Phi_{\Gamma_{3E}(\gamma_{10}, \gamma_{20}, \gamma_{30})}$  in the blue region rendered in Figure 5.3.12 using the result (3.3.21).

$$\begin{aligned} Q(\Phi_{\Gamma_{3E}(\gamma_{10}, \gamma_{20}, \gamma_{30})}) &= \max_{\rho^{(diag)}} I_c(\rho^{(diag)}, \Phi_{\Gamma_{3E}(\gamma_{10}, \gamma_{20}, \gamma_{30})}), \\ \forall \gamma_{10}, \gamma_{20}, \gamma_{30} : 0 \leq \gamma_{10} \leq \frac{1}{2} \wedge 0 \leq \gamma_{20} \leq \frac{1}{2} \wedge 0 \leq \gamma_{30} \leq \frac{1}{2}. \end{aligned} \quad (5.3.18)$$

This computation was performed for 5 choices of  $\gamma_{10}$  in the degradability region and plotted in Figure 5.3.13.

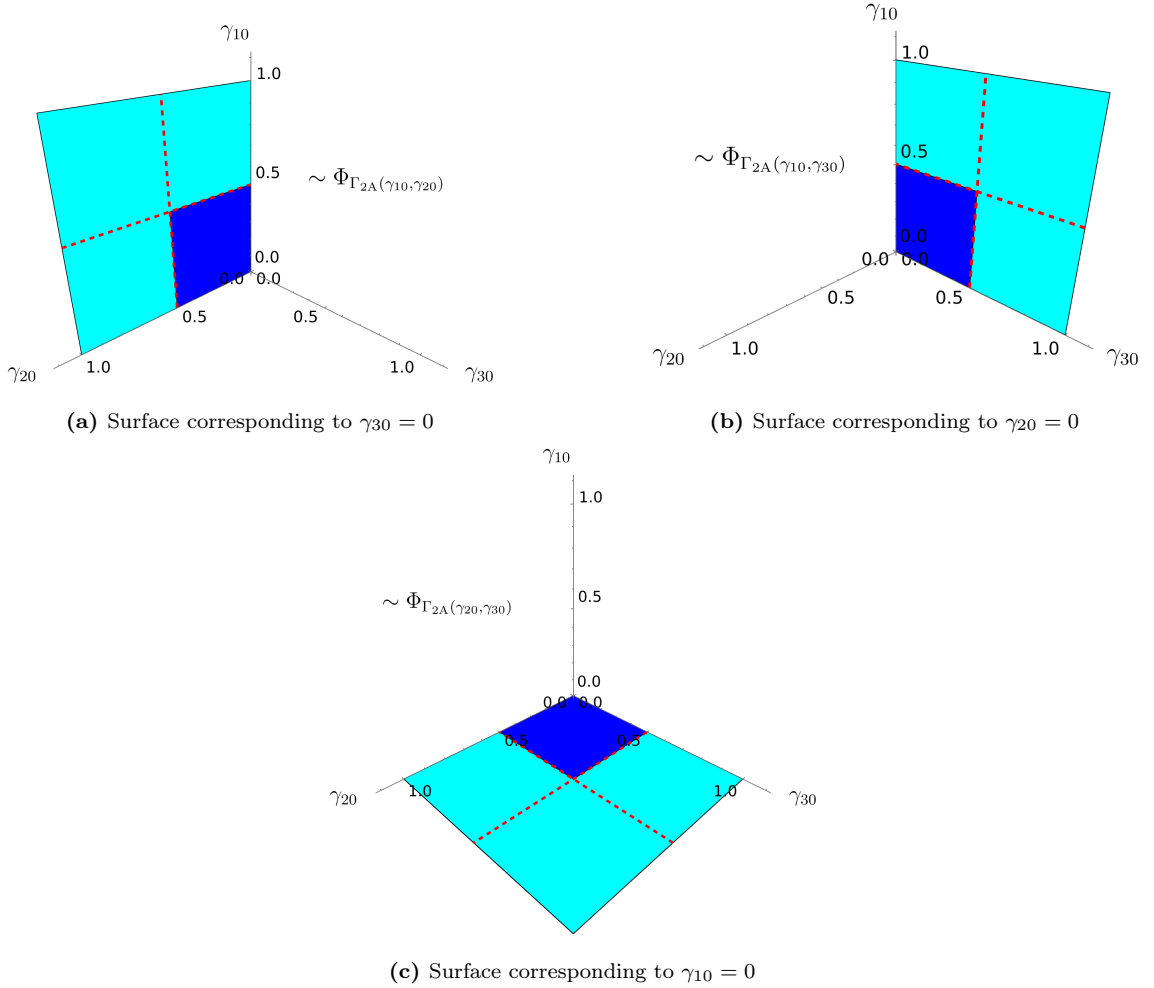


**Figure 5.3.14:** Surfaces in the parameter space of  $\Phi_{\Gamma_{3E}}(\gamma_{10}, \gamma_{20}, \gamma_{30})$  corresponding to setting one of the transition probabilities  $\gamma_{10}, \gamma_{20}, \gamma_{30}$  to 0.

### Quantum capacity on borders of the parameter region

Consider the 2-dimensional borders of the cyan region in Figure 5.3.12; it is possible to compute the quantum capacity of  $\Phi_{\Gamma_{3E}}(\gamma_{10}, \gamma_{20}, \gamma_{30})$  on any of those surfaces.

When either  $\gamma_{10}, \gamma_{20}, \gamma_{30}$  is 0 (these surfaces are represented in Figure 5.3.14),  $\Phi_{\Gamma_{3E}}(\gamma_{10}, \gamma_{20}, \gamma_{30})$  reduces to a channel belonging in Class 2A. The results in Subsection 5.2.a allow for the computation of the quantum capacity on those surfaces. Assume complete damping of a single level of the qudit, i.e. either one of  $\gamma_{10}, \gamma_{20}, \gamma_{30}$  is 1; given the invariance of  $Q(\Phi_{\Gamma_{3E}}(\gamma_{10}, \gamma_{20}, \gamma_{30}))$  under swap of the parameters, one could study, without loss of generality, the case  $\gamma_{30} = 1$ . Using (4.10.9), the quantum capacity of

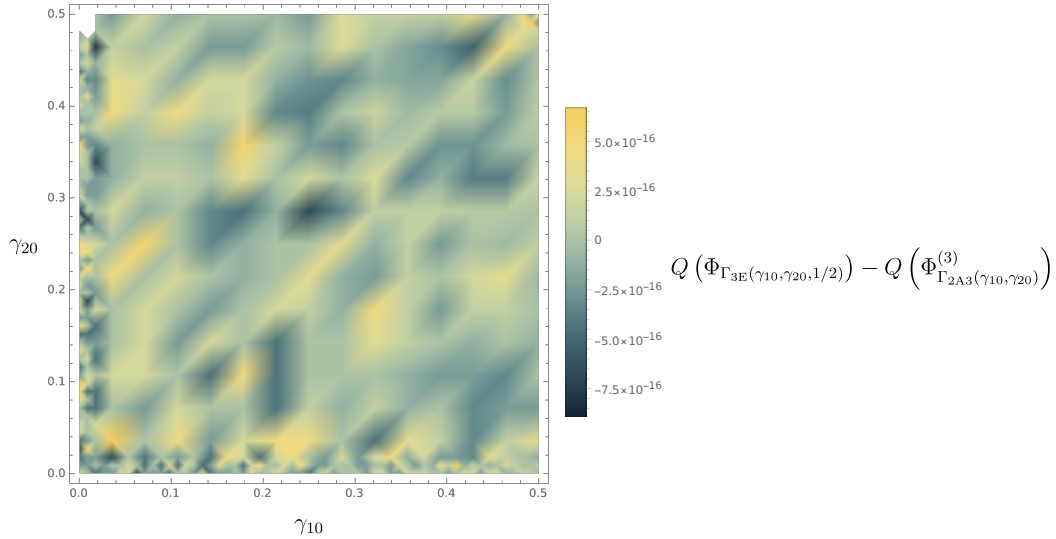


**Figure 5.3.15:** Density plot of the difference between  $Q(\Phi_{\Gamma_{3E}(\gamma_{10}, \gamma_{20}, \gamma_{30}=1/2)})$  and  $Q(\Phi_{\Gamma_{2A3}(\gamma_{10}, \gamma_{20})}^{(3)})$ . The discrepancies from 0 are to be attributed to the precision of the machine used for the computation.

$\Phi_{\Gamma_{3E}(\gamma_{10}, \gamma_{20}, \gamma_{30})}$  in the case of complete damping for a level of the qudit is:

$$\begin{aligned} Q(\Phi_{\Gamma_{3E}(\gamma_{10}, \gamma_{20}, \gamma_{30}=1)}) &= Q(\Phi_{\Gamma_{2A3}(\gamma_{10}, \gamma_{20})}^{(3)}), \\ Q(\Phi_{\Gamma_{3E}(\gamma_{10}, \gamma_{20}=1, \gamma_{30})}) &= Q(\Phi_{\Gamma_{2A3}(\gamma_{10}, \gamma_{30})}^{(3)}), \\ Q(\Phi_{\Gamma_{3E}(\gamma_{10}=1, \gamma_{20}, \gamma_{30})}) &= Q(\Phi_{\Gamma_{2A3}(\gamma_{20}, \gamma_{30})}^{(3)}), \end{aligned} \quad (5.3.19)$$

where  $\Phi_{\Gamma_{2A3}(\gamma_{10}, \gamma_{20})}^{(3)}$  is a 3-dimensional MAD channel whose identifying transition matrix is:

$$\Gamma_{2A3}(\gamma_{10}, \gamma_{20}) = \mathbb{1}_3 + \gamma_{10} |1\rangle\langle 0| + \gamma_{20} |2\rangle\langle 0| - \gamma_{10} |1\rangle\langle 1| - \gamma_{20} |2\rangle\langle 2|. \quad (5.3.20)$$

The quantum capacity of  $\Phi_{\Gamma_{2A3}(\gamma_{10}, \gamma_{20})}^{(3)}$  can be obtained exploiting the results from [CG21a].

**Extension to**  $\frac{1}{2} \leq \gamma_{30} \leq 1$ ,  $0 \leq \gamma_{20} \leq \frac{1}{2}$ ,  $0 \leq \gamma_{10} \leq \frac{1}{2}$

$Q(\Phi_{\Gamma_{2A3}(\gamma_{10}, \gamma_{20})}^{(3)})$  is a lower bound on  $Q(\Phi_{\Gamma_{3E}(\gamma_{10}, \gamma_{20}, \gamma_{30})})$ , as it is the emergent quantum capacity from a fixed choice of encoding. Furthermore, numerically computing the difference between these values at  $\gamma_{30} = \frac{1}{2}$  and  $0 \leq \gamma_{10} \leq \frac{1}{2} \wedge 0 \leq \gamma_{20} \leq \frac{1}{2}$ , one finds that (refer to Figure 5.3.15):

$$\begin{aligned} Q(\Phi_{\Gamma_{3E}(\gamma_{10}, \gamma_{20}, \gamma_{30}=1/2)}) &= Q(\Phi_{\Gamma_{3E}(\gamma_{10}, \gamma_{20}, \gamma_{30}=1)}) \stackrel{(5.3.19)}{=} Q(\Phi_{\Gamma_{2A3}(\gamma_{10}, \gamma_{20})}^{(3)}), \\ \forall \gamma_{10}, \gamma_{20} : 0 \leq \gamma_{10} \leq \frac{1}{2} \wedge 0 \leq \gamma_{20} \leq \frac{1}{2}. \end{aligned} \quad (5.3.21)$$

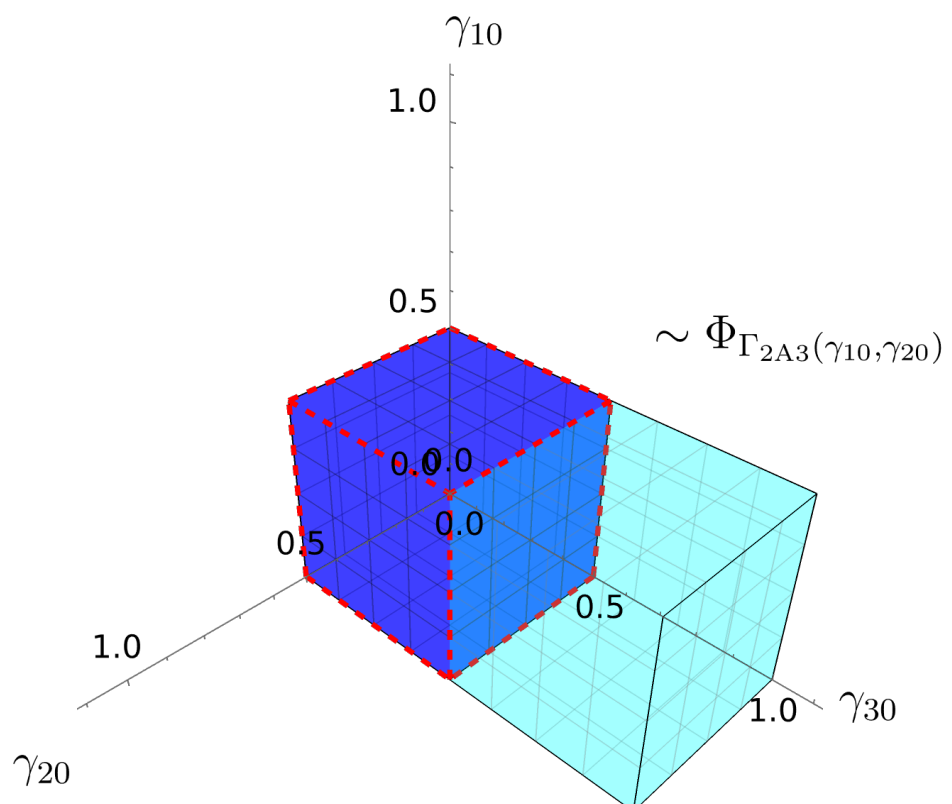


**Figure 5.3.16:** (5.3.22) permits the calculation of the quantum capacity in the cyan region, extending the computation performed in the degradable (blue) region

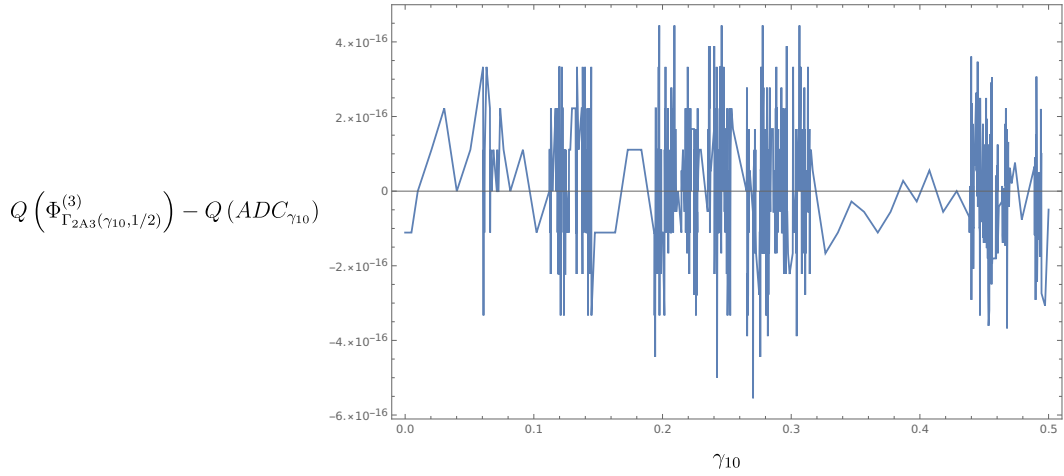


**Figure 5.3.17:** plot of the difference between  $Q\left(\Phi_{\Gamma_{2A3}(\gamma_{10}, \gamma_{20}=1/2)}^{(3)}\right)$  and  $Q(ADC_{\gamma_{10}})$ . The discrepancies from 0 are to be attributed to the precision of the machine used for the computation.

The Equation (5.3.21), together with the non-increasing monotonous property of  $Q\left(\Phi_{\Gamma_{3E}(\gamma_{10}, \gamma_{20}, \gamma_{30})}\right)$  in its parameters and its invariance under swap of the parameters, allow to infer the value of the latter quantity in the regions , the first of which is plotted in Figure 5.3.16.

$$\begin{aligned} Q\left(\Phi_{\Gamma_{3E}(\gamma_{10}, \gamma_{20}, \gamma_{30})}\right) &= Q\left(\Phi_{\Gamma_{2A3}(\gamma_{10}, \gamma_{20})}^{(3)}\right), \\ \forall \gamma_{10}, \gamma_{20}, \gamma_{30} : 0 \leq \gamma_{10} \leq \frac{1}{2} \wedge 0 \leq \gamma_{20} \leq \frac{1}{2} \wedge \frac{1}{2} \leq \gamma_{30} \leq 1. \end{aligned} \quad (5.3.22)$$

$$\begin{aligned} Q\left(\Phi_{\Gamma_{3E}(\gamma_{10}, \gamma_{20}, \gamma_{30})}\right) &= Q\left(\Phi_{\Gamma_{2A3}(\gamma_{10}, \gamma_{30})}^{(3)}\right), \\ \forall \gamma_{10}, \gamma_{20}, \gamma_{30} : 0 \leq \gamma_{10} \leq \frac{1}{2} \wedge 0 \leq \gamma_{30} \leq \frac{1}{2} \wedge \frac{1}{2} \leq \gamma_{20} \leq 1. \end{aligned} \quad (5.3.23)$$

$$\begin{aligned} Q\left(\Phi_{\Gamma_{3E}(\gamma_{10}, \gamma_{20}, \gamma_{30})}\right) &= Q\left(\Phi_{\Gamma_{2A3}(\gamma_{20}, \gamma_{30})}^{(3)}\right), \\ \forall \gamma_{10}, \gamma_{20}, \gamma_{30} : 0 \leq \gamma_{20} \leq \frac{1}{2} \wedge 0 \leq \gamma_{30} \leq \frac{1}{2} \wedge \frac{1}{2} \leq \gamma_{10} \leq 1. \end{aligned} \quad (5.3.24)$$

**Extension to**  $\frac{1}{2} \leq \gamma_{30} \leq 1$ ,  $\frac{1}{2} \leq \gamma_{20} \leq 1$ ,  $0 \leq \gamma_{10} \leq \frac{1}{2}$

Following along the previous line of reasoning, one could prove that:

$$\begin{aligned} Q\left(\Phi_{\Gamma_{3E}(\gamma_{10}, \gamma_{20}, \gamma_{30})}\right) &= Q(ADC_{\gamma_{10}}), \\ \forall \gamma_{10}, \gamma_{20}, \gamma_{30} : 0 \leq \gamma_{10} \leq \frac{1}{2} \wedge \frac{1}{2} \leq \gamma_{20} \leq 1 \wedge \frac{1}{2} \leq \gamma_{30} \leq 1, \end{aligned} \quad (5.3.25)$$

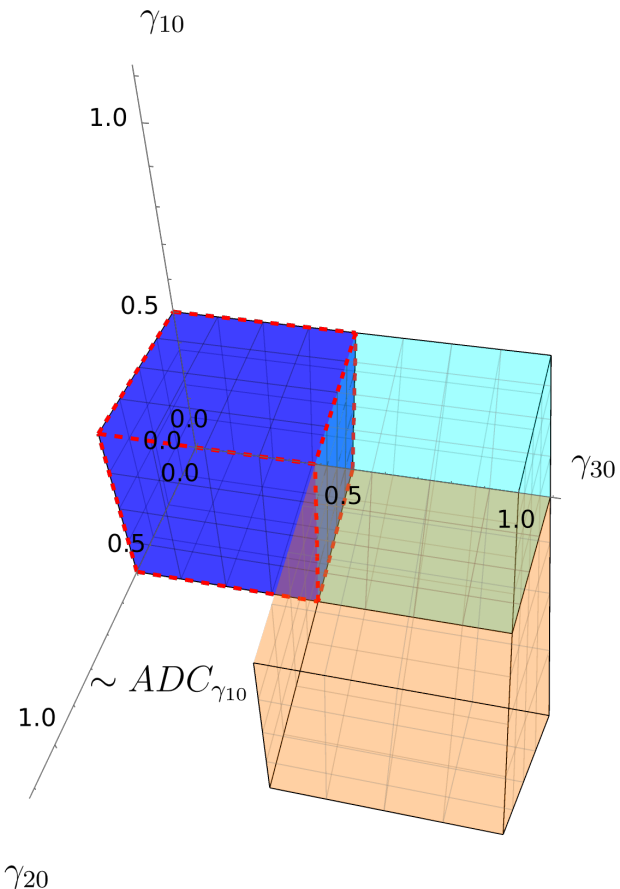


**Figure 5.3.18:** (5.3.25) permits the calculation of the quantum capacity in the orange region, extending the computation performed in the cyan region, possible thanks to (5.3.22).

where  $ADC_{\gamma_{10}}$  was defined in (3.1.3), by proving that

$$\begin{aligned} Q(\Phi_{\Gamma_{3E}(\gamma_{10}, \gamma_{20}=1/2, 1/2 \leq \gamma_{30} \leq 1)}) &\stackrel{(5.3.22)}{=} Q(\Phi_{\Gamma_{2A3}(\gamma_{10}, \gamma_{20}=1/2)}^{(3)}) \\ &= Q(\Phi_{\Gamma_{2A3}(\gamma_{10}, \gamma_{20}=1)}^{(3)}) \\ &\stackrel{[CG21a]}{=} Q(ADC_{\gamma_{10}}), \\ \forall \gamma_{10} : 0 \leq \gamma_{10} \leq \frac{1}{2}. \end{aligned} \quad (5.3.26)$$

A numerical computation of the difference between  $Q(\Phi_{\Gamma_{2A3}(\gamma_{10}, \gamma_{20}=1/2)}^{(3)})$  and  $Q(ADC_{\gamma_{10}})$  was performed and plotted in Figure 5.3.18. Note that, as a consequence of the invariance of  $Q(\Phi_{\Gamma_{3E}(\gamma_{10}, \gamma_{20}, \gamma_{30})})$  under swap of its parameters, from (5.3.25) one could also infer that:

$$\begin{aligned} Q(\Phi_{\Gamma_{3E}(\gamma_{10}, \gamma_{20}, \gamma_{30})}) &= Q(ADC_{\gamma_{20}}), \\ \forall \gamma_{10}, \gamma_{20}, \gamma_{30} : 0 \leq \gamma_{20} \leq \frac{1}{2} \wedge \frac{1}{2} \leq \gamma_{10} \leq 1 \wedge \frac{1}{2} \leq \gamma_{30} \leq 1, \end{aligned} \quad (5.3.27)$$

$$\begin{aligned} Q(\Phi_{\Gamma_{3E}(\gamma_{10}, \gamma_{20}, \gamma_{30})}) &= Q(ADC_{\gamma_{30}}), \\ \forall \gamma_{10}, \gamma_{20}, \gamma_{30} : 0 \leq \gamma_{30} \leq \frac{1}{2} \wedge \frac{1}{2} \leq \gamma_{10} \leq 1 \wedge \frac{1}{2} \leq \gamma_{20} \leq 1. \end{aligned} \quad (5.3.28)$$

Combining the symmetry under swap of the parameters of  $Q(\Phi_{\Gamma_{3E}(\gamma_{10}, \gamma_{20}, \gamma_{30})})$ , (5.3.25), (5.3.22) and (5.3.18), the quantum capacity of  $\Phi_{\Gamma_{3E}(\gamma_{10}, \gamma_{20}, \gamma_{30})}$  is found in the whole of its parameter space.

### 5.3.f Class 3F

Consider the sample channel  $\Phi_{\Gamma_{3F}(\gamma_{30}, \gamma_{31}, \gamma_{32})}$  belonging in Class 3F, identified by the transition matrix:

$$\begin{aligned} \Gamma_{3F}(\gamma_{30}, \gamma_{31}, \gamma_{32}) &= \mathbb{1}_4 + \gamma_{30}|3\rangle\langle 0| + \gamma_{31}|3\rangle\langle 1| + \gamma_{32}|3\rangle\langle 2| \\ &\quad - (\gamma_{30} + \gamma_{31} + \gamma_{32})|3\rangle\langle 3|. \end{aligned} \quad (5.3.29)$$

The degradability conditions for class 3E, reported in (4.7.15), translate to:

$$\Phi_{\Gamma_{3F}(\gamma_{30}, \gamma_{31}, \gamma_{32})} \text{ degradable} \Leftrightarrow 0 \leq \gamma_{30} + \gamma_{31} + \gamma_{32} \leq \frac{1}{2}, \quad (5.3.30)$$

these conditions are rendered in Figure 5.3.19. Note that the quantum capacity of  $\Phi_{\Gamma_{3F}(\gamma_{30}, \gamma_{31}, \gamma_{32})}$  is left invariant under any permutation of  $(\gamma_{30}, \gamma_{31}, \gamma_{32})$ . It is possible to extend the computation performed in the degradability zones to the remainder of the parameter region.

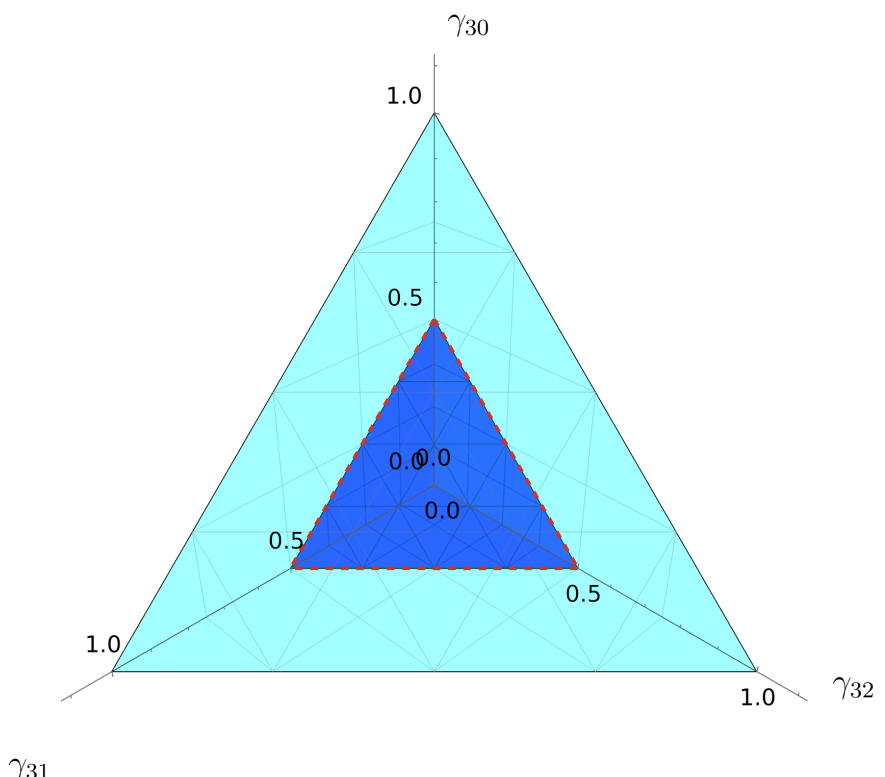


**Figure 5.3.19:** The graph represents the parameter region (cyan) of  $\Phi_{\Gamma_{3F}(\gamma_{30}, \gamma_{31}, \gamma_{32})}$  and its degradability region (blue).

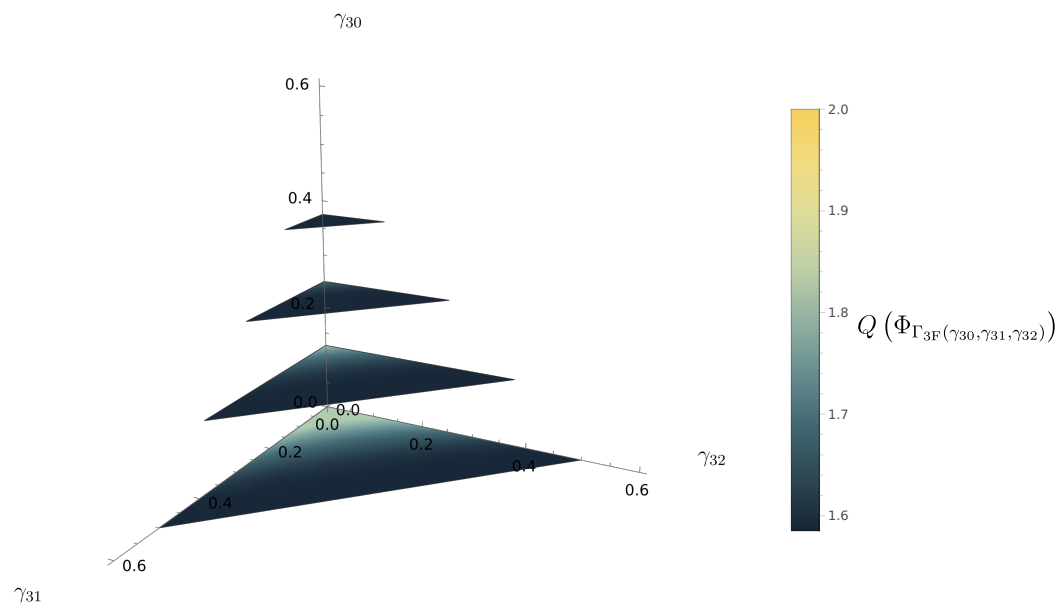


**Figure 5.3.20:** Slices of the quantum capacity in the 3-dimensional degradable region of  $\Phi_{\Gamma_{3F}(\gamma_{30}, \gamma_{31}, \gamma_{32})}$ .

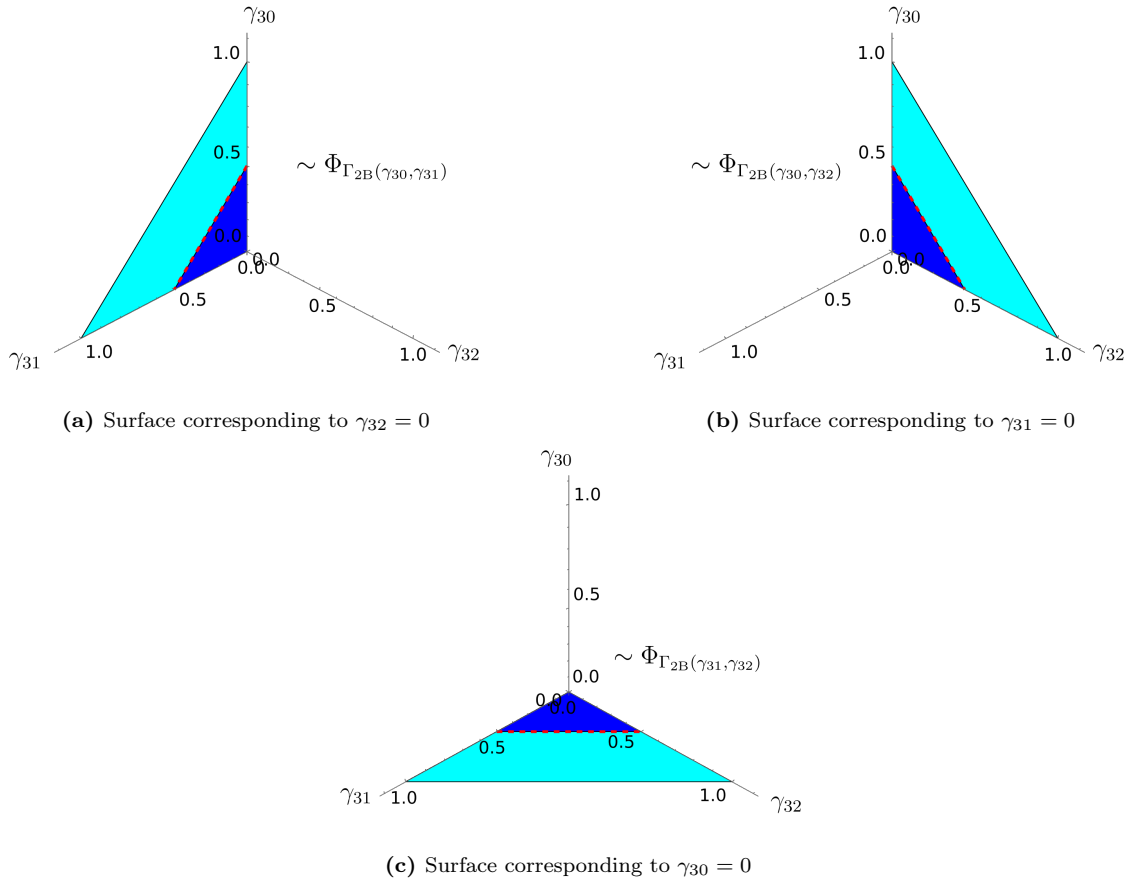


**Figure 5.3.21:** Surfaces in the parameter space of  $\Phi_{\Gamma_{3F}(\gamma_{30}, \gamma_{31}, \gamma_{32})}$  corresponding to setting one of the transition probabilities  $\gamma_{30}, \gamma_{31}, \gamma_{32}$  to 0.

### Quantum capacity in degradability region

One can directly compute the quantum capacity of  $\Phi_{\Gamma_{3F}(\gamma_{30}, \gamma_{31}, \gamma_{32})}$  in the blue region rendered in Figure 5.3.19 using the result (3.3.21).

$$Q(\Phi_{\Gamma_{3F}(\gamma_{30}, \gamma_{31}, \gamma_{32})}) = \max_{\rho^{(diag)}} I_c(\rho^{(diag)}, \Phi_{\Gamma_{3F}(\gamma_{30}, \gamma_{31}, \gamma_{32})}), \quad (5.3.31)$$

$$\forall \gamma_{30}, \gamma_{31}, \gamma_{32} : 0 \leq \gamma_{30} + \gamma_{31} + \gamma_{32} \leq \frac{1}{2}$$

This computation was performed for 4 choices of  $\gamma_{30}$  in the degradability region and plotted in Figure 5.3.20.

### Quantum capacity on borders of the parameter region

Consider the 2-dimensional borders of the cyan region in Figure 5.3.19; it is possible to compute the quantum capacity of  $\Phi_{\Gamma_{3F}(\gamma_{30}, \gamma_{31}, \gamma_{32})}$  on any of those surfaces. When

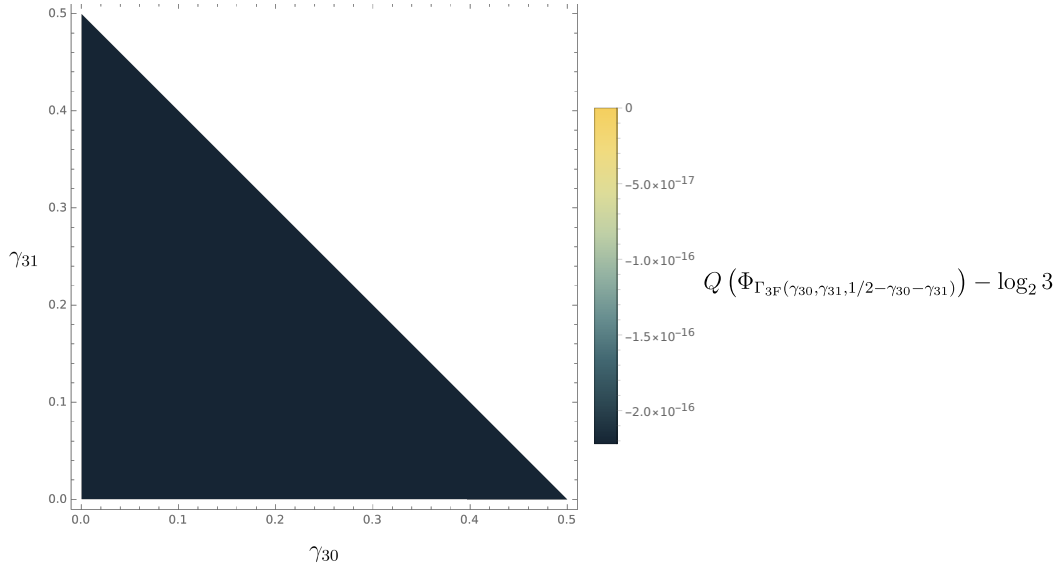


**Figure 5.3.22:** Density plot of the difference between  $Q(\Phi_{\Gamma_{3F}(\gamma_{30}, \gamma_{31}, 1/2 - \gamma_{30} - \gamma_{31})})$  and  $\log_2 3$ . The discrepancies from 0 are to be attributed to the precision of the machine used for the computation.

either  $\gamma_{30}, \gamma_{31}, \gamma_{32}$  is 0 (these surfaces are represented in Figure 5.3.21),  $\Phi_{\Gamma_{3F}(\gamma_{30}, \gamma_{31}, \gamma_{32})}$  reduces to a channel belonging in Class 2B. The results in Subsection 5.2.b allow for the computation of the quantum capacity on those surfaces. In the case of complete damping of level  $|3\rangle$ , i.e. when  $\gamma_{30} + \gamma_{31} + \gamma_{32} = 1$ , from the result (4.10.9) one can infer that:

$$Q(\Phi_{\Gamma_{3F}(\gamma_{30}, \gamma_{31}, 1 - \gamma_{30} - \gamma_{31})}) = \log_2 3. \quad (5.3.32)$$

**Extension to**  $\frac{1}{2} \leq \gamma_{30} + \gamma_{31} + \gamma_{32} \leq 1$

A natural lower bound on  $Q(\Phi_{\Gamma_{3F}(\gamma_{30}, \gamma_{31}, \gamma_{32})})$  is  $\log_2 3$ , as it is the emergent quantum capacity from a fixed choice of encoding. Furthermore, numerically computing the difference between these values at  $\gamma_{32} = \frac{1}{2} - \gamma_{31} - \gamma_{30}$  and  $0 \leq \gamma_{30} + \gamma_{31} \leq \frac{1}{2}$ , one finds that (refer to Figure 5.3.22):

$$\begin{aligned} Q(\Phi_{\Gamma_{3F}(\gamma_{30}, \gamma_{31}, 1/2 - \gamma_{30} - \gamma_{31})}) &= Q(\Phi_{\Gamma_{3F}(\gamma_{30}, \gamma_{31}, 1 - \gamma_{30} - \gamma_{31})}) \stackrel{(5.3.32)}{=} \log_2 3, \\ \forall \gamma_{30}, \gamma_{31} : 0 \leq \gamma_{30} + \gamma_{31} &\leq \frac{1}{2} \end{aligned} \quad (5.3.33)$$

The Equation (5.3.33), together with the non-increasing monotonous property of  $Q(\Phi_{\Gamma_{3F}(\gamma_{30}, \gamma_{31}, \gamma_{32})})$  in its parameters, allow to infer the value of the latter quantity in the cyan region of Figure 5.3.19.

$$\begin{aligned} Q(\Phi_{\Gamma_{3F}(\gamma_{30}, \gamma_{31}, \gamma_{32})}) &= \log_2 3, \\ \forall \gamma_{30}, \gamma_{31}, \gamma_{32} : \frac{1}{2} \leq \gamma_{30} + \gamma_{31} + \gamma_{32} &\leq 1. \end{aligned} \quad (5.3.34)$$

The equations (5.3.34) and (5.3.31) combined offer the quantum capacity of channels in Class 3F in their entire parameter space.

### 5.3.g Class 3G

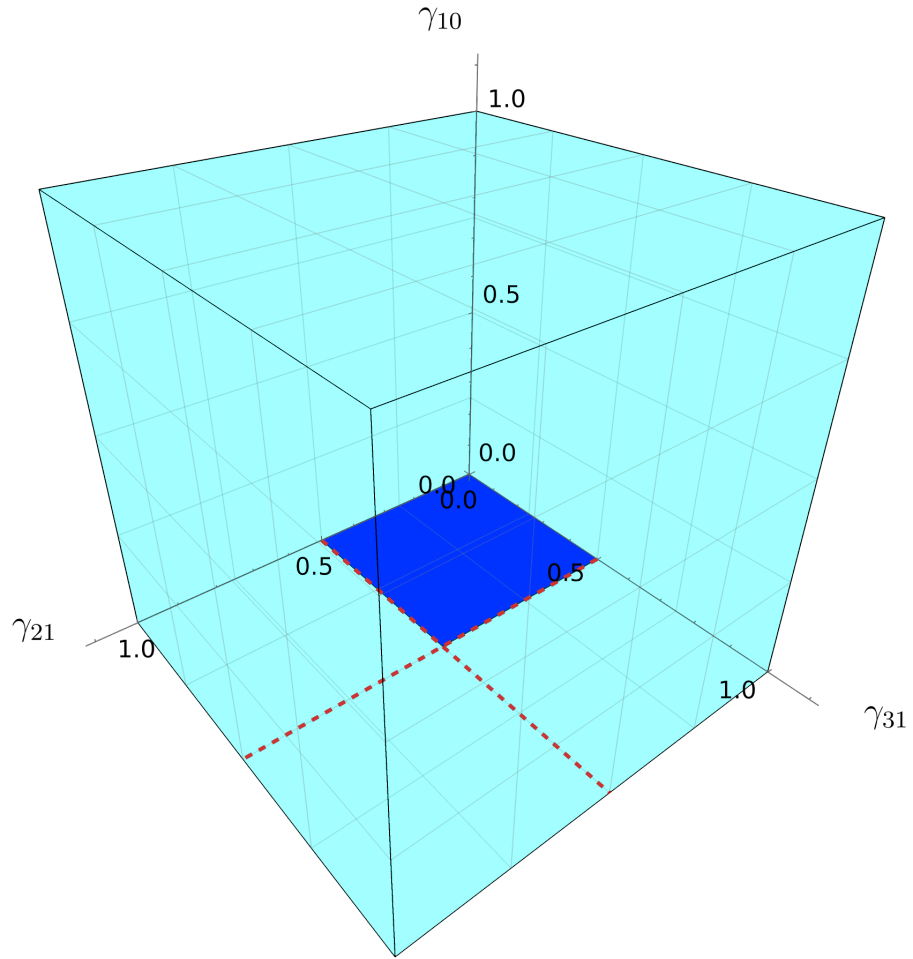


**Figure 5.3.23:** The graph represents the parameter region (cyan) of  $\Phi_{\Gamma_{3G}(\gamma_{10}, \gamma_{21}, \gamma_{31})}$  and its degradability regions (blue).

Consider the sample channel  $\Phi_{\Gamma_{3G}(\gamma_{10}, \gamma_{21}, \gamma_{31})}$  belonging in Class 3G, identified by the transition matrix:

$$\begin{aligned} \Gamma_{3G}(\gamma_{10}, \gamma_{21}, \gamma_{31}) = & \mathbb{1}_4 + \gamma_{10} |1\rangle\langle 0| + \gamma_{21} |2\rangle\langle 1| + \gamma_{31} |3\rangle\langle 1| \\ & - \gamma_{10} |1\rangle\langle 1| - \gamma_{21} |2\rangle\langle 2| - \gamma_{31} |3\rangle\langle 3|. \end{aligned} \quad (5.3.35)$$

As a consequence of the results of Subsection 4.7.1,  $\Phi_{\Gamma_{3G}(\gamma_{10}, \gamma_{21}, \gamma_{31})}$  is never degradable unless  $\gamma_{10}$  is 0, at which point the channel reduces to a channel belonging in Class 2A. The degradability regions in the parameter space of  $\Phi_{\Gamma_{3G}(\gamma_{10}, \gamma_{21}, \gamma_{31})}$  are plotted in Figure 5.3.23.

### 5.3.h Class 3H

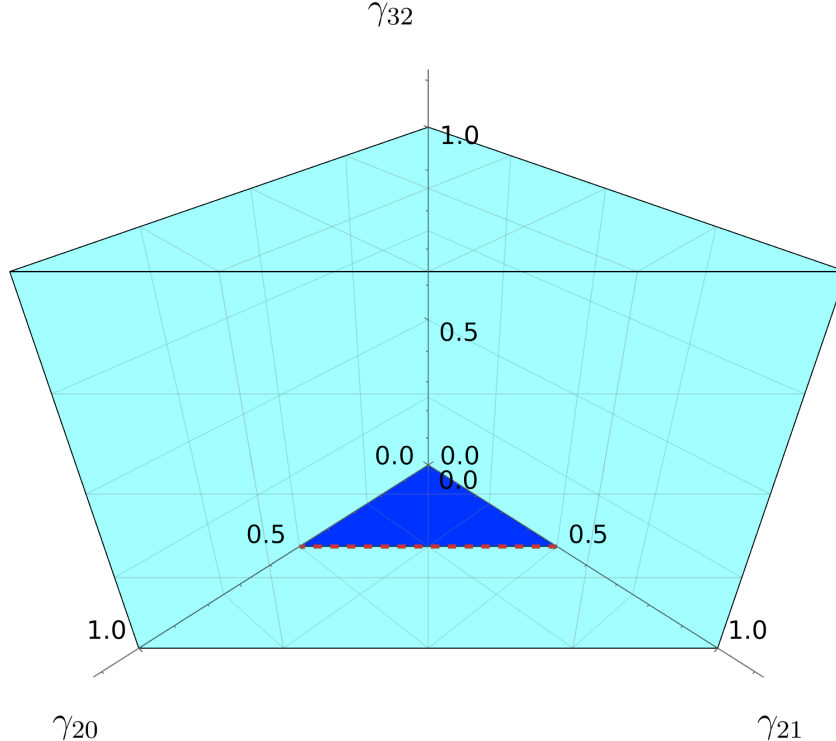


**Figure 5.3.24:** The graph represents the parameter region (cyan) of  $\Phi_{\Gamma_{3H}(\gamma_{20}, \gamma_{21}, \gamma_{32})}$  and its degradability regions (blue).

Consider the sample channel  $\Phi_{\Gamma_{3H}(\gamma_{20}, \gamma_{21}, \gamma_{32})}$  belonging in Class 3H, identified by the transition matrix:

$$\begin{aligned} \Gamma_{3H}(\gamma_{20}, \gamma_{21}, \gamma_{32}) = & \mathbb{1}_4 + \gamma_{20} |2\rangle\langle 0| + \gamma_{21} |2\rangle\langle 1| + \gamma_{32} |3\rangle\langle 2| \\ & - (\gamma_{20} + \gamma_{21}) |2\rangle\langle 2| - \gamma_{32} |3\rangle\langle 3|. \end{aligned} \quad (5.3.36)$$

As a consequence of the results of Subsection 4.7.m,  $\Phi_{\Gamma_{3H}(\gamma_{20}, \gamma_{21}, \gamma_{32})}$  is never degradable unless  $\gamma_{32}$  is 0, at which point the channel reduces to a channel belonging in Class 2B. The degradability regions in the parameter space of  $\Phi_{\Gamma_{3H}(\gamma_{20}, \gamma_{21}, \gamma_{32})}$  are plotted in Figure 5.3.24.

### 5.3.i Class 3I

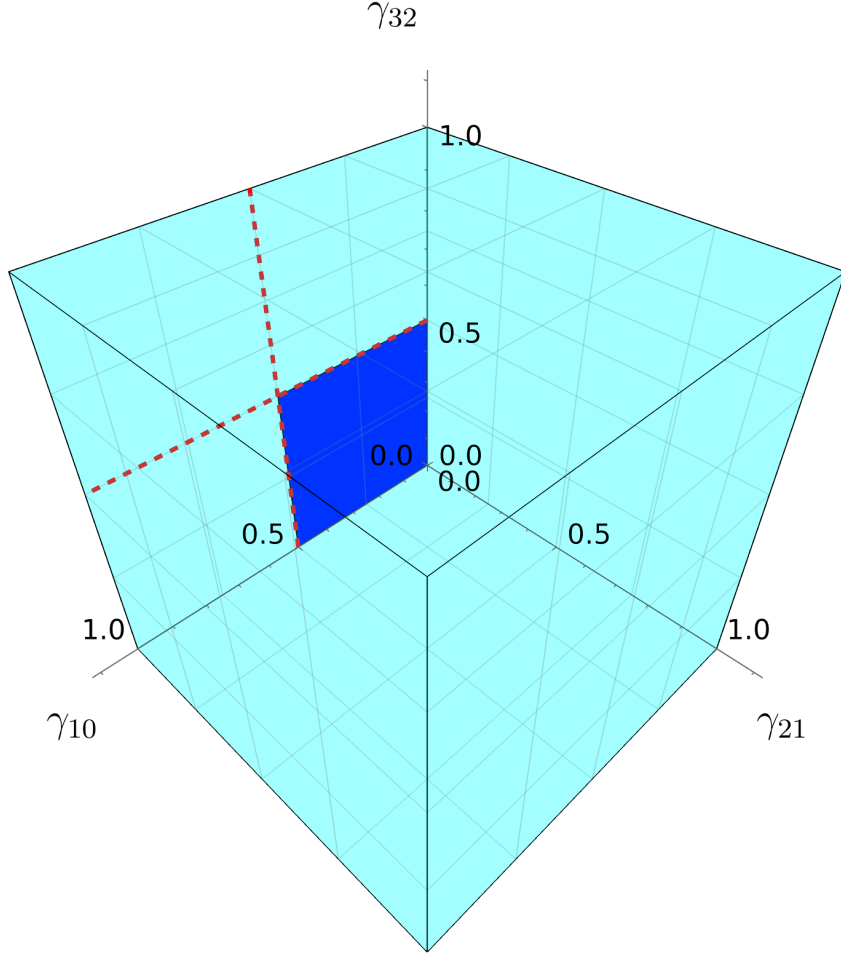


**Figure 5.3.25:** The graph represents the parameter region (cyan) of  $\Phi_{\Gamma_{3I}(\gamma_{10}, \gamma_{21}, \gamma_{32})}$  and its degradability regions (blue).

Consider the sample channel  $\Phi_{\Gamma_{3I}(\gamma_{10}, \gamma_{21}, \gamma_{32})}$  belonging in Class 3I, identified by the transition matrix:

$$\begin{aligned} \Gamma_{3I}(\gamma_{10}, \gamma_{21}, \gamma_{32}) = & \mathbb{1}_4 + \gamma_{10} |1\rangle\langle 0| + \gamma_{21} |2\rangle\langle 1| + \gamma_{32} |3\rangle\langle 2| \\ & - \gamma_{10} |1\rangle\langle 1| - \gamma_{21} |2\rangle\langle 2| - \gamma_{32} |3\rangle\langle 3|. \end{aligned} \quad (5.3.37)$$

As a consequence of the results of Subsection 4.7.n,  $\Phi_{\Gamma_{3I}(\gamma_{10}, \gamma_{21}, \gamma_{32})}$  is never degradable unless  $\gamma_{21}$  is 0, at which point the channel reduces to a channel belonging in Class 2D. The degradability regions in the parameter space of  $\Phi_{\Gamma_{3I}(\gamma_{10}, \gamma_{21}, \gamma_{32})}$  are plotted in Figure

**5.3.25.** Note that Class 3I is the only Class of 3-decay 4-dimensional MAD channels whose capacities were not shown to be monotonous in all their parameters; in fact,  $Q(\Phi_{\Gamma_{3I}(\gamma_{10}, \gamma_{21}, \gamma_{32})})$  is generally not monotonous in  $\gamma_{21}$  under (4.9.7) in every parameter configurations.

## 5.4 4-decay 4-dimensional MAD channels

As mentioned in Subsection 4.7.g, there exists a Class of 4-decay 4-dimensional MAD channels which present 4-dimensional degradability conditions. This Class is unique for 4-dimensional MAD's and can be obtained by "turning on" an additional decay starting from a channel belonging in Class 3B.

### 5.4.a Class 4A

Consider a the channel belonging in [Class 3B](#) identified by the transition matrix:

$$\begin{aligned}\Gamma'_{3B}(\gamma_{20}, \gamma_{30}, \gamma_{31}) = & \mathbb{1}_4 + \gamma_{20} |2\rangle\langle 0| + \gamma_{30} |3\rangle\langle 0| + \gamma_{31} |3\rangle\langle 1| \\ & - \gamma_{20} |2\rangle\langle 2| - (\gamma_{30} + \gamma_{31}) |3\rangle\langle 3|;\end{aligned}\quad (5.4.1)$$

by allowing for an additional decay from level  $|2\rangle$  to level  $|1\rangle$ , one obtains a channel belonging in Class 4A  $\Phi_{\Gamma_{4A}(\gamma_{20}, \gamma_{21}, \gamma_{30}, \gamma_{31})}$ , identified by the transition matrix:

$$\Gamma_{4A}(\gamma_{20}, \gamma_{21}, \gamma_{30}, \gamma_{31}) = \Gamma'_{3B}(\gamma_{20}, \gamma_{30}, \gamma_{31}) + \gamma_{21} |2\rangle\langle 1| - \gamma_{21} |2\rangle\langle 2|. \quad (5.4.2)$$

The degradability conditions for class 4A, reported in (4.7.9), translate to :

$$\Phi_{\Gamma_{4A}(\gamma_{20}, \gamma_{21}, \gamma_{30}, \gamma_{31})} \text{ degradable} \Leftrightarrow 0 \leq \gamma_{20} + \gamma_{21} \leq \frac{1}{2} \wedge 0 \leq \gamma_{31} + \gamma_{30} \leq \frac{1}{2}; \quad (5.4.3)$$

For obvious reasons, a visual rendering of these conditions in a 4-dimensional parameter space is not possible in this context. It is possible to extend the computation of the quantum capacity  $\Phi_{\Gamma_{4A}(\gamma_{20}, \gamma_{21}, \gamma_{30}, \gamma_{31})}$  in its entire parameter space. Note that the quantum capacity  $Q(\Phi_{\Gamma_{4A}(\gamma_{20}, \gamma_{21}, \gamma_{30}, \gamma_{31})})$  presents the following symmetries:

$$Q(\Phi_{\Gamma_{4A}(\gamma_{20}, \gamma_{21}, \gamma_{30}, \gamma_{31})}) = Q(\Phi_{\Gamma_{4A}(\gamma_{30}, \gamma_{31}, \gamma_{20}, \gamma_{21})}), \quad (5.4.4)$$

$$Q(\Phi_{\Gamma_{4A}(\gamma_{20}, \gamma_{21}, \gamma_{30}, \gamma_{31})}) = Q(\Phi_{\Gamma_{4A}(\gamma_{21}, \gamma_{20}, \gamma_{31}, \gamma_{30})}). \quad (5.4.5)$$

### Quantum capacity in degradability region

The quantum capacity in the region described in (5.4.3) can be computed directly using (3.3.21):

$$\begin{aligned}Q(\Phi_{\Gamma_{4A}(\gamma_{20}, \gamma_{21}, \gamma_{30}, \gamma_{31})}) = & \max_{\rho^{(diag)}} I_c(\rho^{(diag)}, \Phi_{\Gamma_{4A}(\gamma_{20}, \gamma_{21}, \gamma_{30}, \gamma_{31})}), \\ \forall \gamma_{20}, \gamma_{21}, \gamma_{30}, \gamma_{31} : & 0 \leq \gamma_{20} + \gamma_{21} \leq \frac{1}{2} \wedge 0 \leq \gamma_{31} + \gamma_{30} \leq \frac{1}{2}.\end{aligned}\quad (5.4.6)$$

### Quantum capacity on borders of the parameter region

Aside from the 3-dimensional borders obtained by setting one of the decay probabilities of  $\Phi_{\Gamma_{4A}(\gamma_{20}, \gamma_{21}, \gamma_{30}, \gamma_{31})}$  to 0, which reduce it to a channel belonging in Class 3B, one may find the quantum capacities on the borders corresponding to  $\gamma_{20} + \gamma_{21} = 1$  and, by (5.4.4), to  $\gamma_{30} + \gamma_{31} = 1$ . Suppose then  $\gamma_{30} + \gamma_{31} = 1$ ; by (4.10.9), the quantum capacity on this border is:

$$Q(\Phi_{\Gamma_{4A}(\gamma_{20}, \gamma_{21}, \gamma_{30}, 1-\gamma_{30})}) = Q(\Phi_{\Gamma_{2B3}(\gamma_{20}, \gamma_{21})}^{(3)}), \quad (5.4.7)$$

where  $\Phi_{\Gamma_{2B3}(\gamma_{20}, \gamma_{21})}^{(3)}$  is defined in (5.3.8) and whose capacity can be found using the results in [CG21a].

Equation (5.4.4) implies that:

$$Q(\Phi_{\Gamma_{4A}(\gamma_{20}, 1-\gamma_{20}, \gamma_{30}, \gamma_{31})}) = Q(\Phi_{\Gamma_{2B3}(\gamma_{30}, \gamma_{31})}^{(3)}). \quad (5.4.8)$$

**Extension to**  $\frac{1}{2} \leq \gamma_{30} + \gamma_{31} \leq 1 \wedge 0 \leq \gamma_{20} + \gamma_{21} \leq \frac{1}{2}$

$Q(\Phi_{\Gamma_{2B3}(\gamma_{20}, \gamma_{21})}^{(3)})$  is a lower bound on  $Q(\Phi_{\Gamma_{4A}(\gamma_{20}, \gamma_{21}, \gamma_{30}, \gamma_{31})})$  as it is the emergent quantum capacity from a fixed choice of encoding. Furthermore, a numerical evaluation of the difference between  $Q(\Phi_{\Gamma_{4A}(\gamma_{20}, \gamma_{21}, \gamma_{30}, 1/2-\gamma_{30})})$  and  $Q(\Phi_{\Gamma_{2B3}(\gamma_{20}, \gamma_{21})}^{(3)})$  yields discrepancies of the order  $\lesssim 10^{(-15)}$ , likely due to the machine's precision, which, together with the monotonicity rules Section 4.9, implies that:

$$\begin{aligned} Q(\Phi_{\Gamma_{4A}(\gamma_{20}, \gamma_{21}, \gamma_{30}, \gamma_{31})}) &= Q(\Phi_{\Gamma_{2B3}(\gamma_{20}, \gamma_{21})}^{(3)}), \\ \forall \gamma_{20}, \gamma_{21}, \gamma_{30}, \gamma_{31} : \frac{1}{2} \leq \gamma_{30} + \gamma_{31} \leq 1 \wedge 0 \leq \gamma_{20} + \gamma_{21} \leq \frac{1}{2}. \end{aligned} \quad (5.4.9)$$

The (5.4.4) also implies that:

$$\begin{aligned} Q(\Phi_{\Gamma_{4A}(\gamma_{20}, \gamma_{21}, \gamma_{30}, \gamma_{31})}) &= Q(\Phi_{\Gamma_{2B3}(\gamma_{30}, \gamma_{31})}^{(3)}), \\ \forall \gamma_{20}, \gamma_{21}, \gamma_{30}, \gamma_{31} : \frac{1}{2} \leq \gamma_{20} + \gamma_{21} \leq 1 \wedge 0 \leq \gamma_{30} + \gamma_{31} \leq \frac{1}{2}. \end{aligned} \quad (5.4.10)$$

**Extension to**  $\frac{1}{2} \leq \gamma_{30} + \gamma_{31} \leq 1 \wedge \frac{1}{2} \leq \gamma_{20} + \gamma_{21} \leq 1$

A natural lower bound on  $Q(\Phi_{\Gamma_{4A}(\gamma_{20}, \gamma_{21}, \gamma_{30}, \gamma_{31})})$  is offered by the  $\log_2$  of the dimension of the noiseless subspace of the channel, which corresponds to 1; a numerical evaluation yields  $Q(\Phi_{\Gamma_{4A}(1/2-\gamma_{20}, \gamma_{30}, 1/2-\gamma_{30})}) = Q(\Phi_{\Gamma_{2B3}(1/2, 1/2-\gamma_{20})}^{(3)}) \stackrel{[CG21a]}{=} 1$ . By the non-increasing properties of  $Q(\Phi_{\Gamma_{4A}(\gamma_{20}, \gamma_{21}, \gamma_{30}, \gamma_{31})})$  in its arguments, it is possible to conclude that:

$$\begin{aligned} Q(\Phi_{\Gamma_{4A}(\gamma_{20}, \gamma_{21}, \gamma_{30}, \gamma_{31})}) &= 1, \\ \forall \gamma_{20}, \gamma_{21}, \gamma_{30}, \gamma_{31} : \frac{1}{2} \leq \gamma_{20} + \gamma_{21} \leq 1 \wedge \frac{1}{2} \leq \gamma_{30} + \gamma_{31} \leq 1. \end{aligned} \quad (5.4.11)$$

Combining (5.4.9), (5.4.10), (5.4.11) and (5.4.6), one is able to obtain the quantum capacity of  $\Phi_{\Gamma_{4A}(\gamma_{20}, \gamma_{21}, \gamma_{30}, \gamma_{31})}$  in the entirety of its parameter space. TODO graph if you have time.



## 6

## 2-way capacity for 3-dimensional MAD channels

The relation (2.13.4) provides an easier to compute lower bound for the 2-way capacity of a quantum channel; in the case of 3-dimensional MAD channels (2.13.4) offers a lower bound on  $Q_2$  for any given choice of the decay probabilities  $(\gamma_{10}, \gamma_{20}, \gamma_{21})$ . Thanks to the results in [CG21a], it is possible to compare this bound to the natural lower bound given by the quantum capacity  $Q$  where this quantity was found. This comparison was performed and reported in the following sections.

### 6.1 2-way capacity for Class 1A3 MAD's - lower bound

Consider a single decay 3-dimensional MAD channel  $\Phi_{\Gamma_{1A3}(\gamma_{10}, 0, 0)}^{(3)}$ , identified by the transition matrix:

$$\Gamma_{1A3}(\gamma_{10}, 0, 0) \equiv \mathbb{1}_3 + \gamma_{10} |1\rangle\langle 0| - \gamma_{10} |1\rangle\langle 1|. \quad (6.1.1)$$

Comparing (2.13.4) with the results of [CG21a] one obtains the plot reported in Figure 6.1.1

### 6.2 2-way capacity for Class 2A3 MAD's - lower bound

Consider a double decay 3-dimensional MAD channel  $\Phi_{\Gamma_{2A3}(\gamma_{10}, \gamma_{20}, 0)}^{(3)}$ , identified by the transition matrix:

$$\begin{aligned} \Gamma_{2A3}(\gamma_{10}, 0, 0) \equiv & \mathbb{1}_3 + \gamma_{10} |1\rangle\langle 0| + \gamma_{20} |2\rangle\langle 0| \\ & - \gamma_{10} |1\rangle\langle 1| - \gamma_{20} |2\rangle\langle 2|. \end{aligned} \quad (6.2.1)$$

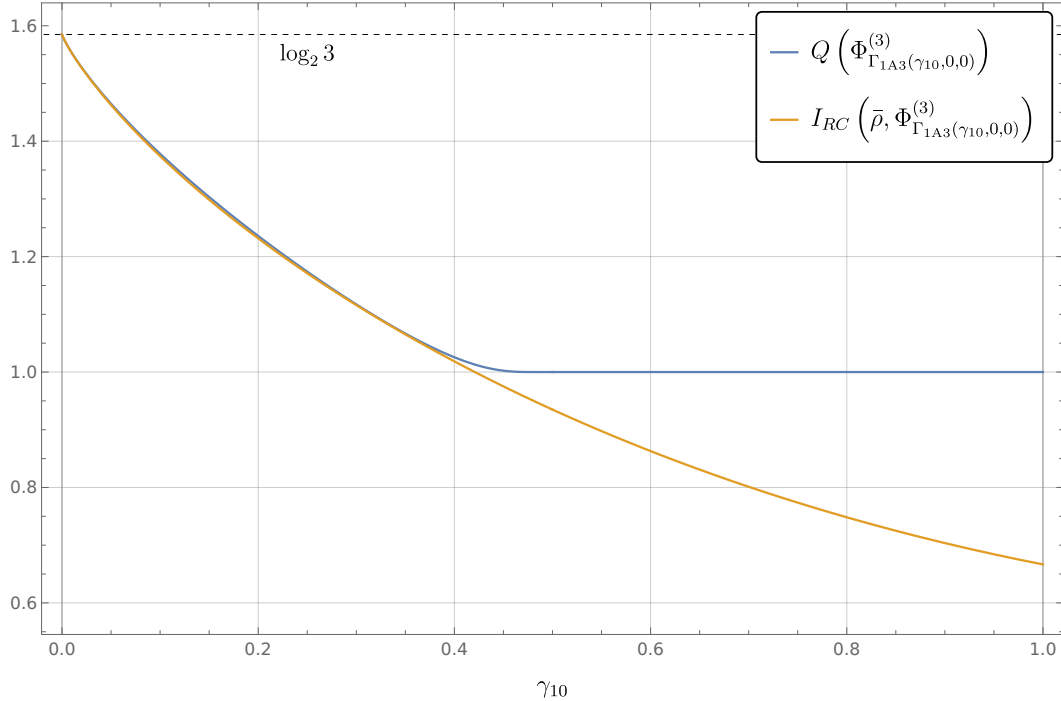


**Figure 6.1.1:** Comparison of lower bounds for the 2-way capacity of  $\Phi_{\Gamma_{1A3}(\gamma_{10}, 0, 0)}^{(3)}$ .

Comparing (2.13.4) with the results of [CG21a] one obtains the plot reported in Figure 6.2.1

### 6.3 2-way capacity for Class 2B3 MAD's - lower bound

Consider a double decay 3-dimensional MAD channel  $\Phi_{\Gamma_{2B3}(0, \gamma_{20}, \gamma_{21})}^{(3)}$ , identified by the transition matrix:

$$\begin{aligned} \Gamma_{2B3}(\gamma_{10}, 0, 0) \equiv & \mathbb{1}_3 + \gamma_{20} |2\rangle\langle 0| + \gamma_{21} |2\rangle\langle 1| \\ & - (\gamma_{20} + \gamma_{21}) |2\rangle\langle 2|. \end{aligned} \tag{6.3.1}$$

Comparing (2.13.4) with the results of [CG21a] one obtains the plot reported in Figure 6.3.1

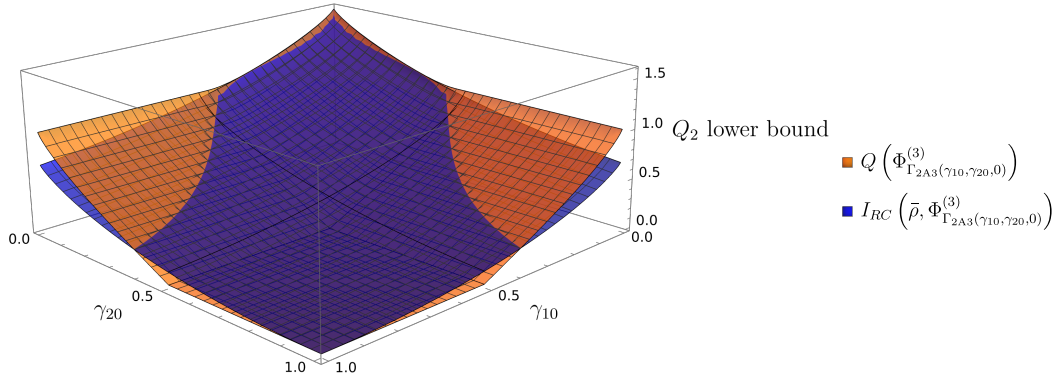


**Figure 6.2.1:** Comparison of lower bounds for the 2-way capacity of  $\Phi_{\Gamma_{2A3}(\gamma_{10}, \gamma_{20}, 0)}^{(3)}$ .

## 6.4 2-way capacity for Class 2C3 MAD's - lower bound

Consider a double decay 3-dimensional MAD channel  $\Phi_{\Gamma_{2C3}(\gamma_{10}, 0, \gamma_{21})}^{(3)}$ , identified by the transition matrix:

$$\begin{aligned} \Gamma_{2C3}(\gamma_{10}, 0, 0) \equiv & \mathbb{1}_3 + \gamma_{10} |1\rangle\langle 0| + \gamma_{21} |2\rangle\langle 1| \\ & - \gamma_{10} |1\rangle\langle 1| - \gamma_{21} |2\rangle\langle 2|. \end{aligned} \quad (6.4.1)$$

Comparing (2.13.4) with the results of [CG21a] one obtains the plot reported in Figure 6.4.1

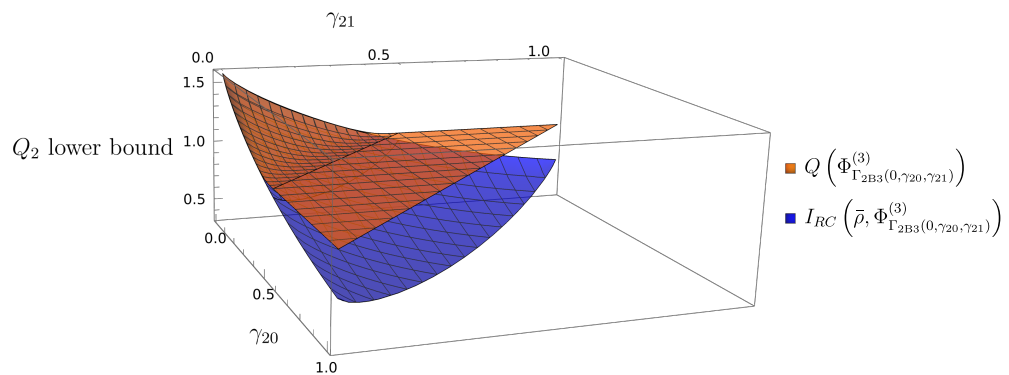


**Figure 6.3.1:** Comparison of lower bounds for the 2-way capacity of  $\Phi_{\Gamma_{2B3}(0,\gamma_{20},\gamma_{21})}^{(3)}$ .

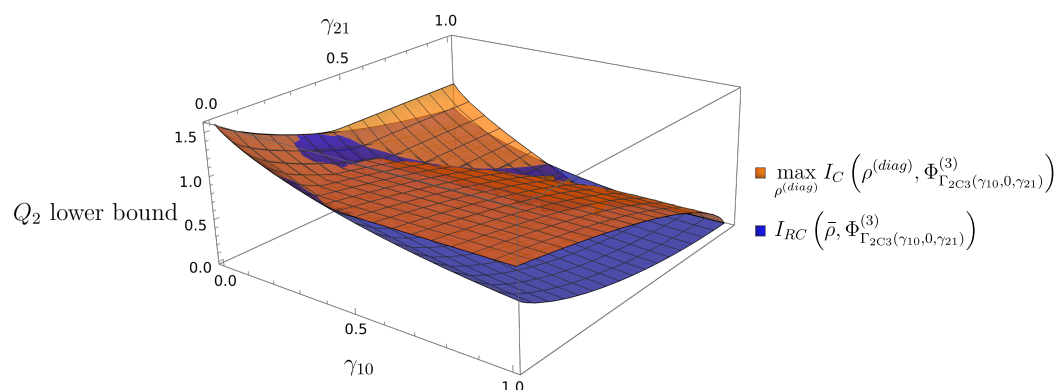


**Figure 6.4.1:** Comparison of lower bounds for the 2-way capacity of  $\Phi_{\Gamma_{2C3}(\gamma_{10},0,\gamma_{21})}^{(3)}$ .

# Conclusion

What has been exposed in this Thesis work is the continuation of an effort of the scientific community to better understand the long distance communication capabilities of qudit-based systems. In fact, MAD channels describe an energy decay process when transmitting messages over long distances, and the capacities of those channels quantify how much the induced noise degrades the signal. Given that energy decays in these processes are very likely to happen (although they are not the only possible kind of noise), the study of their capacities would serve as an important headlight for the development of quantum communication technologies based upon qudits.

## 7.1 Summary

The study mentioned above, for 4-dimensional MAD channels, was achieved for the quantum capacity during this Thesis work in 4 main steps:

- Explore general properties of MAD channels, such as composition rules and monotonicity of capacity functionals.
- Find degradability regions in the parameter space for MAD channels.
- Compute the quantum capacity in the degradability regions.
- Extend the computations performed in the degradability regions to some non-degradable regions.

During the first step of this process, a number of results were found which were reported in Chapter 4. Particularly, the results in Section 4.9 on the monotonicity of the capacities of MAD channels meant that the technique for extending the computation of the capacities first developed in [CG21a] could also be applied to the wide range of Classes of 4-dimensional MAD channels, listed in Section 4.7, which admit degradability regions. These degradability regions were found thanks to the relation (4.6.1) using the methods outlined in Section 7.2. The computation of the quantum capacity, thanks to

the result (3.3.21), was performed as illustrated in Section 7.2. The resulting plots are reported in Chapter 5, along with the explanations of the extension to non-degradable regions.

Finally, a lower bound on the 2-way capacity was computed using (2.13.4)

## 7.2 Future research

The next step in the research of MAD channels consists in setting upper bounds on the 2-way capacity, as to this date there exists no literature in this regard. MAD channels do not seem to be telecovariant (see (2.13.10)), therefore the bound (2.13.13) would not work for this family of channels. The upper bound given by the squashed entanglement (2.13.7) is valid for any channel, however it is hard to compute; a simplification may be possible on MAD channel: in [PLOB17], it was shown that the search of the sup in (2.13.5), for the case of ADC's, can be restricted to purification of diagonal density matrices. This may also hold for higher dimensional settings. Furthermore, one could also study a kind of channels closely related to MAD channels, Resonant Multi-level Amplitude Damping (ReMAD) channels. These channels describe an energy decay process for a qudit under the assumption that the qudit is encoded in a harmonic oscillator, meaning that the energy gaps between successive energy levels of the qudit are fixed. Just as MAD's, they can be identified by a transition matrix (3.3.4), but their Kraus set is different:

$$\begin{aligned} K_{\Gamma}^{(i)} &\equiv \sum_{l=0}^{d-i-1} \sqrt{\gamma_{i+l,l}} |l\rangle\langle i+l|, \quad \forall 0 \leq i \leq d-1, \\ \Phi_{\Gamma}^{(\text{ReMAD})}(\rho) &= \sum_{i=0}^{d-1} K_{\Gamma}^{(i)} \rho K_{\Gamma}^{(i)\dagger}. \end{aligned} \tag{7.2.1}$$

The analysis of the quantum capacity of ReMAD channels for  $d = 3$  has been performed in [CG23] and is based upon the same concept as the quantum capacity analysis of MAD channels. The literature for the 2-way capacity of ReMAD channel, however, is lacking.

The lower bound on the 2-way capacity of ReMAD can always be found using (2.13.2). The squashed entanglement is always an upper bound on the 2-way capacity, and the simplification on its computation given in [PLOB17] for ADC's may also hold for ReMAD's. However, for a specific kind of ReMAD's, it might be possible to set an upper bound on  $Q_2$  using (2.13.13). By setting the transition probabilities so that:

$$\gamma_{jk}^{(\eta)} \equiv \binom{j}{k} \eta^{j-k} (1-\eta)^k, \tag{7.2.2}$$

the corresponding ReMAD channel resembles a beam-splitter of transmittance  $\eta$  which gets passed through by a harmonic oscillator. In this setting, the ReMAD channel

can be mapped into a gaussian channel (see e.g. [CEGH08]); gaussian channels are always telecovariant [PLOB17], therefore their 2-way capacity is upper-bounded by the relative entropy of entanglement and, as a consequence of (2.14.1) and of the mapping between beam-splitter-type ReMAD's and gaussian channels, this bound is also an upper bound for that type of ReMAD's. As a final note, the capacity analysis of MAD's and ReMAD's seems to be highly scalable: in fact, the quantum capacities in some non-degradable regions found in this Thesis work for MAD channels reduced to quantum capacities in lower dimensional systems found in [CG21a]. The "new" computations corresponded to those of the maxima of the coherent information of the degradable regions. This suggests that, when considering higher dimensional systems, much of the work previously performed could be easily exported to future researches on this type of lossy finite-dimensional channels.

## Acknowledgement

First, I like to thank my daily supervisor ..., for there support. Also, I wan to thank my first supervisor ... for his insight into.

Thanks to ..... for all the insights into ..... . Thanks to .... for all the intense but fruitful scientific debate about ..... . Thanks to ... , who always had an open door for ..... .

Also, I would like to thank the ..... .

And last but not least, thanks to .... , who helped ..... . As well as .... for the help with ..... .

# Bibliography

- [Bel64] J. S. Bell. [On the Einstein Podolsky Rosen paradox](#). *Physics Physique Fizika*, 1:195–200, November 1964.
- [CDLBO19] Daniele Cozzolino, Beatrice Da Lio, Davide Bacco, and Leif Katsuo Oxenlowe. High-dimensional quantum communication: Benefits, progress, and future challenges. [Advanced Quantum Technologies](#), 2(12):1900038, 2019.
- [CEGH08] F Caruso, J Eisert, V Giovannetti, and A S Holevo. [Multi-mode bosonic Gaussian channels](#). *New Journal of Physics*, 10(8):083030, August 2008.
- [CG21a] Stefano Chessa and Vittorio Giovannetti. [Quantum capacity analysis of multi-level amplitude damping channels](#). *Communications Physics*, 4(1):22, February 2021.
- [CG21b] Stefano Chessa and Vittorio Giovannetti. [Partially Coherent Direct Sum Channels](#). *Quantum*, 5:504, July 2021.
- [CG23] Stefano Chessa and Vittorio Giovannetti. [Resonant Multilevel Amplitude Damping Channels](#). *Quantum*, 7:902, January 2023.
- [Cho75] Man-Duen Choi. [Completely positive linear maps on complex matrices](#). *Linear Algebra and its Applications*, 10(3):285–290, 1975.
- [Chr06] Matthias Christandl. [The Structure of Bipartite Quantum States - Insights from Group Theory and Cryptography](#). *arXiv: Quantum Physics*, 2006.
- [CWY04] N. Cai, A. Winter, and R. W. Yeung. [Quantum privacy and quantum wiretap channels](#). *Problems of Information Transmission*, 40(4):318–336, October 2004.
- [Dev05] I. Devetak. [The private classical capacity and quantum capacity of a quantum channel](#). *IEEE Transactions on Information Theory*, 51(1):44–55, 2005.
- [DS05] I. Devetak and P. W. Shor. [The Capacity of a Quantum Channel for Simultaneous Transmission of Classical and Quantum Information](#). *Communications in Mathematical Physics*, 256(2):287–303, June 2005.
- [DSS98] David P. DiVincenzo, Peter W. Shor, and John A. Smolin. [Quantum-channel capacity of very noisy channels](#). *Phys. Rev. A*, 57:830–839, February 1998.

- [Dys49] F. J. Dyson. [The Radiation Theories of Tomonaga, Schwinger, and Feynman](#). *Phys. Rev.*, 75:486–502, February 1949.
- [EPR35] A. Einstein, B. Podolsky, and N. Rosen. [Can Quantum-Mechanical Description of Physical Reality Be Considered Complete?](#) *Phys. Rev.*, 47:777–780, May 1935.
- [FW07] Motohisa Fukuda and Michael M. Wolf. [Simplifying additivity problems using direct sum constructions](#). *Journal of Mathematical Physics*, 48(7):072101, July 2007.
- [GF05] Vittorio Giovannetti and Rosario Fazio. [Information-capacity description of spin-chain correlations](#). *Phys. Rev. A*, 71:032314, March 2005.
- [Gor62] J. P. Gordon. [Quantum Effects in Communications Systems](#). *Proceedings of the IRE*, 50(9):1898–1908, 1962.
- [HG12] A S Holevo and V Giovannetti. [Quantum channels and their entropic characteristics](#). *Reports on Progress in Physics*, 75(4):046001, March 2012.
- [Hol07] A.S. Holevo. [Complementary Channels and the Additivity Problem](#). *Theory of Probability & Its Applications*, 51(1):92–100, 2007.
- [Hol13] Alexander S. Holevo. [Quantum Systems, Channels, Information](#). De Gruyter, 2013.
- [Jam72] A. Jamiołkowski. [Linear transformations which preserve trace and positive semidefiniteness of operators](#). *Reports on Mathematical Physics*, 3(4):275–278, 1972.
- [KSW20] Sumeet Khatri, Kunal Sharma, and Mark M. Wilde. [Information-theoretic aspects of the generalized amplitude-damping channel](#). *Phys. Rev. A*, 102:012401, July 2020.
- [KW20] Sumeet Khatri and Mark M. Wilde. [Principles of Quantum Communication Theory: A Modern Approach](#), 2020.
- [NC10] Michael A. Nielsen and Isaac L. Chuang. [Quantum Computation and Quantum Information: 10th Anniversary Edition](#). Cambridge University Press, 2010.
- [PEW<sup>+</sup>15] S. Pirandola, J. Eisert, C. Weedbrook, A. Furusawa, and S. L. Braunstein. [Advances in quantum teleportation](#). *Nature Photonics*, 9(10):641–652, October 2015.
- [PLOB17] Stefano Pirandola, Riccardo Laurenza, Carlo Ottaviani, and Leonardo Banchi. [Fundamental limits of repeaterless quantum communications](#). *Nature Communications*, 8(1):15043, April 2017.

- [Sha48] C. E. Shannon. [A mathematical theory of communication](#). *The Bell System Technical Journal*, 27(3):379–423, 1948.
- [Sti55] W. Forrest Stinespring. [Positive Functions on C\\*-Algebras](#). *Proceedings of the American Mathematical Society*, 6(2):211–216, 1955.
- [WHSK20] Yuchen Wang, Zixuan Hu, Barry C. Sanders, and Sabre Kais. [Qudits and High-Dimensional Quantum Computing](#). *Frontiers in Physics*, 8, November 2020.
- [YHD08] Jon Yard, Patrick Hayden, and Igor Devetak. [Capacity theorems for quantum multiple-access channels: classical-quantum and quantum-quantum capacity regions](#). *IEEE Transactions on Information Theory*, 54(7):3091–3113, 2008.



# Appendix

## Computation methods

The values for the quantum capacities and the lower bounds on the 2-way capacity reported in this document were obtained thanks to the **Mathematica** framework. The version that was used for the computations is **Mathematica** 13.0. The most basic function necessary for quantum channels, such as the creation of a channel from its Kraus set, were provided by the [QuantumUtils](#) package.

```
"      Needs["QuantumUtils`"]
```

However, most of the functions needed were created specifically for this project. The notebooks can be found at [my GitHub page](#). The problem of finding the degradability regions of MAD channels 4.7 reduces to finding the eigenvalues of the Choi matrix of the map built in (4.6.1). The Choi matrix of this map was built using the following function:

```
" ChoiMatrixConnecting[mat_]:=(
nkr=nK[mat];
CM1=ConstantArray[0,{d nkr,d nkr}];
dm=ConstantArray[0,{d,d}];
Do[
dm[[ik,jk]]=1;
dm1=InverseMAD[dm,mat];
dm2=ComplMAD[dm1,Kraus[KrausList[mat]]];
dm[[ik,jk]]=0;
Do[
CM1[[((ik-1) nkr+iik,(jk-1) nkr+jjk)]] = FullSimplify[dm2[[iik,jjk]]],
{iik,1,nkr},{jjk,1,nkr}
],
{ik,1,d},{jk,1,d}
];
Simplify[CM1]
);
```

where `nkr` is the number of Kraus operators and `mat` is the transition matrix of the channel. Once the Choi matrix is created, it is possible to use the built-in **Mathematica** function `Eigenvalues` to compute the eigenvalues of the matrix; if those eigenvalues are  $\geq 0$ , the channel is degradable.

The computation of the maximum of the coherent information in the degradable regions, corresponding to the quantum capacity in those regions, was a bit trickier. In

order to help **Mathematica** understand the bounds where the search of the maximum was to be performed, a trigonometric formulation of the input density matrices was used:

```
"      BuildDensity[par_]:=(
  ρSys=ConstantArray[0,{d,d}];
  Do[
    ρSys[[j1,j1]]=(
      Product[Sin[ToExpression[ToString[par]<>ToString[j2-1]]]^2)
      ,{j2,1,j1-1}];
    ρSys[[d,d]]=Product[Sin[ToExpression[ToString[par]<>ToString[j2-1]]]^2,
      {j2,1,d-1}];
    Simplify[ρSys]
  )
)
```

Then, the numerical maxima over the parameters (par)<sub>j</sub> were reported in the plots of 5.